Theoretical Investigation into Asymmetric Iminium Ion Organocatalysis

Gareth J.S. Evans

A thesis submitted to Cardiff University in accordance with the requirements for the degree of Philosophiae Doctor in the faculty of Science, Department of Chemistry, Cardiff University.

UMI Number: U492422

UMI

Dissertation Publishing

ProQuest

Abstract

The scope of this thesis covered three topics and creates a picture of an emerging area of chemistry. A reaction pathway is proposed for the formation of iminium ion intermediates from the reaction of secondary amines with carbonyl compounds.

Molecular properties were used to describe a range of secondary amines with an aim to find a relationship between composition, reactivity and enantioselectivity. A number of catalytic candidates were suggested for synthesis.

Two reaction types that directly and indirectly utilise iminium ions as catalysts or intermediates were covered. The Diels-Alder reaction was studied in depth for a number of iminium ions. The α-acyloxylation of simple enamine compounds was investigated highlighting possible areas for further investigation of reactivity and enanotioselectivity

Acknowledgements

The important thing in science is not so much to obtain new facts as to discover new ways of thinking about them.

<div align="right">
Sir William Bragg
British physicist (1862 - 1942)
</div>

TABLE OF CONTENTS

1. – Introduction

Chemistry can be seen as the process by which one system is transformed into another. This simplistic view obviously encapsulates hundreds of years of alchemy and experimentation which has spawned numerous disciplines within an enormous subject. Far from an insular subject chemistry embraces other sciences through the need for answers. Spectroscopy and kinetic experiments have been used to identify structure and rates giving experimental data from which to base ideas. The twentieth century bought a new way of thinking in the advent of quantum theory; the use of computer aided simulation has allowed old problems to be seen through fresh eyes and create a new and powerful discipline.

1.1.   Use of catalysts in Synthetic Chemistry

Reactions in chemistry take place at a certain rate at given temperatures, some have low energy requirements, such as dimerisation of cyclopentadiene that happens at room temperature, others are energetically unfavourable such as producing hydrocarbons from carbon monoxide and hydrogen. An entity that can increase the rate at which a process can occur without being consumed in the process is known as a catalyst. A catalyst can be as simple as a single proton in acid catalysis or as complex as the vast enzyme structures found in nature.

It is the efficiency of a catalyst that is of paramount importance, with constant efforts being made to increase the molecule's effectiveness. There are many forms of catalyst, each with both advantages and limitations. Catalysis has allowed for mass production of compounds ranging from organic solvents to large molecular weight polymers. The reliance on these molecules to consistently produce products of specific design has lead to advancement in all areas of chemistry from material science to pharmacology.

Many molecules exist as optical isomers (enantiomers), these are non-superimposable mirror images that only differ in the rotation of plane polarised light . Nature deals with this variety by using complex enzymes to create, modify or metabolise chiral forms of a molecule, allowing for superior reactivity and stereoselectivity.

Asymmetric catalysis allows a chemist to control the three-dimensional nature of a product by creating a system in which one enantiomer is favoured over another. As the understanding of reaction mechanisms becomes more advanced, catalytic moieties can be tailored to specific reactions to increase the sense of asymmetric induction, yields and purity. This ability to design effective chiral catalysts has become an area of rapid growth within the chemical community. It is of particular interest in the preparation of biologically active molecules, where optical purity can have major effect on the potency and efficacy of the molecule. The majority of synthetically preferred compounds used for catalysis are metal based, and have historically given the best yields and stereoselectivites for numerous reactions.

Simple Lewis acids such as boron trifluoride (BF_3), aluminium trichloride ($AlCl_3$) and titanium tetrachloride ($TiCl_4$) have all been used in a number of C – C bond forming reactions, mostly in stoichiometric amounts. It is the complexation of the Lewis acid to a carbonyl group that promotes a reaction to occur. Modification of these simple Lewis acids can create versatile asymmetric catalysts. A number of chiral organoaluminium Lewis acids (example given in Figure 1.1) have been found to be effective in hetero Diels-Alder reactions.[1] There has also been much success with organotitanium Lewis acids for Diels alder reactions.[2] The most effective Lewis acids for Diels-Alder reactions have been derived from borane. This can be seen to be due to their affinity for carbonyl groups with acyloxyboranes shown to give excellent results for a wide range of unsaturated aldehydes in the Diels-Alder reaction.[3]
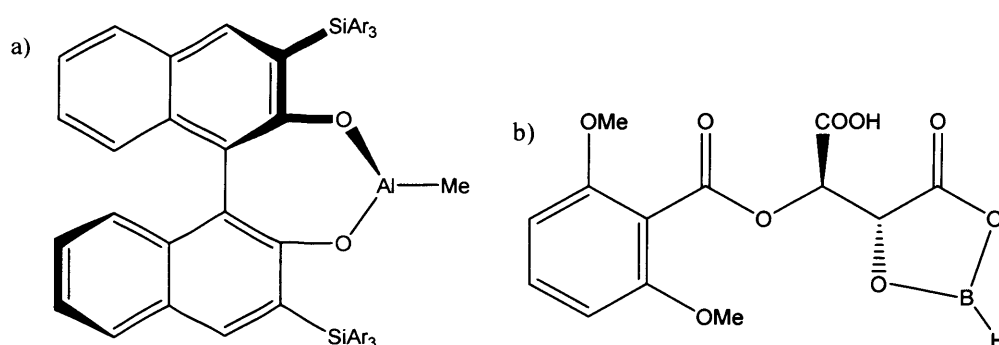
Figure 1.1 Structures of a) chiral organoaluminium reagent, b) chiral (Acyloxy)borane (CAB) Reagent I

1.2. Organocatalysis

The use of organic compounds in catalysis has become a breeding ground for innovation. The term "organocatalysis" was first coined by MacMillan in 2000[4] to describe a processes where the catalyst contains only "organic" elements, that is, they contain carbon, hydrogen, nitrogen, sulphur or phosphorus. The subject area of amino catalysis first appeared in the 1970's when Hajos and Parish[5] and separately Eder, Sauer and Wiechert[6] reported the catalytic properties of (*S*)-(-)-proline for the intramolecular aldol cyclisation of triketones (Figure 1.2).
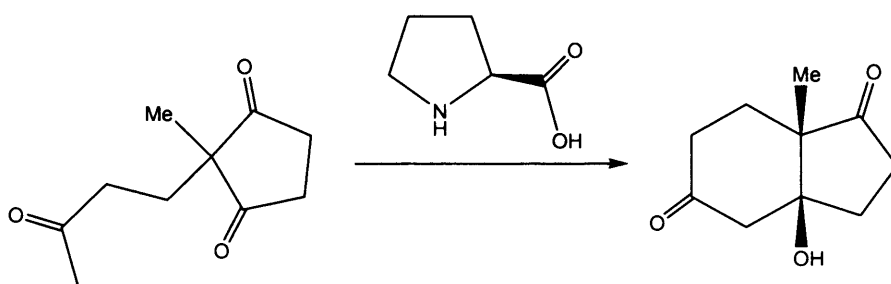
Figure 1.2 (*S*)-(-)-Proline catalysis of intramolecular aldol cyclisation of triketones.

Since MacMillan's initial publication of a Diels-Alder reaction catalysed by an imidazolidinone based molecule, a torrent of papers have been published on the effectiveness of asymmetric organocatalysis in an ever increasing range of reactions, some of which will be reported within this work. Two excellent reviews have been published by Dalko[7,8] documenting many of the recent advances found in the literature.

1.3. Reasons for organocatalysis

Most catalytic processes employed by a chemist use organometallic compounds as the catalyst. These have at their centre, one or more metal atoms, often one of the transition-metals. There are many advantages to using metals: their high coordination numbers allow for structural diversity, while the ability to fine tune ligands to suit individual classes of reactions gives a large amount of control of the range of reactions available.

Although metal-mediated catalysis has a number of advantages, there are some economic and environmental disadvantages which are becoming increasingly important. These include the high price of refined metal, along with the costs of correct disposal of the catalysts once used. Metals are sensitive to environmental factors such as oxidation and moisture, which can make them troublesome to work with and also susceptible to degradation. The inherent toxicity of metals increases the need for effective waste treatment and also the risk of contamination by the metal is of particular concern with pharmaceutical products.[9] Such considerations are amplified for large-scale industrial processes.

Many of the difficulties that arise due to metal-based catalysts can be bypassed by using metal-free processes which includes organocatalytic transformations. The absence of a metal means that the cost and toxicity are both reduced. Also, the stability of the organic catalysts frequently allows the user to carry out reactions in both aerobic and wet conditions. The typical low molecular weight with respect to metal complexes also means that many catalysts can be attached to solid supports for easier use than their metal equivilants.[10] All of these factors allow for easier control and more flexible working environments in which the catalyst can operate, leading to potential for use in a wider range of applications in cheaper, more environmentally benign operations.

1.4. Iminium ion catalysis using α,β-unsaturated carbonyl compounds

Traditionally, Lewis acids are used to facilitate reactions of compounds that contain α,β-unsaturated carbonyl groups. The standard reasoning for their activity is that they lower the energy of the lowest unoccupied molecular orbital (LUMO) of the carbonyl system making the molecule more susceptible to nucleophilic attack.
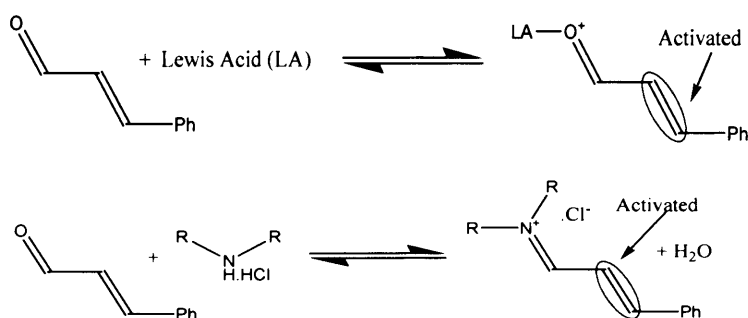
Figure 1.3 Analogy between Lewis acid and iminium ion catalysis

4

Although secondary amine organocatalysis had been known since the seventies, it was the group of MacMillian that first proposed that the reasoning for the reactivity of Lewis acids toward carbonyl compounds could be applied to catalysis via secondary amines.[4] The paper highlighted that Lewis acid catalysts could be mimicked by secondary amines in the enantioselective Diels-Alder reaction of cinnamaldehyde and cyclopentadiene via a proposed iminium ion intermediate (Figure 1.3).

Early results showed that secondary amines can be used to catalyse reactions of α,β-unsaturated carbonyl compounds, the best results came using imidazolidinone based catalysts. Subsequently, there have been a number of variations to this catalyst architecture, mainly to the nature of the groups attached to the α-carbon. The original catalyst had geminal methyl groups at this position (Figure 1.4a), but the catalyst evolved to use t-butyl[11-16] (Figure 1.4b) and furan[12] based groups (Figure 1.4c) creating a series of molecules that show efficient catalytic properties over a range of substrates.[17]
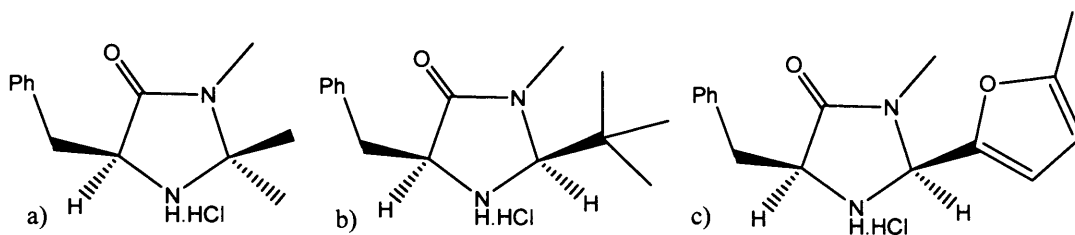
Figure 1.4 Catalysts developed by MacMillan

It is commonly believed that deprotonation of the amine is the rate determining step of iminium ion formation. Experimental work covered by Jencks[18] has shown that under acidic conditions (pH 2-5), with strongly basic amines, the rate determining step of iminium ion formation is the deprotonation to form the iminium ion catalyst.

The increase in use of iminium ion catalysis has invited theoretical investigations into the subject area. Much of the work has focused on accounting for the observed stereoselectivities and yields. The pioneering synthetic work by MacMillan has attracted the most attention due to its commercial importance. The greatest volume of theoretical data on organocatalysis by imidazolidinone based molecules has been compiled by Houk et $al.$ who modelled the Diels-Alder reaction of a number of imidazolidinone based secondary amines.[19,20] Houk's data is mostly at a standard level of theory (B3LYP/6-31G(d)) describing catalyst geometry, reaction profiles and geometric considerations. The predictions of enantiomeric excess and yield from the

study fitted well with experimental findings with Diels-Alder reactions taking place in an asynchronous concerted manner.

List *et al.* have also contributed to the field in the conjugate reduction of α,β-unsaturated aldehydes via imidazolidinone moieties[21] and a number of simple secondary amines[22] (Figure 1.5). The group has also documented the use of proline in a broad range of asymmetric transformations.[23]

Ph $\diagup$ $\diagdown$ $\overset{+}{\underset{H_2}{N}}$ $\diagup$ $\diagdown$ Ph

$CF_2CO_2^-$

$\overset{+}{NH_2}$

$CF_2CO_2^-$
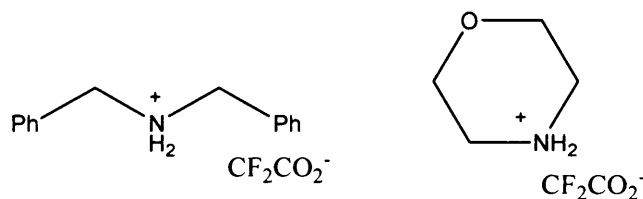
Figure 1.5 Simple secondary amines employed by List *et al.*

Jørgensen has employed organocatalysts similar to those of the MacMillan group, in that they are based around an imidazoline ring. These catalysts have been found to accelerate a number of reactions such as Michael,[24] domino Michael-Aldol,[25,26] Mannich,[27] α-chlorination,[28] allylic amination[29] and other conjugate additions.[30,31]

Me

Ph $\diagdown$ N

N
H

CO_2H
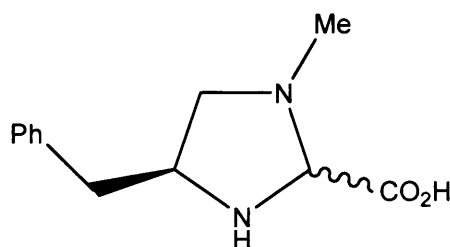
Figure 1.6 Phenylalanine-derived imidazolidine catalyst developed by Jørgensen.

Hydrazine derivatives have been employed by Tomkinson,[32] exploiting the increase in reactivity due to the presence of an atom adjacent to the reactive centre having a lone pair of electrons. This "α-effect"[33] has been used to give increased performance in reaction times. Even with increased use of this α-effect there is still little known about the origins of the observed increase in rate. Many theories exist including speculation on transition state stablisation[34], reduction of solvation of the nucleophile[35,36] and ground state destablisation[37]. The series of catalysts reported show excellent yields over a range of substrates under acidic conditions. An example of some catalysts are shown in Table 1.1. documenting the yields obtained for the Diels-Alder reaction between cyclopentadiene and cinnamaldehyde.
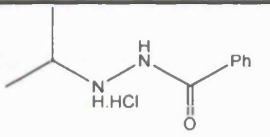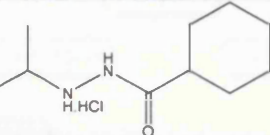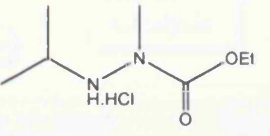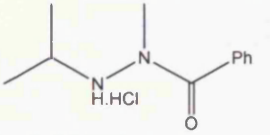
Catalyst	% Yield
	82
	86
	98
	89

Table 1.1 Diels-Alder reaction between cyclopentadiene and cinnamaldehyde at room temperature in wet methanol over 6 hours with 10mol% catalyst.

Another series of chiral catalysts has been prepared by Ogilvie[38] for the asymmetric Diels-Alder reaction. These tricyclic *N*-substituted compounds (Figure 1.7) show promise in explaining the observed stereoselectivity of the catalyst. The Ogilvie catalyst was subjected to kinetic studies and it was reported that for this moiety, the rate determining step was the cycloaddition itself with formation of the reactive iminium ion being rapid. It was also found that the reaction proceeded quickest in water with strong acid cocatalysts which had no detrimental effect on enantioselectivity.[39]
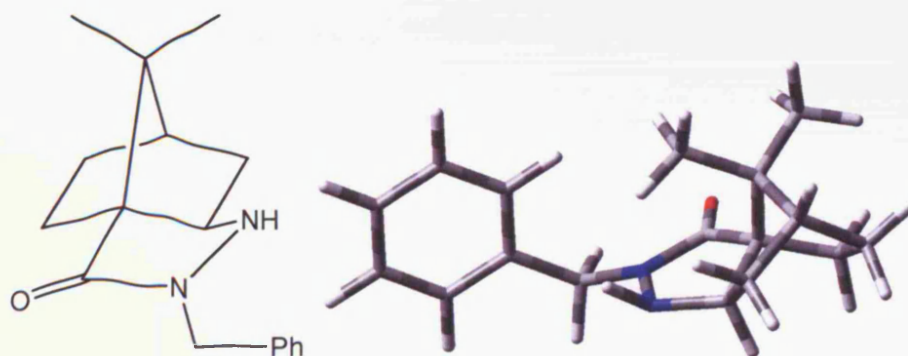
Figure 1.7 Catalyst developed by Ogilvie *et al* with optimised geometry (B3LYP/6-31+G(d,p)).

These researchers, along with a number of other groups, have begun to not only use small organic molecules as efficient catalysts but to look deeper into the mechanisms that control the reactions. Since 2000 the number of reactions directly catalysed *via* an iminium ion has grown in size to contain a group of synthetically useful reactions (Figure 1.8).
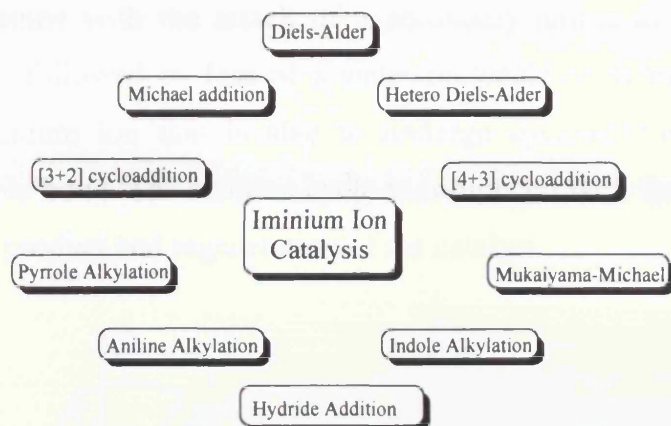
Figure 1.8 Reactions catalysts *via* an iminium ion intermediary

Each of the reactions noted in Figure 1.8 initially proceed *via* addition to the β carbon of the conjugated system. In the case of cycloaddition this is seen as an asynchronous approach of the diene. One of the most widely and synthetically useful reactions is the Diels-Alder reaction, due to the importance of this reaction in this field further discussion is provided in section 1.4.1.

1.4.1. Diels-Alder reaction

The Diels-Alder reaction[40] is one of the most important methods of carbon-carbon bond formation in organic chemistry. In one step, an unsaturated six-membered ring can be formed from a cycloaddition reaction of a conjugated diene with a double or triple bond. This reaction is used as the standard benchmark to measure activity in the activation of α,β-unsaturated carbonyl compounds.
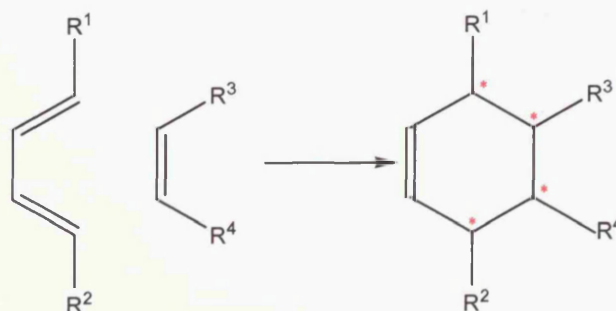
Figure 1.9 Diels-Alder reaction between diene and dienophile.

The reaction can create up to four contiguous stereogenic centres (marked with an asterisk in Figure 1.9). Understandably, control of the stereochemistry and regiochemistry of these centres is of much interest to synthetic chemists.

The accepted catalytic cycle for iminium ion activated Diels-Alder reactions is given in (Figure 1.10). The reaction begins with the attack of a secondary amine at the carbonyl of an α,β-unsaturated compound, followed by loss of a water molecule or dehydration. This produces a positively charged iminium ion that is able to undergo cycloaddition with a diene *via* the conjugated C – C double bond. The reaction cycle is completed with the hydrolysis of the N = C bond and formation of product and regeneration of the catalyst.
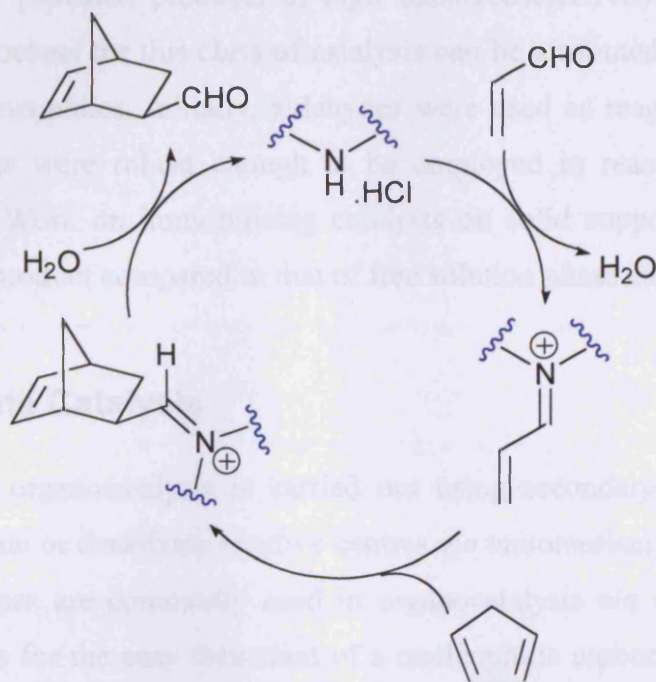
Figure 1.10 Iminium ion catalysed cycloaddition of acrolein and cyclopentadiene.

There are a number of ways to achieve selectivity within a Diels-Alder reaction for example by controlling the endo/exo selectivity (Figure 1.11) further discussion of which is given in Chapter 4. Chirality can be present in the diene, dienophile or induced *via* a chiral catalyst. Corey reported the first highly stereoselective Diels-Alder reaction in 1975,[41] spurring a plethora of chiral auxiliaries for [4+2] cycloadditions. The scope of this reaction has led it to be the staple benchmark of many synthetic chemists. The use of iminium ion catalysis for this reaction was first documented by MacMillan in 2000.[4]
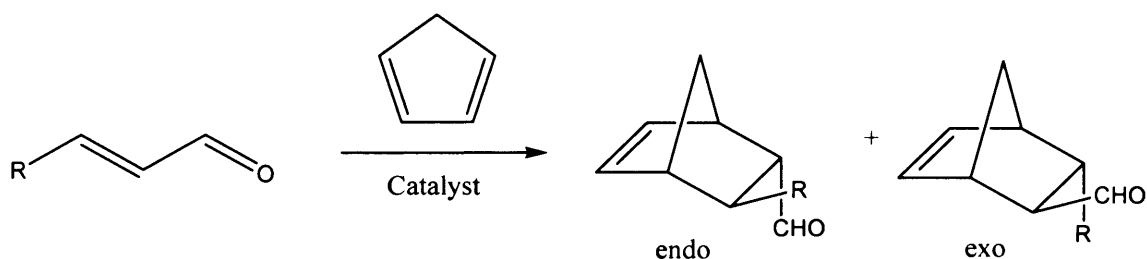
Figure 1.11 General reaction of cyclopetadiene and an α,β-unsaturated aldehyde showing two possible bicyclic diastereomeric products.

The MacMillan group developed the first highly enantioselective and general asymmetric organocatalytic Diels-Alder reaction, using HCl salts of α-amino acid-derived imidazolidinones (see Figure 1.4). The reaction was thought to proceed *via* an iminium ion intermediate. This group of catalysts has provided products in high diastereoselectivity and high enantiomeric excess.[4] Much of the success for this class of catalysis can be attributed to its robustness with a range of diene and dieneophiles. Initially, aldehydes were used as reagents, but it was quickly found that the catalysts were robust enough to be employed in reactions of sterically more challenging ketones.[12] Work on immobilising catalysts on solid supports[42] has led to equally good or better yield of product compared to that of free solution phase catalysis.

1.5. Enamine Catalysis

A large proportion of organocatalysis is carried out using secondary amines. The ability of amines to readily activate or deactivate reactive centres *via* tautomerism makes them particularly suited. Secondary amines are commonly used in organocatalysis *via* enamine pathways. This class of reaction allows for the easy formation of a nucleophilic carbon centre, where the lone-pair of the nitrogen is the driving force for the attack on electron deficient species such as a carbonyl carbon. Many of the reactions documented in the literature occur *via* the generalised enamine catalytic cycle. Here, secondary amines react with a carbonyl group to form an iminium ion, which can readily convert to the neutral enamine (Figure 1.12) allowing for a vast number of reactions to take place via the β carbon rather than the conjugated system of the iminium ion.
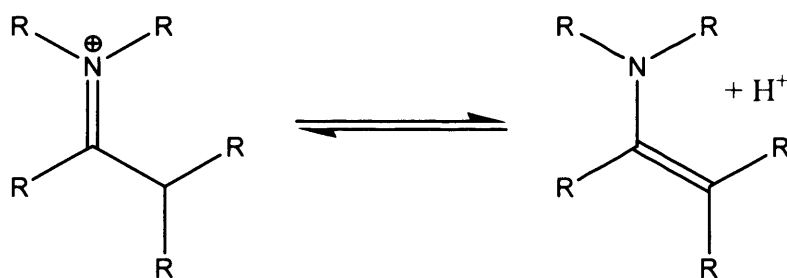
Figure 1.12 Iminium ion - Enamine tautomerisation.

The use of iminium ions as the reactive species in catalysis is relatively small in the numbers of transformations, when compared to enamine catalysis. Much research in the field of asymmetric catalysis begins from the observation of what nature does best; enzymes have the ability to catalyse hordes of reactions under benign conditions at rates synthetic chemists can only dream of. In an attempt to mimic the class of enzymes called aldolases,[43] chemists looked to harness enamines as a potent source of synthetic catalytic activity.[44]

Iminium ions are the intermediates in the formation of an enamine. Catalysis using this type of species was first developed in the 1970's by Hajos, Parrish and Oliveto[5] and separately by Eder, Sauer and Wiechert[6]. Both reactions used an intramolecular aldol reaction to produce bicyclic ketone homologues (Figure 1.2). This form of reaction has been used numerous times for the production of steroids and terpenoids[45] showing the importance of the reaction.

Enamine catalysis has grown since the work of Hajos and others to encompass a wide range of reactions. The most prolific enamine catalysed reaction studied has been the aldol reaction. Much work has gone into describing mechanisms of catalysis with the most accurate interpretation of intermediate structure proposed by List[46] and similarly Houk[47] using computational means. Proline derivatives are most commonly found in the literature but variations have been found with Barbas[48], Jørgenson[49] and MacMillan[50] all having had success with catalysts.

The nucleophilic addition to a carbonyl group is better known as conjugate addition, this class of reaction covers a vast section of chemical transformation with catalysed and uncatalysed mechanisms found in most chemistry textbooks. The area is dominated by metal-based Lewis acid catalysis, but an increasing number of metal-free processes are being employed. An example of this conjugate addition via organocatalyis can be found in the amine catalysed Michael addition which is the conjugative addition of carbon nucleophiles to activated double bonds (Figure 1.13).
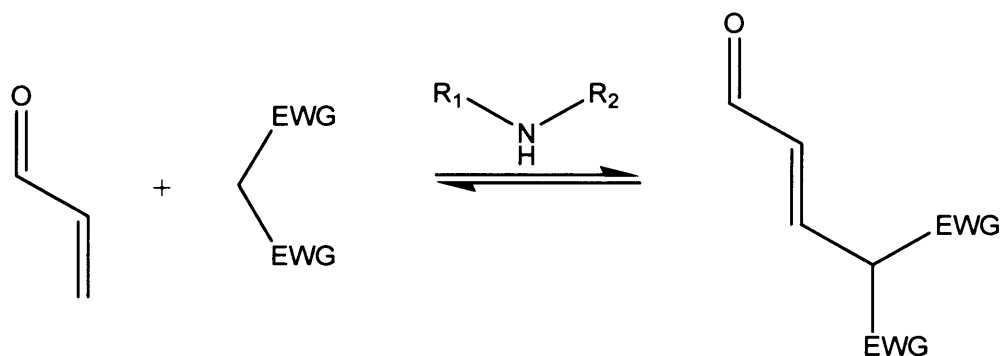
Figure 1.13 General Michael addition

Recent work exploring the reaction has been reported by List[51], Barbas[44] and Alexakis[52], each giving account of the reaction with a range of amines investigating variables such as solvent effect. Other reactions catalysed by enamines include the Robinson annulation which combines Michael and aldol reactions to synthesise six-membered rings[53] and Mannich reactions for the production of chiral nitrogen-containing compounds.[27,47]

1.6. Reasons for calculations

This investigation was embarked upon to address a number of questions unanswered in the present literature and increase understanding of a new, rapidly expanding subject area. The ultimate goal of the research was to produce a predictive scale to attribute, for example functional groups, structure and geometry to reactivity.
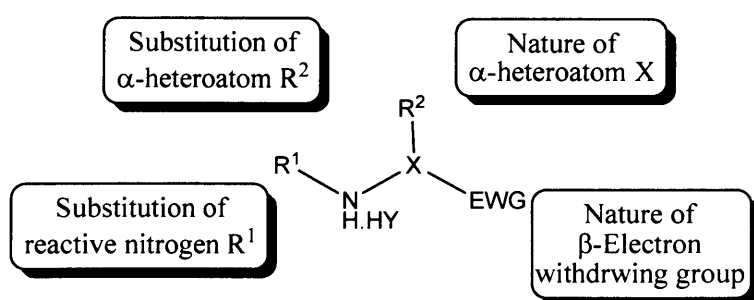
Figure 1.14 Areas of investigation.

To accomplish this a number of other important goals must be met. A library of data for structurally interesting secondary amines must be created to examine possible trends in properties that may affect reactivity. Investigation into the elements of the catalysts shown in Figure 1.14 show the direction the research could progress.

The initial formation of an iminium ion from the respective amine and α,β-unsaturated carbonyl compound has yet to be studied in depth through computational means. It was therefore thought necessary to model the system of a number of amines to determine the mechanism of reaction. By constructing a model system for the reaction, a framework would be available for further calculations to be performed, and therefore discern the effect of amine structure on this initial phase.

Reactions of iminium ions are mostly carried out in a solvent with specific properties, also containing counter-ions that are associated with the amine. The effect of solvent and counter ion must be therefore examined to determine the extent of influence upon reactions.

In essence, this research was undertaken to extend the knowledge of using iminium ions as catalysts to promote efficient, enantioselective alternatives to the metal containing catalysts dominating the field today. This invigorating field of organocatalysis represents a synthetic alternative to established organometallic transformations to both augment and complement existing methodology.

1.7. References

(1)   Maruoka, K.; Itoh, T.; Shirasaka, T.; Yamamoto, H. *Journal of the American Chemical Society* **1988**, *110*, 310-312.

(2)   Corey, E. J.; Matsumura, Y. *Tetrahedron Letters* **1991**, *32*, 6289-6292.

(3)   Ojima, I. *Catalytic asymmetric synthesis*; Wiley-VCH, 1993.

(4)   Ahrendt, K. A.; Borths, C. J.; MacMillan, D. W. C. *Journal of the American Chemical Society* **2000**, *122*, 4243-4244.

(5)   Hajos, Z. G.; Parrish, D. R. *Journal of Organic Chemistry* **1974**, *39*, 1615-1621.

(6)   Eder, U.; Sauer, G.; Weichert, R. *Angewandte Chemie-International Edition* **1971**, *10*, 496-&.

(7)   Dalko, P. I.; Moisan, L. *Angewandte Chemie-International Edition* **2001**, *40*, 3726-3748.

(8)   Dalko, P. I.; Moisan, L. *Angewandte Chemie-International Edition* **2004**, *43*, 5138-5175.

(9)   Fubini, B.; Arean, C. O. *Chemical Society Reviews* **1999**, *28*, 373-381.

(10)   Benaglia, M.; Puglisi, A.; Cozzi, F. *Chemical Reviews* **2003**, *103*, 3401-3429.

(11)   Brown, S. P.; Goodwin, N. C.; MacMillan, D. W. C. *Journal of the American Chemical Society* **2003**, *125*, 1192-1194.

(12)   Northrup, A. B.; MacMillan, D. W. C. *Journal of the American Chemical Society* **2002**, *124*, 2458-2460.

(13)   Austin, J. F.; MacMillan, D. W. C. *Journal of the American Chemical Society* **2002**, *124*, 1172-1173.

(14)   Paras, N. A.; MacMillan, D. W. C. *Journal of the American Chemical Society* **2002**, *124*, 7894-7895.

(15)   Ouellet, S. G.; Tuttle, J. B.; MacMillan, D. W. C. *Journal of the American Chemical Society* **2005**, *127*, 32-33.

(16)   Huang, Y.; Walji, A. M.; Larsen, C. H.; MacMillan, D. W. C. *Journal of the American Chemical Society* **2005**, *127*, 15051-15053.

(17)   Lelais, G.; MacMillan, D. W. C. *Aldrichimica Acta* **2006**, *39*, 79-87.

(18)   Jencks, W. P. *Catalysis in Chemistry and Enzymology*; Dover Publications, New York, 1987.

(19)   Gordillo, R.; Houk, K. N. *Journal of the American Chemical Society* **2006**, *128*, 3543-3553.

(20)   Gordillo, R.; Carter, J.; Houk, K. N. *Advanced Synthesis & Catalysis* **2004**, *346*, 1175-1185.

(21)   Yang, J. W.; Fonseca, M. T. H.; Vignola, N.; List, B. *Angewandte Chemie-International Edition* **2005**, *44*, 108-110.

(22)   Yang, J. W.; Fonseca, M. T. H.; List, B. *Angewandte Chemie-International Edition* **2004**, *43*, 6660-6662.

(23)   List, B. *Tetrahedron* **2002**, *58*, 5573-5590.

(24)   Halland, N.; Hansen, T.; Jørgensen, K. A. *Angewandte Chemie-International Edition* **2003**, *42*, 4955-4957.

(25)   Pulkkinen, J.; Aburel, P. S.; Halland, N.; Jørgensen, K. A. *Advanced Synthesis & Catalysis* **2004**, *346*, 1077-1080.

(26)   Halland, N.; Aburel, P. S.; Jørgensen, K. A. *Angewandte Chemie-International Edition* **2004**, *43*, 1272-1277.

(27)   Poulsen, T. B.; Alemparte, C.; Saaby, S.; Bella, M.; Jørgensen, K. A. *Angewandte Chemie-International Edition* **2005**, *44*, 2896-2899.

(28)   Marigo, M.; Bachmann, S.; Halland, N.; Braunton, A.; Jørgensen, K. A. *Angewandte Chemie-International Edition* **2004**, *43*, 5507-5510.

(29)   Poulsen, T. B.; Alemparte, C.; Jørgensen, K. A. *Journal of the American Chemical Society* **2005**, *127*, 11614-11615.

(30)   Marigo, M.; Wabnitz, T. C.; Fielenbach, D.; Jørgensen, K. A. *Angewandte Chemie-International Edition* **2005**, *44*, 794-797.

(31)   Prieto, A.; Halland, N.; Jørgensen, K. A. *Organic Letters* **2005**, *7*, 3897-3900.

(32)   Cavill, J. L.; Peters, J. U.; Tomkinson, N. C. O. *Chemical Communications* **2003**, 728-729.

(33)   Edwards, J. O.; Pearson, R. G. *Journal of the American Chemical Society* **1962**, *84*, 16-24.

(34)   Hoz, S. *Journal of Organic Chemistry* **1982**, *47*, 3545-3547.

(35)   Um, I.-H.; Buncel, E. *Journal of Organic Chemistry* **2000**, *65*, 577-582.

(36)   Herschlag, D.; Jencks, W. P. *Journal of the American Chemical Society* **1990**, *112*, 1951-1956.

(37)   Buncel, E.; Hoz, S. *Tetrahedron Letters* **1983**, *24*, 4777-4780.

(38)   Lemay, M.; Ogilvie, W. W. *Journal of Organic Chemistry* **2006**, *71*, 4663-4666.

(39)   Lemay, M.; Ogilvie, W. W. *Organic Letters* **2005**, *7*, 4141-4144.

(40)   Diels, O. A., K. *Justus Liebigs Annalen Der Chemie* **1928**, *460*, 98.

(41)   Corey, E. J.; Ensley, H. E. *Journal of the American Chemical Society* **1975**, *97*, 6908-6909.

(42)   Selkala, S. A.; Tois, J.; Pihko, P. M.; Koskinen, A. M. P. *Advanced Synthesis & Catalysis* **2002**, *344*, 941-945.

(43)   Machajewski, T. D. W., C.-H. *Angewandte Chemie International Edition* **2000**, 1352-1374.

(44)   Notz, W.; Tanaka, F.; Barbas, C. F. *Accounts of Chemical Research* **2004**, *37*, 580-591.

(45)   Danishefsky, S. J.; Masters, J. J.; Young, W. B.; Link, J. T.; Snyder, L. B.; Magee, T. V.; Jung, D. K.; Isaacs, R. C. A.; Bornmann, W. G.; Alaimo, C. A.; Coburn, C. A.; DiGrandi, M. J. *Journal of the American Chemical Society* **1996**, *118*, 2843-2859.

(46)   Bahmanyar, S.; Houk, K. N.; Martin, H. J.; List, B. *Journal of the American Chemical Society* **2003**, *125*, 2475-2479.

(47)   Allemann, C.; Gordillo, R.; Clemente, F. R.; Cheong, P. H. Y.; Houk, K. N. *Accounts of Chemical Research* **2004**, *37*, 558-569.

(48)   Notz, W.; Tanaka, F.; Barbas, C. F. *Accounts of Chemical Research* **2004**, *37*, 580-591.

(49)   Bogevig, A.; Juhl, K.; Kumaragurubaran, N.; Zhuang, W.; Jørgensen, K. A. *Angewandte Chemie-International Edition* **2002**, *41*, 1790-1793.

(50)   Northrup, A. B.; MacMillan, D. W. C. *Journal of the American Chemical Society* **2002**, *124*, 6798-6799.

(51)   List, B. *Chemical Communications* **2006**, 819-824.

(52)   Alexakis, A.; Andrey, O. *Organic Letters* **2002**, *4*, 3611-3614.

(53)   Bui, T.; Barbas, C. F. *Tetrahedron Letters* **2000**, *41*, 6951-6954.

(54)   Brochu, M. P.; Brown, S. P.; MacMillan, D. W. C. *Journal of the American Chemical Society* **2004**, *126*, 4108-4109.

2. Computational Methods

To be able to gain meaningful results from information gathered via computational calculations, one must be able to understand what is needed to construct that calculation and how reliable the results will be. Knowledge extending from fundamental principles to experimental techniques is required to give validity to results. With the increase of computer power and the availability of parallelised computing, numerically intense calculations can be carried out on larger and more complex systems at greater accuracy, all in less time than it would have previously taken. This allows for the study of more realistic model systems in a feasible amount of time. This chapter will cover the necessary background to be able to understand the results presented later.

2.1.   Fundamentals

Modern quantum theory is based on the premise that all information about a system is available from a single source, the wavefunction (Ψ) of the system. Manipulation of the wavefunction by an operator allows the abstraction of the data required, in the majority of calculations this will be the total energy of a system.

2.1.1.   Schrödinger equation

To obtain our desired system energy, we start from the non-relativistic time-independent Schrödinger equation:

$$\hat{H}\Psi(r,R) = E\Psi(r,R) \qquad\qquad \text{Equation 2.1}$$

Where ($\hat{H}$) is the Hamiltonian operator and (E) is the total system energy. The operator is described in terms of the position of the electrons (r) and the position of the nuclei (R). To find the solution to the equation of a system of N electrons and M nuclei the Hamiltonian operator can be expressed as:

$$\hat{H} = -\sum_{i=1}^{N}\frac{1}{2}\nabla_i^2 - \sum_{A=1}^{M}\frac{1}{2M_A}\nabla_A^2 - \sum_{i=1}^{N}\sum_{A=1}^{M}\frac{Z_A}{r_{iA}} + \sum_{i=1}^{N}\sum_{j>i}^{N}\frac{1}{r_{ij}} + \sum_{A=1}^{M}\sum_{B>A}^{M}\frac{Z_A Z_B}{R_{AB}} \qquad \text{Equation 2.2}$$

Where i and j are electrons and A and B are nuclei, Z is the charge on the nuclei and the Laplacian operator is given as:

$$\nabla^2 = \frac{\partial^2}{\partial x^2} + \frac{\partial^2}{\partial y^2} + \frac{\partial^2}{\partial z^2}$$

<div align="right">Equation 2.3</div>

The first term on the right hand side of equation 2.2 is the kinetic energy of the electrons, the second term the kinetic energy of the nuclei, the third the electron-nucleus attraction, with the fourth and fifth terms the electron-electron and nucleus-nucleus repulsion terms, respectively.

2.1.2. Born-Oppenheimer Approximation

For anything more than the simplest system, such as the hydrogen atom, the Schrödinger equation is impossible to solve exactly, mainly due to the correlated motion of particles. Fortunately the Born-Oppenheimer approximation allows us to detach the motion of the nuclei from that of the electrons. This is possible because the mass of an electron much smaller than that of a nucleus, therefore the change in electron position is effectively instantaneous. This gives a simplified Schrödinger equation where the electrons move in a fixed field of nuclei:

$$\hat{H}_{elec}\Psi_{elec} = E_{elec}\Psi_{elec}$$

<div align="right">Equation 2.4</div>

With the total wave function of:

$$\Psi_{tot} = \Psi_{elec}\Psi_{nuc}$$

<div align="right">Equation 2.5</div>

The full Hamiltonian:

$$\hat{H}_{tot} = \hat{H}_{elec} + \hat{H}_{nuc}$$

<div align="right">Equation 2.6</div>

And the electronic Hamiltonian is:

$$H_{elec} = -\sum_{i=1}^{N}\frac{1}{2}\nabla_i^2 - \sum_{i=1}^{N}\sum_{A=1}^{M}\frac{Z_A}{r_{iA}} + \sum_{i=1}^{N}\sum_{j>i}^{N}\frac{1}{r_{ij}}$$

<div align="right">Equation 2.7</div>

Once the electronic problem is solved the nuclear problem can be solved within an average electronic field by simply adding the nuclear – nuclear interaction which is constant for a given geometry. Therefore the Born-Oppenheimer approximation of the Schrödinger equation is complete.

$$E_{tot} = E_{elec} + \sum_{A=1}^{M}\sum_{B>A}^{M}\frac{Z_A Z_B}{R_{AB}}$$

<div align="right">Equation 2.8</div>

All wavefunctions from here on are electronic only, and the 'elec' subscript shall be omitted. Mathematically a wavefunction is quite simple to follow, but giving it a physical form is a harder task. Born proposed an interpretation which is related to a wavefunction's complex conjugate Ψ^*:

$$|\Psi|^2 = \Psi^*\Psi \qquad\qquad \text{Equation 2.9}$$

$|\Psi|^2 d\tau$ represents the probability of finding an electron in a certain volume of space $d\tau$ or the electron density (ρ). Integrating this probability over all space should give the number of the electrons in the system, N:

$$\rho(r) = \Psi^*(r)\Psi(r) = \left|\Psi(r)\right|^2 \qquad\qquad \text{Equation 2.10}$$

$$\int \Psi^*\Psi d\tau = N \qquad\qquad \text{Equation 2.11}$$

If an operator $\hat{A}$ acts upon the wavefunction , the property (A) of that operator can be found:

$$\int \Psi^*\hat{A}\Psi d\tau = A \qquad\qquad \text{Equation 2.12}$$

As we are investigating electrons we must not only be aware of their positions in space but also their spin orientation. An electron spin can be described by one of two functions $\alpha(\omega)$ or $\beta(\omega)$ where ω is the spin variable, which can only be $\pm1/2$, this addition to the spatial location of a electron gives a spin orbital.

A wavefunction can be constructed in the form of a Slater determinant in which the columns are the spin orbitals and the rows permute the electron coordinates. For N electrons and N spin orbitals (ϕ), it has the form:

$$\Psi_{SD} = \frac{1}{\sqrt{N!}}\begin{vmatrix} \phi_1(1) & \phi_2(1) & \cdots & \phi_N(1) \\ \phi_1(2) & \phi_2(2) & \cdots & \phi_N(1) \\ \vdots & \vdots & \ddots & \vdots \\ \phi_1(N) & \phi_2(N) & \cdots & \phi_N(N) \end{vmatrix} \qquad\qquad \text{Equation 2.13}$$

The wavefunction obeys the Pauli exclusion principle, since if two rows of the Slater determinant are equal the determinant would be zero. Also, interchanging the coordinates of two

electrons corresponds to interchanging two rows of the Slater determinant, resulting in a change of sign of the determinant.

These antisymmetric functions account for the indistinguishability of the electrons, such that two electrons may not occupy the same set of quantum numbers, thus satisfying the Pauli principle. This is achieved by ensuring that the position of any two electrons causes the sign of the wavefunction to change.

2.2.   Hartree – Fock Approach

The Hartree-Fock approximation was a major advance in the solution of the Schrödinger equation of atoms and molecules. It allowed the interaction of electrons with each other to be separated into an effect of an average electronic field (Coulomb repulsion) and an exchange term. The Fock operator is an effective one-electron operator:

$$\hat{f} = \hat{h} + v^{HF}$$ Equation 2.14

Where $\hat{h}$ is the one electron Hamiltonian of an electron moving in the field of the nuclei;

$$h = -\frac{1}{2}\nabla^2 - \sum_{A}^{M}\frac{Z_A}{r_{iA}}$$ Equation 2.15

The remaining term of the Fock operator v^{HF} represents the average potential felt by the electron :

$$v^{HF} = \sum_{b}\hat{J}_b - \hat{K}_b$$ Equation 2.16

Where $\hat{J}_b$ accounts for the Columbic repulsion between electrons and $\hat{K}_b$ describes the spin correlation or exchange of electrons.

A way of solving such equations for generic closed-shell systems was developed independently by Roothaan and Hall. By using a Linear Combination of Atomic Orbitals (LCAO) approach they created a matrix calculation which can be described as.

19

$$\phi_i = \sum_{v}^{K} c_{vi} \chi_v \qquad \text{Equation 2.17}$$

$$\mathbf{F}c = \mathbf{S}c\varepsilon \qquad \text{Equation 2.18}$$

where c is a matrix of coefficients, ε is a diagonal matrix whose elements are the orbital energies. $\mathbf{S}$ is the overlap matrix with elements S_{ij}, and $\mathbf{F}$ is the Fock matrix with elements F_{ij}.

$$S_{ij} = \int \chi_i \chi_j d\tau \qquad \text{Equation 2.19}$$

$$F_{ij} = \int \chi_i f \chi_j d\tau \qquad \text{Equation 2.20}$$

This representation allows the use of non-orthonormal basis sets, and is more commonly referred to as Restricted Hartree-Fock theory. The equations have to be solved iteratively as the Fock matrix depends on the orbital coefficients, therefore the Hartree-Fock equation is a self consistent field (SCF) method. According to the Variational theorem no energy from an SCF calculation can be below the exact energy, therefore the iterations can continue until the convergence criteria are met, *i.e.* the lowest energy is reached.

2.3. Correlation Energy

For all its simplicity, Hartree-Fock theory gives reasonable geometries and energies when compared with experiment. This is partly due to the use of an antisymmetric wavefunction which takes into account the position of parallel spin electrons and therefore the exchange energy. It does not however include the interaction of anti-parallel electrons or the correlation energy, meaning that the electrons will not avoid each other. It is possible that HF sometimes gives good results simply due to fortuitous cancellation of errors, but the neglect of electron correlation is the major drawback to HF theory and difference between the HF energy and the real energy is one definition of the correlation energy.

2.4.   Post HF methods

The inability of HF to account for the correlation energy of a system has been addressed by a number of post Hartree-Fock methods. These aim to explicitly include the correlation of electrons and are briefly covered in this section. All of these theories are more computationally demanding than HF, but one method which has been heavily used is Møller-Plesset theory.

Møller-Plesset (MP) perturbation theory is principally based upon Rayleigh-Schrödinger theory, in which the true Hamiltonian operator $\hat{H}$ is expressed as the sum of a 'zeroth-order' Hamiltonian $\hat{H}^0$ and a perturbation term, V :

$$\hat{H} = \hat{H}^0 + \lambda V$$

<div align="right">Equation 2.21</div>

where λ is a parameter that can vary from 0 and 1.

In this way the Hamiltonian, and subsequently the wave function and the energy, can be expressed as powers of λ. The zeroth-order energy represents the one-electron Fock operators for N electrons. Also, it can be shown that the sum of the zeroth and first-order energies is equal to the Hartree-Fock energy. Thus, in order to estimate the contribution of electron correlation, further terms have to be computed. MP2 corresponds to the second-order perturbation terms, MP3 to the third, etc. MP theory is not variational but is size consistent with MP2 scaling to N^5 where N is the number of basis functions.

A particular problem in post-HF methods is the evaluation of the 4-index 2-electron integrals and their transformation from atomic orbitals into the molecular orbital basis. These integrations can be a bottleneck in the calculations, a method to remove this obstacle is the use of density fitting methods. In theory this method replaces these difficult integrals with an approximation constructed of 2- and 3-index 2- electron integrals. In practice the DF-MP2 (also known as RI-MP2) calculation can increase the speed of a calculation by an order of magnitude without significant loss in accuracy.

2.5.   Density Functional Theory

Density Functional Theory (DFT) has been used extensively in recent times as a computationally inexpensive theory which reports good geometries and accounts for electron correlation. The theory is based upon the reasoning that the ground state electronic energy of a system is fully explained by its electron density ρ; the difficulty is that the functional that links these properties is unknown. The electron density has the advantage over wavefunction approaches that it is independent of the size of the system (the number of electrons). Within the electron density each nucleus is found as a local maximum therefore its position can be located. Initial attempts to resolve a system's energy from the electron density were led by Thomas and Fermi (TF) but large flaws in the work such as the inability to predict bonding hindered any practical use. The first real progress in using DFT for molecules came in 1964 by the hands of Hohenberg and Kohn in the form of two theorems. Their Existence theorem gave proof that a non-degenerate ground state electron density defines the position and charges of the nuclei (the external potential) and therefore the wave function. This was achieved by *reductio ad absurdum*, or showing the opposite of the statement is not true. The second theorem provided was that the density obeys a variational principle, so that any trial density will give an energy greater than or equal to the exact energy of the system. What is not shown by these theorems is how these densities are chosen or the exact mathematical form of the functional linking energy to density. True implementation of DFT as a viable method for computational chemistry came from Kohn and Sham in 1965.

2.5.1. Kohn-Sham Equations

The inadequacies of TF-DFT come in the description of the kinetic energy of a system $T[\rho(r)]$, therefore affecting such properties as binding energy. Kohn and Sham borrowed the ∇^2 operator from wavefunction theory to represent this energy, giving good representation of the kinetic energy but meaning that orbitals have to be employed in an iterative procedure similar to HF theory.

The problem with DFT up until this point is that we still have to solve the Kohn-Sham equations, thus there is no improvement to a molecular orbital approach as we still have to deal with electron – electron interactions. Kohn and Sham[1] ignored this interaction and therefore the

Hamiltonian could be constructed of one electron operators, with the eigenvalue being a sum of the one electron eigenvalues. This would suffer the same fate as Thomas and Fermi's theory if not for the condition that this non-interacting system has the same ground state density as the real system. From the existence theorem, the density of the fictitious and real interacting system must be identical. Knowing this we can write an expression for the energy functional:

$$E[\rho(r)] = T_{ni}[\rho(r)] + V_{ne}[\rho(r)] + V_{ee}[\rho(r)] + E_{xc}[\rho(r)] \qquad \text{Equation 2.22}$$

From the left the terms are: the kinetic energy of the non-interacting electrons, the nuclear – electron interaction, the classical electron – electron repulsion, and the exchange correlation energy. This last term contains the terms for the kinetic energy correction for the interaction of electrons and all non-classical electron interactions. This is more commonly know as the exchange-correlation energy and is the area of the equation that is unsolved and most interest is focused upon.

2.5.2. Exchange-Correlation Functionals

An exact exchange correlation functional would provide a theoretically perfect solution for all systems. Unfortunately such a function is not known and much research effort has focused on formulating functionals that perform well for various types of system. Up until this point DFT has been variational, but this very useful property is lost due to the approximate calculation of E_{xc}. Most modern functionals attempt to estimate E_{xc} by creating a hole function using empirical parameters. An advantage of DFT is that even a simple representation of E_{xc} gives reasonable results. The approximation of E_{xc} is usually performed via one of three methods; the local-density approximation (LDA), the generalised gradient approximation (GGA), or by using hybrid combinations of these methods.

2.5.3. Local Density Approximation

The simplest approach to estimation E_{xc} is to use only the electron density at a single point thus giving the integral:

$$E_{xc}[\rho(r)] = \int \rho(r) \varepsilon_{xc}(\rho(r)) dr \qquad \text{Equation 2.23}$$

where ε_{xc} is the exchange-correlation. In some functionals the exchange and correlation values are separated. LDA assumes that the spin at a specific point is zero, much the same as a restricted HF calculation. LDA has been superseded by Local Spin Density Approximation (LSDA) which allows for open shell systems to be modelled more accurately, although for a closed system LDA and LSDA are identical. The exchange energy is approximated from calculations of the uniform electron gas model with a common form for LDA:

$$E_X^{LDA} = -\frac{3}{2}\left(\frac{3}{4\pi}\right)^{1/3} \int \rho(r)^{4/3} dr \qquad \text{Equation 2.24}$$

Representation of the correlation energy is often seen as the approximation of Vosko, Wilk and Nusair[2] (VWN) which was fitted to calculated Monte Carlo based data for the uniform electron gas.

2.5.4. Gradient corrected functionals

For an increase in accuracy in an approximation, systems other that a uniform electron gas must be taken into account. This can be done by including the gradient of the electron density into the parameterisation of E_{xc}. These gradient corrected or generalised gradient approximation (GGA) approaches are still based on local properties and are considered a correction to the LDA energy. A popular example of this is by Becke[3]:

$$E_X^{B88} = E_X^{LDA} - \gamma \sum_s \int \frac{\rho_s(r)^{\frac{4}{3}} x_s^2}{1 + 6\gamma x_s \sinh^{-1} x_s} \, dr \qquad \text{Equation 2.25}$$

$$\text{with} \quad x_s = \rho_s(r)^{-\frac{4}{3}} \left| \nabla \rho_s(r) \right|$$

where γ is a parameter chosen to fit the known exchange energies of the inert gas atoms.

2.5.5. Hybrid DFT Methods

2.5.5.1. B3LYP

The use of Becke three parameter exchange functional (B3) with the LYP[4] correlation functional gives one of the most widely used DFT methods available today. Although there are numerous other functionals available, B3LYP performs well in a wide range of systems and is often the first choice of functional for calculating geometries and approximate energies.

$$E_{XC}^{B3LYP} = E_X^{LDA} + 0.20(E_X^{HF} - E_X^{LDA}) + 0.72 E_X^{B88} + E_C^{VWN} + 0.81(E_C^{LYP} - E_C^{VWN})$$

Equation 2.26

Becke determined the parameter values by fitting several molecular properties, such as atomisation energies, ionisation potentials etc. Thus, the HF and LDA exchange expressions are combined and adjusted by Becke's gradient-corrected exchange. In a similar manner, the local VWN energy correlation is used and corrected by the Lee, Yang, Parr's (LYP)[4] correlation energy which gives both local and non-local components.

2.5.5.2. BH&H

Recently the use of Becke's "half-and-half" functional has been reported to give good energies for a number of non-bonding interactions[5]. This is an ad hoc mixture of exact (HF) and local density approximation exchange, coupled with Lee, Yang, and Parr's expression for the correlation energy

$$E_{xc} = \left(\frac{1}{2} E_x^{HF} + \frac{1}{2} E_x^{LDA} \right) + E_c^{LYP} \qquad \text{Equation 2.27}$$

2.5.5.3. mPW1PW91

A third hybrid functional employed in this research was mPW1PW91[6]. Developed by Adamo and Barone, it is a modified Perdew-Wang One parameter hybrid functional, with 25:75 mixture of Hartree-Fock and PW91 exchange with PW91 correlation[7]. The functional is modified for better reproduction of long-range interactions and barriers to model reactions such as S_n2.

2.6. Basis Sets

In most modern quantum chemistry, we take as the fundamental descriptor of electronic motion the shapes and forms of atomic orbitals, obtained from the solution of the Schrödinger equation for the hydrogen atom i.e. atomic orbitals. A molecular orbital can be given the form:

$$\phi_i = \sum_{\alpha}^{N} c_{\alpha i} \chi_\alpha$$

Equation 2.28

where $c_{\alpha i}$ are molecular orbital expansion coefficients and χ_α are the basis functions. This is known as the linear combination of atomic orbitals (LCAO) approach. A basis set must include enough flexiblity to give meaningful results but still be computationally feasible. Basis sets are commonly made up from one of two types of functions centred over nuclei, both having specific advantages over the other:

Slater Type Orbitals[8] (STO) have the correct exponential dependence on the distance between the nucleus and the electron, which allows for rapid convergence with increasing numbers of functions. STO can not analytically calculate three- and four-centre two-electron integrals so are mainly used for high accuracy atomic and diatomic systems and semi-empirical methods which neglect or parameterise the above integrals.

Gaussian Type Orbitals[9] (GTO) are less accurate than STO both near the nucleus, due the lack of description of the cusp at the nucleus, and at distance, with the GTO decaying too quickly, both of these failures are due to the e^{-r^2} dependency. (Figure 2.1)
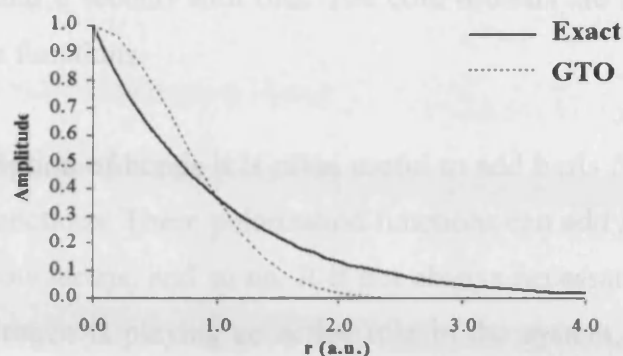
Figure 2.1 Exact and GTO behaviour as distance from the nucleus increases showing failures of GTO

In comparison, STO are more accurate when using the same number of orbitals. GTO need approximately three times the number of basis functions to be as accurate, but the integrals are far easier to calculate, and this outweighs the increase in the number of functions. One approach to improve the speed of self-consistent calculations is to form each member of a basis set from a linear combination of GTO to give an approximate STO this is known as a contraction of Gaussian functions the coefficients required are seen as part of the basis set and only the combined function enters the SCF procedure.

Describing a GTO in polar coordinates can improve performance as a d-type GTO has six components in a Cartesian system where as in a polar coordinate system there are only five. This difference in representation is more prominent in larger functions, e.g. a f-function has ten Cartesian components but only seven spherical components. This has a some saving on calculation times.

The smallest basis set that can describe all of the electrons of the molecule in their ground state configuration is known as a minimal basis set or a single-ζ basis set. This means there is only one function describing each of the occupied orbitals present. To increase the flexibility one can de-contract the basis functions, or more specifically the primitive Gaussians that make up the functions. The number of primitive Gaussians need not differ from an analogous single-ζ basis set, therefore there would be no increase in the number of integrals calculated, but the number of molecular orbital coefficients c calculated is increased. If each valence function is constructed from two basis functions, the basis set is said to be double-ζ. It is not necessary to do this for core orbitals as they have little effect on the chemistry of chemical reaction, therefore we can treat core and valence functions differently. A common split valence basis set is 6-31G, developed by Pople *et al*[10]. with two functions for valence orbitals, the first made up of three

primitive Gaussians and a second with one. The core orbitals are represented by a set of fully contracted 6 primitive functions.

To improve the description of bonds it is often useful to add basis functions that describe higher angular momentum functions. These polarisation functions can add p-functions for hydrogen and d-functions for first-row atoms, and so on. It is not always necessary to include p- functions for hydrogen, unless hydrogen is playing an active role in the system. A further modification to a standard basis set is helpful to describe negatively charged species or lone pairs. Diffuse functions[11] can encompass these expanded areas of electron density by having smaller exponents allowing for larger spatial extent of molecular orbitals, these are normally denoted as and '+'

The use of contracted Gaussians, polarisation functions and diffuse functions is commonly summarised in the basis set label. So that a 6-31+G(d,p) basis set would consist of two valance shell functions one of which is a contraction of three Gaussians, d and p polarisation functions and the diffuse basis function.

2.7. Quantum Theory of Atoms In Molecules (QTAIM)

2.7.1. Electron Density

QTAIM analysis uses the electron density (ρ) of a system to determine chemical properties of that system, the relationship between ρ and the wavefunction can be defined as:

$$\rho(r) = \int \psi^*(r)\psi(r)dr \qquad \text{Equation 2.29}$$

The spatial distribution of electron density forms a map of a system in which key points can be identified. An example of different representations of ρ can be seen for ethene (Figure 2.2). Slicing through the σ symmetry axis containing all of the atoms Figure 2.2a shows the electron density as the third dimension with the greatest density at the nuclei (cut off used for large densities) from these maxima the ρ falls away rapidly in all direction. ρ is more commonly shown as a 2D contour plot (Figure 2.2b) for the σ-plane of ethene. It can also be shown as an isosurface of constant ρ, which is useful to reveal molecular shape and surfaces. The topic of atoms in molecules is covered extensively in publications by Bader[12] and Popelier[13].
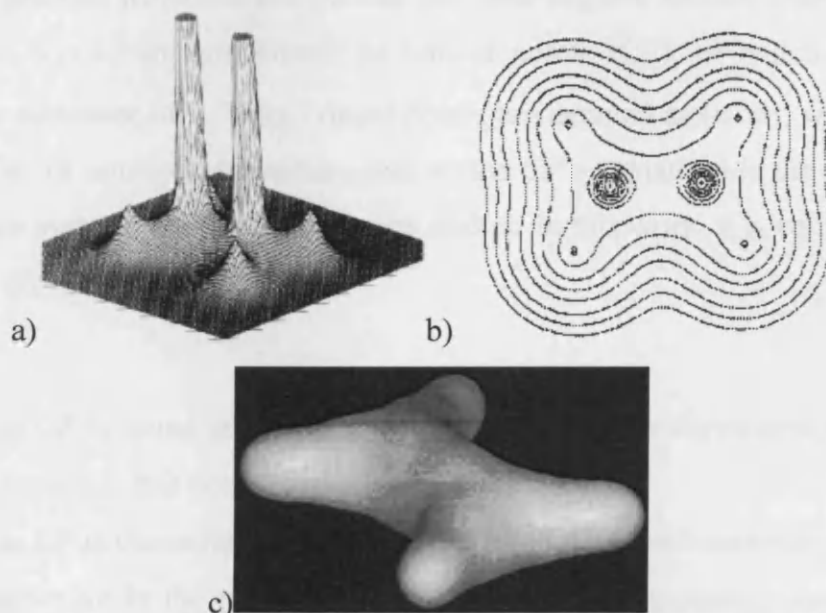
Figure 2.2 Representations of ethene electron density[13] **a)** ρ *as the third dimension* **b)** *2-D contour map* **c)** *isodensity surface*

AIM utilises the gradient of ρ to describe structure of, and bonding within, a molecule. The direction of greatest increase of ρ, known as the gradient vector, $\nabla\rho$, also has the property of

being everywhere perpendicular to a contour of ρ. There can only be one gradient path at one point (assuming $\nabla\rho \neq 0$) the final important property of a gradient path is that it must have a beginning (usually infinity) and an end (usually a nucleus). A number of gradient paths can be seen in Figure 2.3
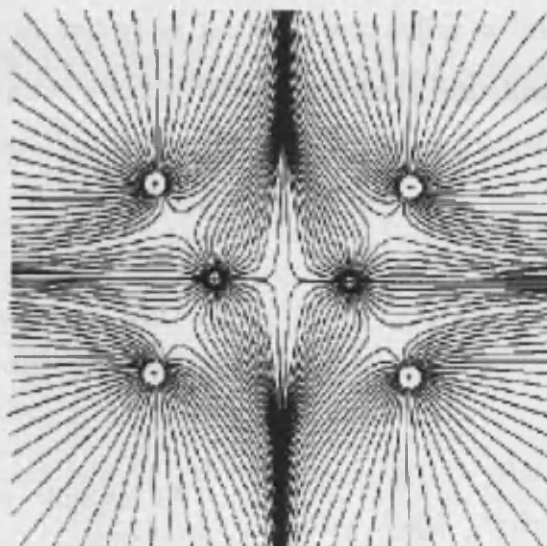
Figure 2.3 Diagram of gradient paths associated with ethene[13]

The majority of gradient paths end at a nucleus but some begin at another type of attractor. These points that have $\nabla\rho = 0$ and are known as critical points (CP), of which there are 4 types classified by the curvature of ρ. Thus, critical points are denoted as (n, m), where n (the rank of CP) is the number of non-zero curvatures, and m (the CP's signature) is the sum of their signs. Usually for stable systems and for all the cases studied in this work, n is equal to three, leading to four different types of critical point:

i.   (3,-3): this CP is found at nuclear positions, where all the curvatures are negative. ρ is a local maximum at this point;

ii. (3,-1): this CP is characteristic of a chemical bond. Here two curvatures are negative, and ρ is a maximum in the plane defined by the two corresponding axes; one curvature is positive, and ρ is a local minimum along the axis;

iii. (3,+1): this point is found within rings. Two curvatures are positive, here ρ is a minimum in the plane defined by the corresponding axes; one curvature is negative, and ρ is a maximum along this axis;

iv.   (3,+3): this point is typical of cage structures. All curvatures are positive and ρ is a local minimum at this point.

Of most interest to the chemistry is the (3,-1) critical point denoting an interaction between two atoms, this is the Bond Critical Point (BCP). There is a unique pair of trajectories originating from the BCP ($\nabla\rho = 0$) and ending at nuclei. They define a line along which the electron density is a maximum in space. At equilibrium geometry, this line is known as a Bond Path. Thus, the lines of maximum electron density linking bonded nuclei form the molecular graph which is the more common representation of an AIM analysis.

2.7.2.   Laplacian of the electron density

The laplacian of electron density ($\nabla^2\rho = \dfrac{\partial^2\rho}{\partial x\partial x} + \dfrac{\partial^2\rho}{\partial y\partial y} + \dfrac{\partial^2\rho}{\partial z\partial z}$) is a measure of local concentrations of the charge density. In particular, regions where $\nabla^2\rho > 0$ present a local depletion of electron density, whereas regions where $\nabla^2\rho < 0$ are locally concentrated charge. In practice, in order to analyse properties of molecules, the quantity $L = -\nabla^2\rho$ is typically employed.

It is therefore possible via simple analysis to characterise covalent, ionic, H-bonds and van der Waals interactions from ρ and L. Of particular interest for this project are the two latter bonding motifs as the electron density is much lower than covalent bond, ca. 10 times and 100 times smaller for H-bond and van der Waals interactions, respectively. Although lower in energy, these interactions can play an important role in determining molecular geometry and reaction mechanisms.

Within the scope of this work, all AIM properties were calculated with the AIM2000[14] program. Generally the analysis is a visual inspection of the resultant molecular graph of a system with most interest in Bond Critical Points, (3,-1). This method was used to evaluate inter- and intra-molecular interactions in the system especially hydrogen bonds and nonbonding interactions, and explain underlying reasons for observed energetic and geometric properties.

2.8.   Practical considerations

2.8.1. Optimisation of stationary points

The potential energy of a system is a function of nuclear positions, so a collection of energies can give a potential energy surface (PES). For N nuclei in a system there are 3N coordinates that define the geometry, three translational and three rotational for movement with respect to three axes. The remaining 3N-6 coordinates describe the internal molecular movement of the nuclei. A PES can be explained with the use of first and second derivatives of energy with respect to some or all of these coordinates.

There are a few areas of interest on a PES, such as local energy minima and the local energy maxima linking them (Figure 2.4). These stationary points are defined by the first derivative of the energy (the gradient) being zero. Using the first derivative of the energy the direction towards a stationary point can be found with the magnitude of the gradient giving the steepness of the slope. This can be translated into the force on the nucleus that can be used for minimisation techniques. The value of the second derivative of the energy is used to further differentiate between a minimum (positive value) and a maximum (negative value), describing the change in direction of the function.
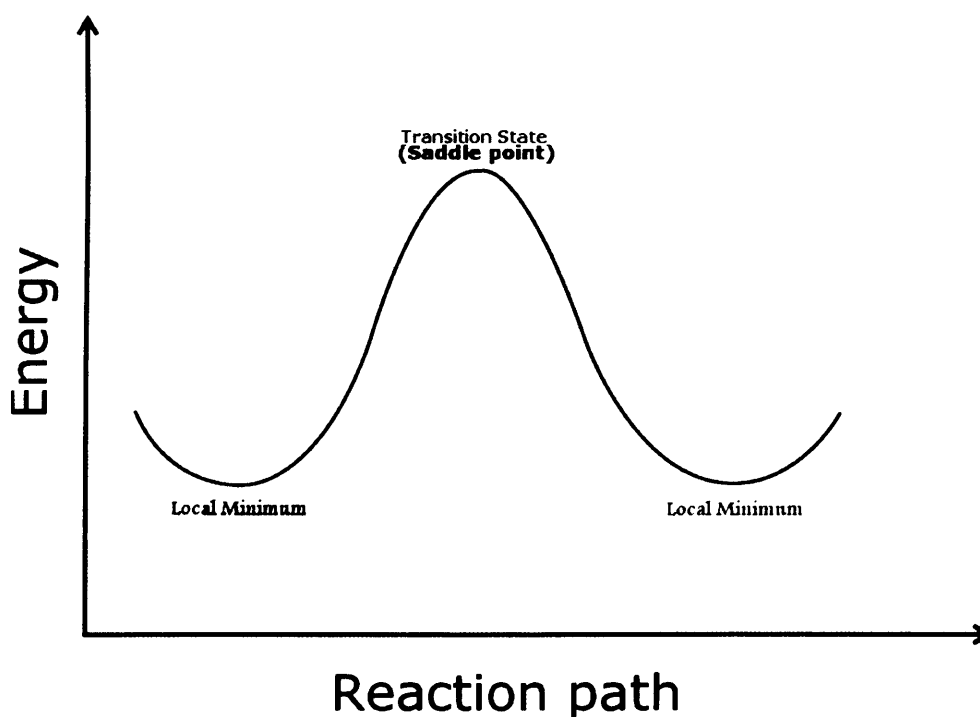

Figure 2.4 2-D representation of energy minimum and saddle point in a PES

A matrix of the second derivatives is constructed and termed the Hessian matrix. The optimisation of structures are carried out using the pseudo-Newton-Raphson Schlegel–Berny algorithm[15]. The advantage of such an algorithm is the speed of convergence, this is due to approximating the Hessian and updating this estimate at each step of the optimisation. The consequence of this is that more optimisation steps are calculated but each cycle is markedly faster than producing an exact Hessian at each step.

To compute a reaction barrier, the geometry of the transition state that lies along the reaction coordinate between the reactant and the product must be optimised. For an algorithm to find a transition state, the geometry must be optimised in such a way so as to increase the magnitude of the negative eigenvalues of the Hessian and to minimise the positive values. This process can be achieved in a number of ways. When using a pseudo-Newton-Raphson method, the starting geometry for the transition state must be close enough to the actual transition state. This is because there is an assumption that the potential energy surface is of a quadratic shape, making the calculation very sensitive to the initial guess compared to other methods. Gaussian 03[16] implements an eigenvalue check that ensures a single negative eigenvalue is found to be optimised. For complex transition states the initial guess at the geometry affords more than one negative value, here disabling this check allows for the most negative value to be optimised while the remaining negative values are minimised. One way to obtain a starting geometry is to perform a constrained optimisation along the coordinate that the reaction is most likely to follow. This is easiest to see in bond dissociation reactions.

A more elegant method of calculating a transition state is to use a Synchronous Transit-Guided Quasi-Newton (STQN) Method. Within the Gaussian 03 package this is an implementation of the work by H. B. Schlegel and coworkers[15]. This approach requires geometries for at least the reactant and product (QST2) but ideally a guess for the transition state (QST3). Using a quadratic synchronous transit approach to get closer to the quadratic region of the transition state and then a quasi-Newton or eigenvector-following algorithm to complete the optimization means that a much quicker and robust convergence to the stationary point is possible.

For a system geometry to be classified as a transition state it must have, with respect to the movement of the nuclear coordinates, both a zero derivative of energy (as in a standard geometry optimisation), and a single negative second derivative of the energy. A vibrational frequency calculation can be used to verify a true transition state by visual inspection of the eigenvector

corresponding to the negative eigenvalue or perturbing a transition state geometry to confirm the link between product and reactants.

2.8.2. Solvent effects

Accurate simulation of many molecules and reactions requires that the effect of solvent must be taken into account, and solvent properties such as the dielectric constant are of particular importance. Solvents can play a passive role in a reaction by simply stabilising transition states and charge species, or take a more active role in the reaction by mediating proton transfers or other reactions. For the latter it is important to explicitly model these molecules, for more general effects created by the solvent a continuum model can be used to give an average affect of the solvent without greatly increasing the calculation time.

The ideal method to describe solvent effects would be to include a large volume of explicit solvent described by an electron correlated *ab initio* method, but this is far too expensive to calculate. A compromise can be made by including less solvent in the explicitly modelled system to include short range solvent – solute interactions. To examine general bulk properties of a sovent, surrounding this region with a continuum model of the solvent allows for a reasonable approximation of a solvent description. Descriptors of this type are normally some sort of self-consistent reaction field (SCRF) model reliant on the dielectric ε of the solvent in question, where the solvent perturbs the molecule which in turn polarises the solvent. Energy is needed to create a suitable cavity in the solvent but there is a stablistation due to the dispersion forces between the solute and solvent.

$$\Delta G_{solvation} = \Delta G_{cavity} + \Delta G_{dispersion} + \Delta G_{electrostatic} \qquad \text{Equation 2.30}$$

Two types of solvation model were employed in this research, firstly an Onsager[17] spherical cavity which takes into account the dipole of the solute. Here the size of the cavity is critical in the energy stabilisation of the solvent. The second type of model is a Polarizable Continuum Model[18] (PCM) that uses a van der Waals surface to describe the cavity produced for the solute, this can be solved self consistently and contains parameterisation to increase the accuracy of the model. This is generally more accurate, but can be slower, at the time of calculation there was a lack of analytical second derivatives for use with PCM within the Gaussian03 package.

2.9. References

(1)   Kohn, W.; Sham, L. J. *Physical Review* **1965**, *140*, A1133 LP - A1138.
(2)   Vosko, S. H.; Wilk, L.; Nusair, M. *Canadian Journal of Physics* **1980**, *58*, 1200-1211.
(3)   Becke, A. D. *Physical Review A* **1988**, *38*, 3098-3100.
(4)   Lee, C. T.; Yang, W. T.; Parr, R. G. *Physical Review B* **1988**, *37*, 785-789.
(5)   Waller, M. P.; Robertazzi, A.; Platts, J. A.; Hibbs, D. E.; Williams, P. A. *Journal of Computational Chemistry* **2006**, *27*, 491-504.
(6)   Adamo, C.; Barone, V. *Journal of Chemical Physics* **1998**, *108*, 664-675.
(7)   Perdew, J. P.; Burke, K.; Ernzerhof, M. *Physical Review Letters* **1996**, *77*, 3865-3868.
(8)   Slater, J. C. *Physical Review* **1930**, *36*, 57 LP - 64.
(9)   **Boys, S. F.** *Royal Society of London Proceedings Series A* **1950**, *200*, 542-554.
(10)   Ditchfie.R; Hehre, W. J.; Pople, J. A. *Journal of Chemical Physics* **1971**, *54*, 724-&.
(11)   Frisch, M. J.; Pople, J. A.; Binkley, J. S. *Journal of Chemical Physics* **1984**, *80*, 3265-3269.
(12)   Bader, R. F. W. *Atoms in Molecules - A Quantum Theory*; Oxford University Press: Oxford, 1990.
(13)   Popelier, P. L. A. *Atoms in Molecules: An Introduction*; Prentice Hall: Harlow, 2000.
(14)   Biegler-König, F.; Schönbohm, J.; Bayles, D. *J. Comp. Chem.* **2001**, *22*, 545-559.
(15)   Schlegel, H. B. *Journal of Computational Chemistry* **1982**, *3*, 214-218.
(16)   M. J. Frisch, G. W. T., H. B. Schlegel, G. E. Scuseria, M. A. Robb, J. R. Cheeseman, J. A. Montgomery, Jr., T. Vreven, K. N. Kudin, J. C. Burant, J. M. Millam, S. S. Iyengar, J. Tomasi, V. Barone, B. Mennucci, M. Cossi, G. Scalmani, N. Rega, G. A. Petersson, H. Nakatsuji, M. Hada, M. Ehara, K. Toyota, R. Fukuda, J. Hasegawa, M. Ishida, T. Nakajima, Y. Honda, O. Kitao, H. Nakai, M. Klene, X. Li, J. E. Knox, H. P. Hratchian, J. B. Cross, V. Bakken, C. Adamo, J. Jaramillo, R. Gomperts, R. E. Stratmann, O. Yazyev, A. J. Austin, R. Cammi, C. Pomelli, J. W. Ochterski, P. Y. Ayala, K. Morokuma, G. A. Voth, P. Salvador, J. J. Dannenberg, V. G. Zakrzewski, S. Dapprich, A. D. Daniels, M. C. Strain, O. Farkas, D. K. Malick, A. D. Rabuck, K. Raghavachari, J. B. Foresman, J. V. Ortiz, Q. Cui, A. G. Baboul, S. Clifford, J. Cioslowski, B. B. Stefanov, G. Liu, A. Liashenko, P. Piskorz, I. Komaromi, R. L. Martin, D. J. Fox, T. Keith, M. A. Al-Laham, C. Y. Peng, A. Nanayakkara, M. Challacombe, P. M. W. Gill, B. Johnson, W. Chen, M. W. Wong, C. Gonzalez, and J. A. Pople.
(17)   Onsager, L. *Journal of the American Chemical Society* **1936**, *158*, 1486.
(18)   Tomasi, J.; Mennucci, B.; Cances, E. *Journal of Molecular Structure: THEOCHEM* **1999**, *464*, 211-226.

3 Iminium ion formation

To investigate a reaction profile and be able to understand the processes associated, it was necessary to start from a position which gives a solid base for progress. All of the reaction types that we endeavoured to examine began with the formation of an iminium ion from a carbonyl compound and secondary amine. The ability of functional groups to increase reactivity and stereoselectivity of a reaction comes at a cost to the theoretical chemist. Increasing the molecular weight and number of heteroatoms can drastically increase the amount of time needed to model the reaction correctly. Due to the nature of these reactions, we cannot rely on symmetry constraints to control the increase in degrees of freedom as more complex systems are created. Therefore, chemical knowledge must be used to simplify the problems at hand.

3.1   Model reaction

We started our theoretical investigation with a model of the reaction conditions in the acid-catalysed formation of iminium ions. The solvent used in experimental work was a 19:1 mixture of methanol and water. These conditions were shown to be vital in many of the catalytic processes studied synthetically.[1] An ensemble was constructed with a hydrochloride salt of dimethylamine, acrolein as the electrophile, and a single explicit water molecule. Due to the charged nature of the system, it was deemed necessary to include some approximation to the bulk solvent of the reaction. The Onsager continuum solvent model[2] was employed to give a crude estimate of the macroscopic properties of the solvent. The presence of a counter ion has also been shown to be necessary for reaction as there was no reactivity unless the catalyst was in a salt form.

The system can be arranged in many ways, but only a small number of distinct geometries would afford a suitable energy minimum for the reaction to proceed. The chloride co-catalyst and explicit water molecule proved to be the most mobile aspects of the ensemble, throughout the initial calculations all low energy geometries had the reacting species (amine plus acrolein) in approximately the same orientation. Optimisation of this reaction mixture from varying starting points revealed stable conformations within 5kJ mol^{-1} of each other, and with negligible barriers of interconversion (Figure 3.1).
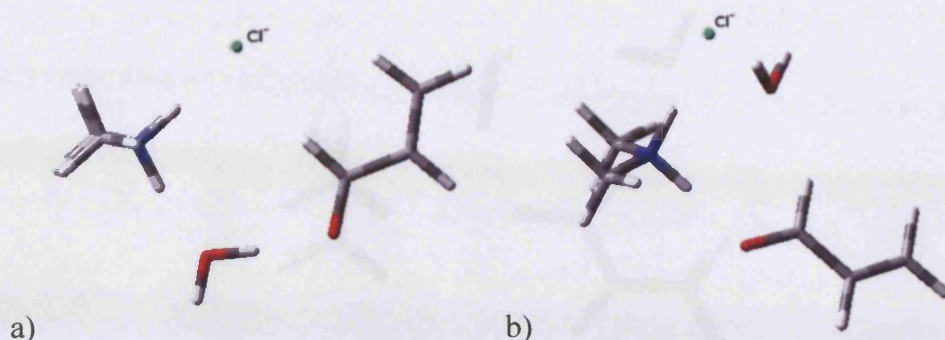
Figure 3.1 Two optimised reactant geometries differing in energy by 2.9kJ mol^{-1}

The most stable minimum found gave a geometry (Figure 3.1a) where the positioning of the chloride ion meant that further reaction gave substantially higher barriers than found for the next lowest energy geometry (Figure 3.1b); the difference in energy between these two minima being 2.9kJ mol^{-1}. On energy minimisation, the reactants form a hydrogen-bonded complex. Non-bonding interactions play an important role in the stabilisation and orientation of reactants at stationary points: the chloride ion positions over one hydrogen of the protonated amine, the carbonyl oxygen of acrolein aligns with the remaining *N—H*, and the main body of acrolein stretches away from the amine with the α-hydrogen coordinating with the water molecule (Figure 3.1b). Starting from the reactant ensemble shown in Figure 3.1b, a pathway containing seven stationary points was determined. Local minima corresponding to the iminium ion product, and an intermediate structure containing a *C—N* single bond (which we term 'protonated aminol'), as well as the reactant geometry shown above, were located and confirmed *via* harmonic frequency calculation. Using the QST procedure, a transition state (TS1, shown in Figure 3.2) linking the reactant and protonated aminol intermediate was located, with a single imaginary frequency of 139.9i cm^{-1}. TS1 was 110kJ mol^{-1} higher in energy than the reactant complex, a sizeable barrier due to the transfer of a proton from the amine to chloride, accompanied by a small re-orientation of acrolein and water. The chloride was covalently bound to the hydrogen with an *H—Cl* distance of 1.32Å (*cf.* 1.29Å for free *HCl* at the same level).

The process of the chloride removing one of the protons forces the amine to 'rock back' to accommodate this change. Hydrogen bonding between the transferring proton and the carbonyl oxygen (*H...O* = 1.96Å) and between the proton and the free nitrogen of the amine (*H...N* = 1.66Å) can be observed.
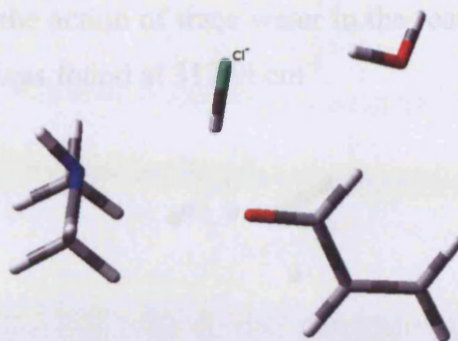
Figure 3.2 Geometry of TS1

Perturbing TS1 in the forward direction led not to the expected protonated aminol structure, but instead to an unexpected local minimum, as shown in Figure 3.3. This structure has an energy 32.6 kJ mol^{-1} below TS1, has no imaginary vibrational frequencies, and differs from that of TS1 solely by rotation of the various moieties, with both acrolein and HCl rotated towards their subsequent orientations. As the amine was symmetric, the two possible directions in which the acrolein may rotate are degenerate, though this will become an important point for asymmetric amines. This intermediate shows a reordering of weak interactions from TS1, including N—$H...Cl$ (2.70Å). At this stage the water molecule performs a role by bridging the hydrogen chloride (Cl—$H...O$ = 1.59Å) and the carbonyl (O—$H...O$ = 1.70Å).

Figure 3.3 Intermediate geometry

The metastable intermediate structure was separated from the protonated aminol species by TS2 (Figure 3.4). The barrier from intermediate to TS2 was 10kJ mol^{-1}, *i.e.* essentially negligible when compared to the barrier associated with TS1. The structure of this transition state was of interest, the water molecule mediates proton transfer from HCl to the carbonyl oxygen, acting as a "proton shuttle". Thus, it appears that only this step requires the presence of an explicit water

molecule, and hence explains the action of trace water in the reaction mixture noted previously.[3] A single imaginary frequency was found at 312.9i cm^{-1}.

Figure 3.4 TS2 geometry

The protonated aminol structure was *ca.* 10 kJ mol^{-1} higher in energy than the reactant complex: the *N—C* bond has formed in this species and a proton transferred from amine to carbonyl (Figure 3.5). Here again, the chloride ion was closely associated with the protonated amine centre, with the water hydrogen bonded to both chloride and hydroxyl group. The *N—C* bond length was 1.56Å, *i.e.* somewhat longer than a typical *N—C* single bond (1.46Å in methylamine, calculated at the same theoretical level). The reactive carbon centre has an approximate sp[3] geometry (*NCO* = 109.0°, *NCC* = 111.4°). Perturbation along the reaction coordinate forward from TS2 results in the protonated aminol geometry shown in Figure 6, but two other conformations can be located. Of these three conformations, the two with H-N-C-O torsion angles of +71.4° and –64.9° are of essentially equal energy, while that with -171.6° was considerably higher in energy. Barriers of 40 kJ mol^{-1} and 54 kJ mol^{-1} separate these minima, such that effective free rotation around the C—N bond was anticipated within the energy profile of the reaction.
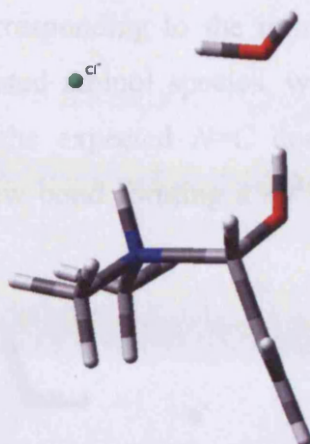
Figure 3.5 Protonated aminol geometry

The final transition state located, TS3 (Figure 3.6), accompanies elimination of water from the protonated aminol intermediate. This was again a proton transfer from amine to oxygen ($Cl...H$ = 1.53Å, $O...H$ = 1.25Å), mediated by the presence of chloride. TS3 was *ca.* 90kJ mol⁻¹ above the protonated aminol species.

Thus, the barrier associated with initial formation of the $N—C$ bond was higher in energy than subsequent elimination of water to the final product. The $N—C$ distance reduces to 1.39Å and the carbon chain of the acrolein begins to flatten. A single imaginary frequency 405.6icm⁻¹ was found.
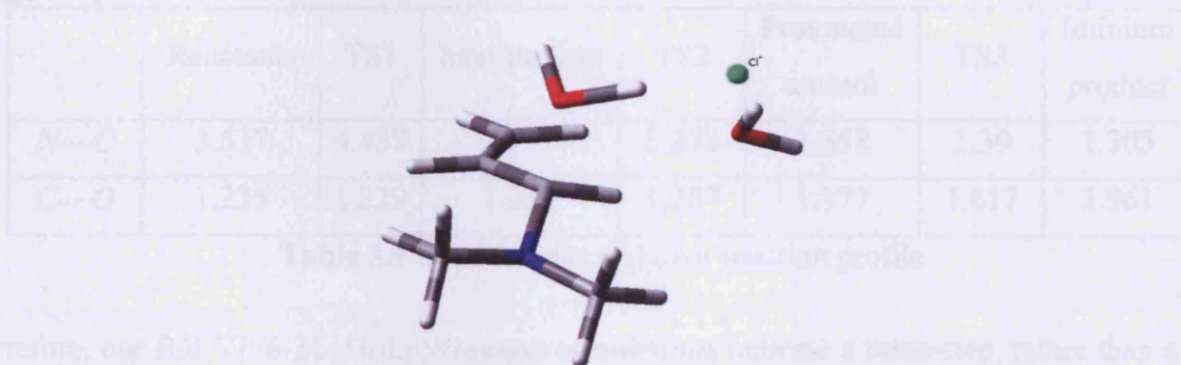
Figure 3.6 TS3 geometry

It could be envisaged that the proton transfer required to move from the protonated aminol to the Iminium ion species could take place in a series of steps similar to the transition between reactant species and protonated aminol. However, from the calculations undertaken within this research, no such points were found but this area of the reaction coordinate could produce further stationary points albeit energetically unimportant similar to TS2.

A final low energy minimum, corresponding to the iminium ion product after elimination of water from the protonated protonated aminol species, was located *ca.* 40 kJ mol^{-1} above the reactants. This product contains the expected $N=C$ double bond, as evident by the planar disposition of groups about the new bond forming a sp^2 hybridised carbon centre, and a $N=C$ length of 1.31Å (Figure 3.7).
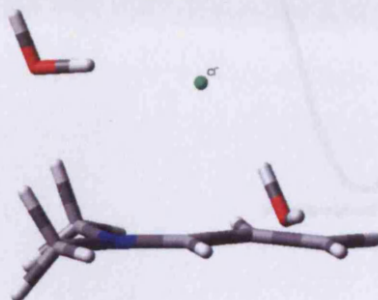

Figure 3.7 Iminium ion product

The chloride ion was now located above the $N=C$ carbon, solvated by two explicit water molecules. Table 3.1 contains inter-atomic distances of $N—C$ and $C—O$ in the model reaction profile.As expected the general trend was toward formation of an $N—C$ double bond and dissociation of $C—O$ to give the iminium ion product.

	Reactants	TS1	Intermediate	TS2	Protonated aminol	TS3	Iminium product
$N—C$	3.637	4.437	2.771	2.272	1.558	1.39	1.305
$C—O$	1.233	1.229	1.232	1.257	1.377	1.617	3.961

Table 3.1 Bond lengths (Å) over reaction profile

Therefore, our B3LYP/6-31+G(d,p)/Onsager calculations indicate a three-step, rather than a two-step mechanism for formation of an iminium ion from dimethylamine hydrochloride and acrolein, albeit with one energetically unimportant step, as shown in Figure 3.8. With this model there was considerable scope for electronic and/or steric effects, through modification of the amine, to alter the kinetics of iminium ion formation.
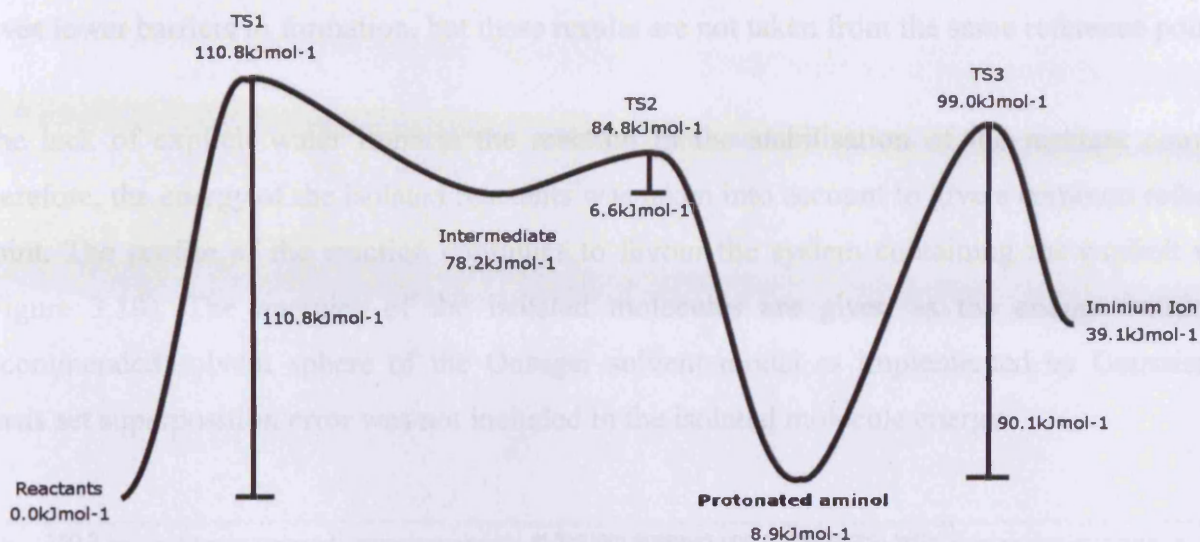
TS1
110.8kJmol-1

TS3
99.0kJmol-1

TS2
84.8kJmol-1

6.6kJmol-1

Intermediate
78.2kJmol-1

Iminium Ion
39.1kJmol-1

110.8kJmol-1

90.1kJmol-1

Reactants
0.0kJmol-1

Protonated aminol
8.9kJmol-1

Figure 3.8 Reaction profile of reaction between dimethylamine hydrochloride and acrolein

3.1.1 Presence of water

In order to determine whether a single explicit water molecule was sufficient to model the behaviour of wet methanol, the effect of additional water molecules on the system was evaluated by adding a further three molecules to the system. In all cases, optimisation led to the chloride occupying a comparable position as the initial system described, *i.e.* forming a close contact with the protonated amine (Cl...H distances vary between 2.17Å and 1.90Å), with minor changes in other geometrical details (Figure 3.9).
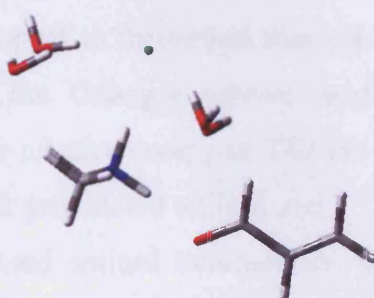
Figure 3.9 Geometry of reactants plus four water molecules

Another possibility for a model system was to exclude the explicit water in favour of a simpler system. Although such a system has less complexity, the same number of minima were found as with the hydrated system. Here TS2 was still associated with protonation of the carbonyl but directly via the counter ion. Calculations on this system were carried out giving very similar

42

barriers to the later stages of the pathway. From initial results it seems that the anhydrous system gives lower barriers to formation, but these results are not taken from the same reference point

The lack of explicit water impacts the reaction in the stabilisation of the reactant complex, therefore, the energy of the isolated reactants was taken into account to give a common reference point. The profile of the reaction continues to favour the system containing the explicit water (Figure 3.10). The energies of the isolated molecules are given as the energy within the recommended solvent sphere of the Onsager solvent model as implemented by Gaussian03[4], Basis set superposition error was not included in the isolated molecule energy.
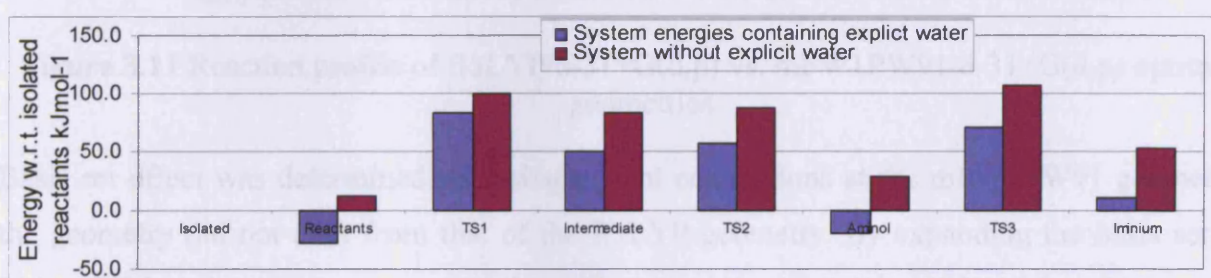

Figure 3.10 Re-referenced data of the reaction profile with and without water.

It was therefore decided to continue with the explicit water as this contained the species present in the experimental reaction mixture and gives a lower energy pathway.

3.1.2 Effect of theory level

Before expanding our investigation into a wider range of secondary amines, we further checked the stability of our results with respect to theoretical method. Optimisation at the mPW1PW91 functional (Figure 3.11) within the Onsager solvent model, has a small effect on TS1, intermediate and iminium ion. The relative energy of TS2 drops to give an even smaller barrier, where the energy of the protonated protonated aminol and TS3 was considerably reduced to the extent that the protonated protonated aminol intermediate was now lower in energy than the reactants. The difference in geometry between B3LYP and mPW1PW91 was negligible.
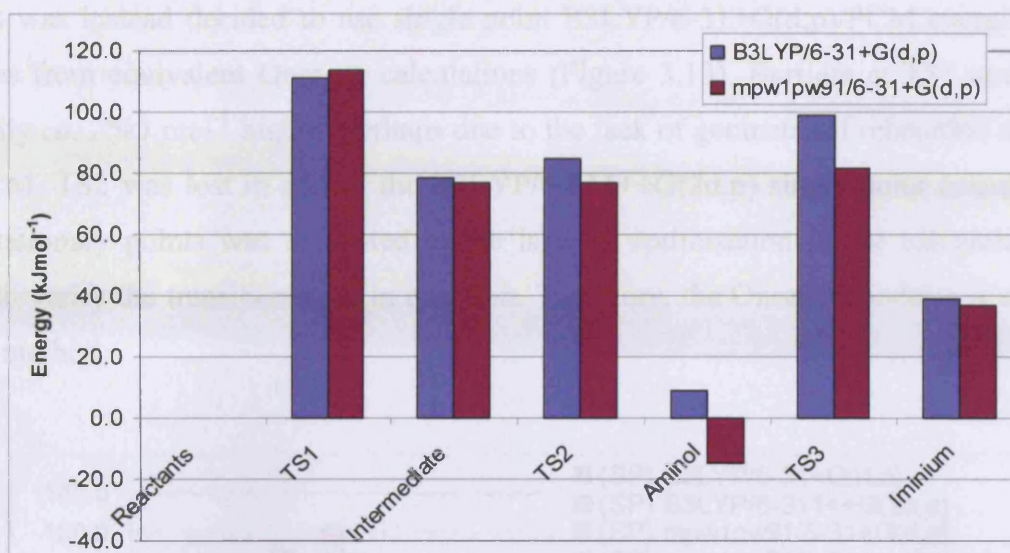
Figure 3.11 Reaction profile of B3LYP/6-31+G(d,p) vs. mPW1PW91/6-31+G(d,p) optimised geometries

Basis set effect was determined with single point calculations at the mPW1PW91 geometry, as the geometry did not alter from that of the B3LYP geometry. By expanding the basis set to 6-311++G(2d,p) the relative energy of the stationary points was reduced in all but the protonated protonated aminol species (Figure 3.12). The largest change in energy being *ca.* 7kJ mol^{-1} in TS1, with rather smaller changes elsewhere. The protonated protonated aminol energy increases by *ca.* 2kJ mol^{-1}, which was maybe due to a better description of the sp^3 nitrogen centre.
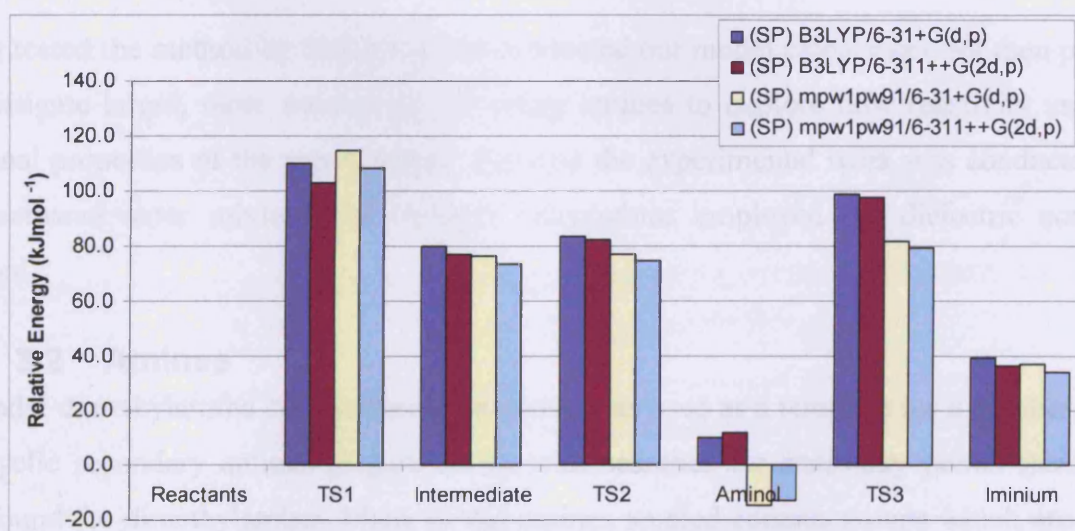

Figure 3.12 Effect of basis set size on reaction profile including Onsager solvent model

We also examined the possible use of the polarisable continuum model (PCM) for solvation. We were unable to recalculate all stationary points shown in Figure 3.8 using this method. There were numerous SCF convergence errors that plagued most optimisations procedure on the model

system. It was instead decided to use single point B3LYP/6-31+G(d,p)/PCM energies found at geometries from equivalent Onsager calculations (Figure 3.13). Barriers at TS1 and TS3 were consistently *ca.* 25kJ mol^{-1} higher, perhaps due to the lack of geometrical relaxation at this level. Using PCM, TS2 was lost in all but the B3LYP/6-311++G(2d,p) single point calculation. This loss of stationary points was attributed to the lack of optimisation in the calculation and the inability to verify the transition state in question. Therefore, the Onsager model was chosen over the PCM method.
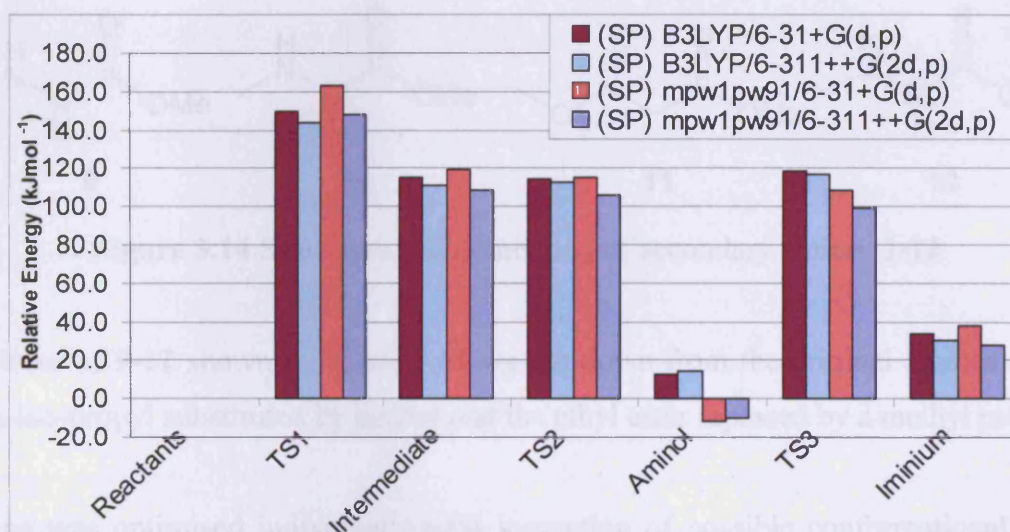

Figure 3.13 Single point calculations at differing theory levels in PCM solvent

Having tested the method by which we had conducted our model calculation, we then proceeded to investigate larger, more interesting secondary amines to explore how reactivity varies with functional properties of the parent amine. Because the experimental work was conducted with a 95:5 methanol:water mixture our Onsager calculations employed the dielectric constant of methanol.

3.2 Amines

The model dimethylamine system discussed above was used as a template for a number of cyclic and acyclic secondary amines (Figure 3.14), with searches for stationary points starting from those found for dimethylamine. Many of the amines studied contain groups which are bulky in nature. A series of calculations were carried out to determine if the bulk associated with these groups was integral to the conformation of the amine and reaction profile itself. These groups increased the calculation time considerably, as they were found not to effect the reaction profile. It was therefore decided to simplify the groups to methyl substituents.
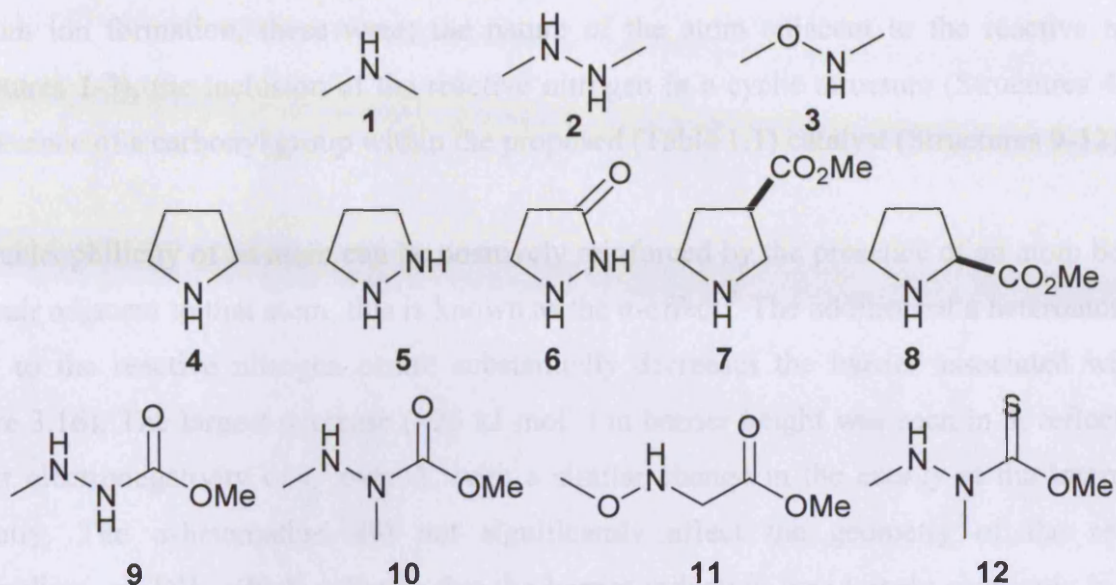
Figure 3.14 Structures and numbering of secondary amines **1-12**

The structures of **9-12** shown in Figure 3.14 are cut down from the original amines synthesised with the α-iso-propyl substituted by methyl and the ethyl ester replaced by a methyl ester.

Each amine was optimised individually with inspection of possible conformational flexibility. This was particularly important within the acyclic carbonyl containing series **9-12**. An example of this can be seen for the full structure of amine **9** (Figure 3.15) where change in position of the hydrogen of the reactive nitrogen can afford two distinct geometries; one featuring the oxygen and reactive nitrogen adjacent, with the other orientation with the carbonyl on the opposite side.
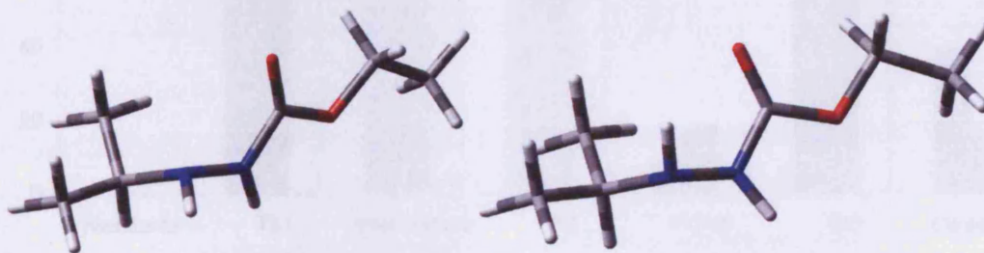

Figure 3.15 possible orientations of amine 9

By overlaying a previously optimised amine over the dimethylamine of the model system an approximation for each stationary point was created. The majority of stationary points were found by standard optimisation techniques, but some more troublesome transition states were found with the QST3 method.

Three main areas of interest were isolated with regards to the effect of functional groups in iminium ion formation, these were; the nature of the atom adjacent to the reactive nitrogen (Structures **1-3**), the inclusion of the reactive nitrogen in a cyclic structure (Structures **4-8**) and the presence of a carbonyl group within the proposed (Table 1.1) catalyst (Structures **9-12**).

The nucleophilicity of an atom can be positively reinforced by the presence of an atom bearing a lone-pair adjacent to that atom, this is known as the α-effect.[5] The addition of a heteroatom (N or O) α- to the reactive nitrogen centre substantially decreases the barrier associated with TS1 (Figure 3.16). The largest decrease (>25 kJ mol^{-1}) in barrier height was seen in **3**, reflecting the greater electronegativity of O over N, with a similar change in the energy at the intermediate geometry. The α-heteroatom did not significantly affect the geometry of the reactants, intermediate, or TS1, which suggests that the barrier reduction was largely electronic in nature. TS3 also lowers notably: in this case, energy differences appear to be due to the extra flexibility of the amine, as rotation around the N—X ($X = N$ or O) bond allows further interactions with water and chloride. The presence of αN—H in **2** allows the formation of hydrogen bonding to O and Cl^-, which could also explain the relative stability of the iminium ion product of **2**.
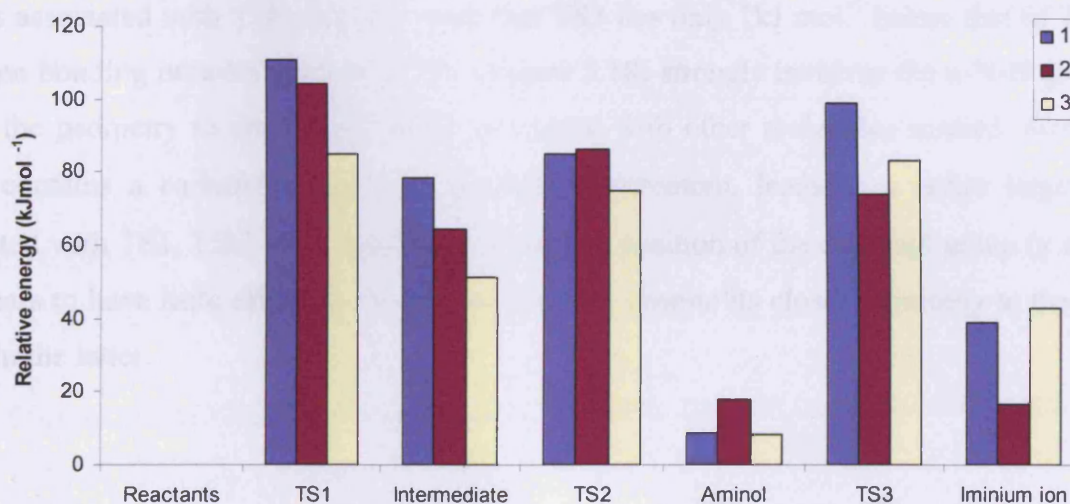
Figure 3.16 Reaction profile for acyclic secondary amines **1 – 3**

The incorporation of the reactive secondary amine into a five-membered ring in pyrrolidine (**4**) increases TS1 to give the largest barrier found (118kJ mol^{-1}). This amine also yields higher energy of both remaining transition states, relative to **1** (Figure 3.17). Substitution with α-nitrogen (**5**) gives a relative energy of TS1 below that of **1**, reinforcing the barrier-lowering effect of an α-heteroatom. Formation of hydrogen bonding between the α-N—H and acrolein

was apparent in TS1, which may contribute to lowering the barrier by 19kJ mol^{-1} *cf.* **4**. A decrease in relative energy *cf.* **4** was observed in the remaining two transition states and intermediate geometry, with corresponding increases in the relative energy of both protonated protonated aminol and iminium ion minimum.
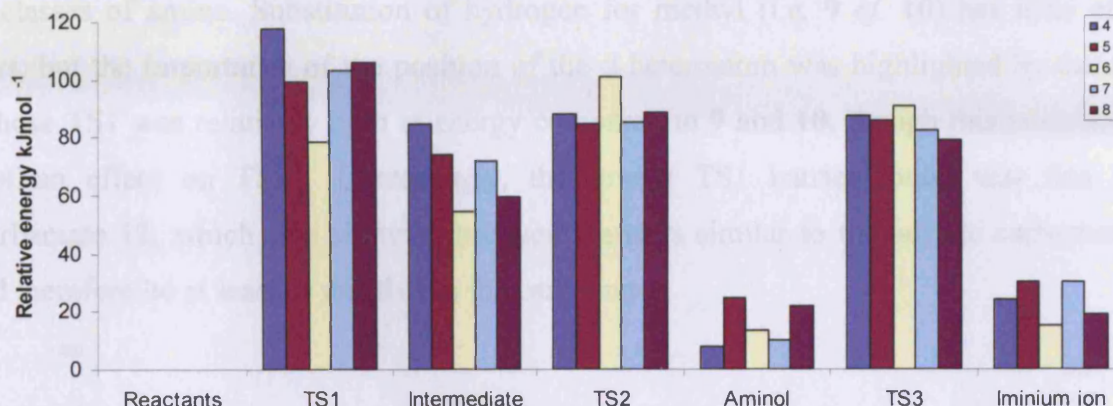
Figure 3.17 Reaction profiles for cyclic secondary amines **4 – 8**

The effect of an endocyclic carbonyl group in the β-position of the five-membered ring can be seen in the data for the lactam **6**. This gives the lowest barrier to TS1 of all the data reported here, suggesting that this should form a useful catalyst. However, **6** also has the largest relative barriers associated with TS2 and TS3, such that TS3 lies only 1kJ mol^{-1} below that of TS1. The hydrogen bonding network present in TS1 (Figure 3.18) strongly involves the α-N-H group, and causes the geometry to alter significantly compared with other molecules studied. Molecule **7**, which contains a carbonyl group but not the α-heteroatom, leads to a rather larger barrier associated with TS1, 15kJ mol^{-1} larger than in **6**. The position of the carbonyl group (γ in **7**, β in **8**) appears to have little effect on the reaction profile, despite its closer proximity to the reactive centre in the latter.

Figure 3.18 Geometry of TS1 of **6**

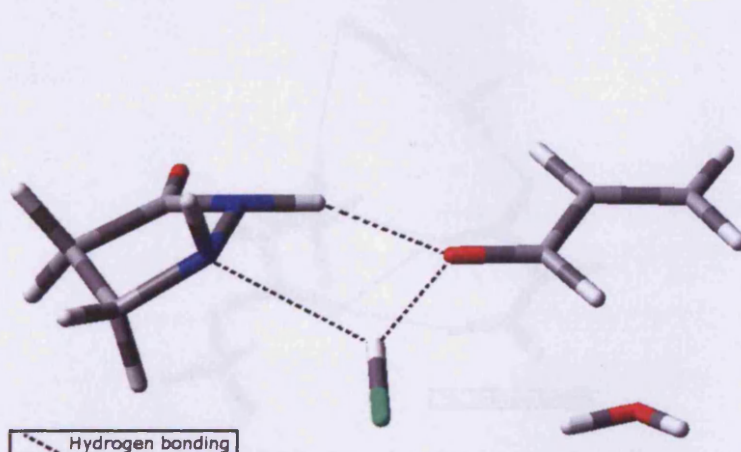The low TS1 barrier for the acyclic carbamates **9** and **10** (Figure 3.19) supports the result for **6** showing that this functionality has a large effect on the reaction profile. In these acyclic cases, however, the relative energies of TS2 and TS3 are also significantly lower than those found for other classes of amine. Substitution of hydrogen for methyl (*i.e.* **9** *cf.* **10**) has little effect on barriers, but the importance of the position of the α-heteroatom was highlighted by the data for **11**, whose TS1 was relatively high in energy compared to **9** and **10**, though this positioning has less of an effect on TS3. Interestingly, the lowest TS1 barrier found was that for the thiocarbamate **12**, which also shows subsequent barriers similar to the acyclic carbamates, and should therefore be at least as reactive as the carbamate.
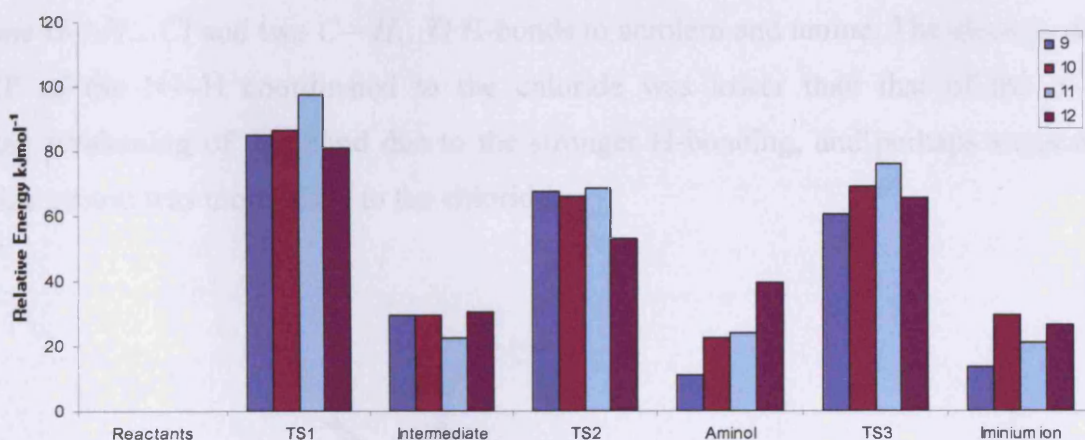
Figure 3.19 Reaction profiles for carbamate derivatives **9–12**

All carbamates considered stabilise the intermediate considerably, and increase the barrier at TS2 to the range between 20–40 kJ mol^{-1}. These carbamates (or thiocarbamates) form extensive hydrogen bonding networks through the carbonyl group (see Figure 3.20), unlike **7** and **8** which are limited by the ring structure.
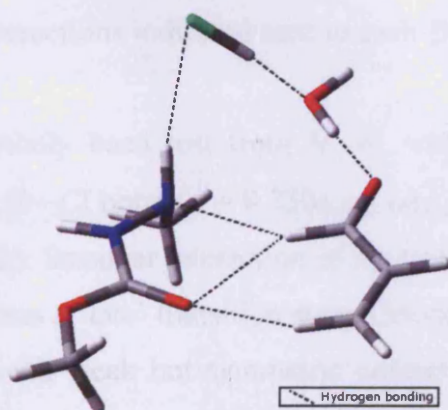
Figure 3.20 Intermediate geometry of **10** showing hydrogen bonding network, including C—H...O interactions between β-carbonyl and acrolein.

3.2.1   Quantum Theory of Atoms in Molecules Analysis

To explore more extensively the role of hydrogen bonding and other intermolecular interactions, and to follow the reaction profile where bonds are formed and broken, we carried out AIM analysis of all stationary points, initially with the model dimethylamine system. Visual inspection can identify the interactions within a certain structure, while the value of the electron density at the BCPs located allows interaction strengths to be quantified. The intermolecular interactions within the reactant ensemble are shown in Figure 3.21. By some distance, the strongest interactions are those involving the protonated amine $N—H$, which forms H-bonds to the carbonyl and chloride. Remaining weaker interactions involve the water molecule, which forms one $O—H...Cl$ and two $C—H...O$ H-bonds to acrolein and amine. The electron density at the BCP of the N—H coordinated to the chloride was lower than that of the $N—H...O$, indicating weakening of this bond due to the stronger H-bonding, and perhaps suggesting that this amine proton was more labile to the chloride.
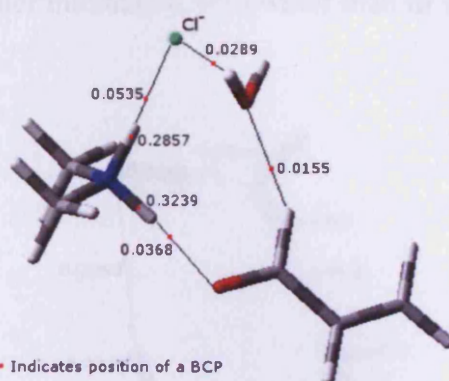
Figure 3.21 Molecular graph of reactant of **1**, with ρ_{BCP} (a.u.) of significant intermolecular interactions indicated next to each BCP.

At TS1, the proton has essentially been lost from $N—H$, with only a very weak interaction remaining: instead, a covalent $H—Cl$ bond ($\rho = 0.230$a.u.) was present, along with a $Cl—H...O$ H-bond to acrolein (Figure 3.22). Stronger interaction of the transferred proton with the carbonyl oxygen than the nitrogen suggests a 'late' transition state. Orientation of the reactants appears to be moderated by H-bonding, with weak but symmetric contacts between carbonyl and methyl protons. The water molecule plays a passive role interacting with the chloride and α-proton of the acrolein similar to that of the reactants.

• Indicates position of a BCP

Figure 3.22 Molecular graph of TS1 of **1,** with ρ_{BCP} (a.u.) of significant intermolecular interactions indicated next to each BCP.

The intermediate geometry was the first in which an interaction between nitrogen and carbon was observed in the dimethylamine system (Figure 3.23). To form this bond, acrolein must rotate relative to dimethylamine, and hence a number of interactions have been lost: the weak $C—H...O$ interactions are replaced by stronger bonds involving the water molecule. Also, the covalent $H—Cl$ bond has greater interaction with water than in TS1.

• Indicates position of a BCP

Figure 3.23 Molecular graph of intermediate of **1,** with ρ_{BCP} (a.u.) of significant intermolecular interactions indicated next to each BCP.

TS2 was associated with a proton shuttle mechanism through H_2O, and hence there was no change in number and type of BCPs present in the intermediate (Figure 3.24). However, AIM analysis shows the progress of proton transfer, with almost equal ρ at the $Cl—H$ and $H—O$

BCPs, such that the water might be better described as a hydronium ion here, along with weakened C—O and enhanced O…H interactions at the carbonyl. The incipient N—C bond was stronger here than in the intermediate, as was the N-H…Cl H-bond, since Cl was more like a chloride ion.
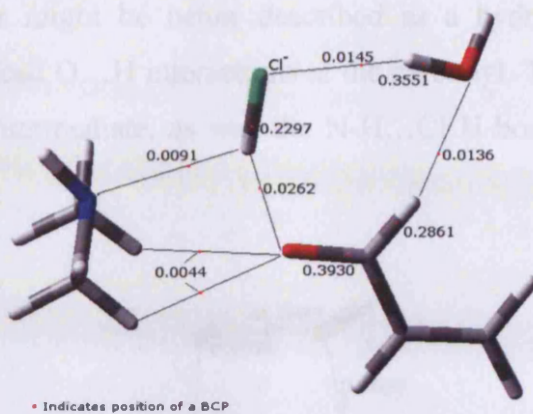

Figure 3.24 Molecular graph of TS2 of **1**, with ρ_{BCP} (a.u.) of significant intermolecular interactions indicated next to each BCP.

The protonated protonated aminol stationary point affords the first 'true' N-C bond (ρ=0.221a.u. *cf.* 0.250a.u. in the N-C bond of dimethylamine), with ρ at the BCP almost five times that found at TS2, along with a protonated *O—H* at the former carbonyl and a weaker, longer *C—O* bond (Figure 3.25). The chloride ion forms a strong H-bond to the remaining amine proton, with similar electron density to that seen in the reactant. A strong *O—H…O* interaction was also seen between water and the now protonated carbonyl.

0.3272
Cl⁻ 0.0322
0.0483
0.0532
0.2929
0.2877
0.2205

• Indicates position of a BCP

Figure 3.25 Molecular graph of protonated protonated aminol of **1,** with ρ_{BCP} (a.u.) of significant intermolecular interactions indicated next to each BCP.

Formation of the final iminium ion product involves dehydration *via* transfer of the amine proton to the 'carbonyl' oxygen, which was accompanied by contraction of the *N—C* bond (Figure 3.26). As in TS1, the chloride ion plays a key role in facilitating proton transfer, with almost equal sharing of electron density between *H—Cl* and *O—H* interactions at this TS. The strength of the *N—C* bond was increased when compared to the protonated protonated aminol species, while the breaking *C—O* bond was considerably weaker. The water molecule interacts weakly with hydrogens from the acrolein and more strongly with the chloride.

Cl⁻
0.1327
0.0201
0.1555
0.0075
0.1616
0.0124
0.3158

• Indicates position of a BCP

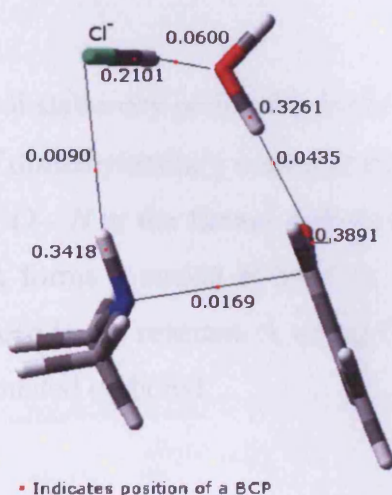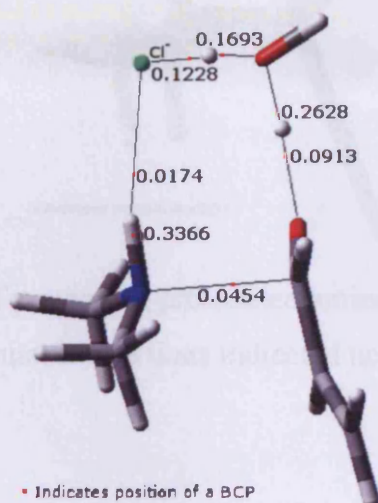**Figure 3.26** Molecular graph of TS3 of **1,** with ρ_{BCP} (a.u.) of significant intermolecular interactions indicated next to each BCP.

The final product of the profile was the iminium ion with $2H_2O + Cl^-$, which, as expected, has the largest ρ for the N—C bond observed thus far (Figure 3.27). The positioning of the two water molecules allows each to have three H-bonding interactions of comparable strength. One water molecule interacts with the chloride and protons of the methyl groups, while the second accepts density from the protons of the alkene as well as donating to the chloride. The chloride centres above the carbon of the newly formed N=C bond, interacting directly with this atom. The essentially planar iminium ion also gives rise to weak $H...H$ interaction between methyl and acrolein protons, a pattern similar to that recently studied by Matta et al.[6]
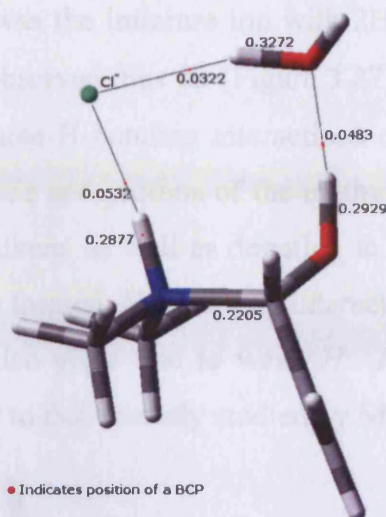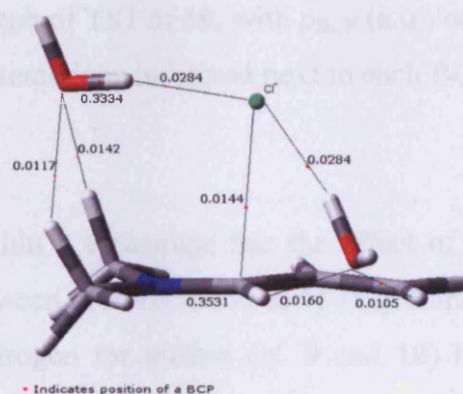

Figure 3.27 Molecular graph of iminium ion of **1**, with ρ_{BCP} (a.u.) of significant intermolecular interactions indicated next to each BCP.

AIM analysis can also be used to shed light on possible reasons for the changes in relative energies with amine structure. For instance, the low TS1 found for acyclic (thio)carbamates indicates that this functional group has direct bearing on the reaction profile: the relative energies of intermediate, TS2 and TS3 geometries are significantly lower than that of other classes of amine studied. These molecules form extensive hydrogen bonded networks, whose formation/disruption can play a role in the energetics of the reaction (Figure 3.28). Such interactions cannot occur in cyclic molecules such as **7** and **8** due to the structural constraints of the ring.
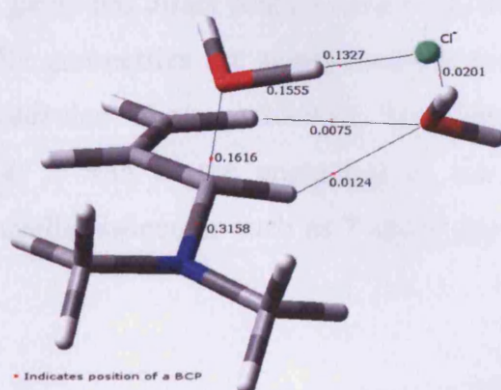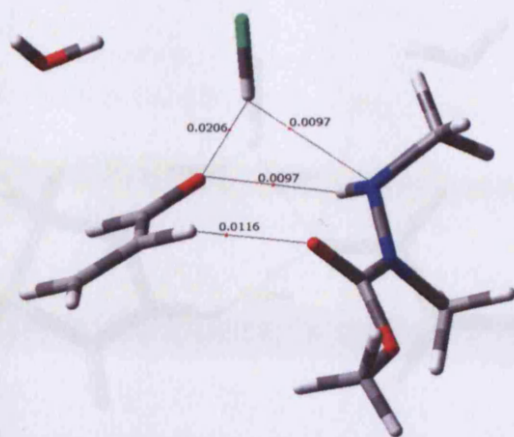
Figure 3.28 Molecular graph of TS1 of **10**, with ρ_{BCP} (a.u.) of significant intermolecular interactions indicated next to each BCP.

The presence of the *C=O* within a carbamate has the effect of controlling the position of the acrolein, with interactions between protons in the early stages once the *N—C* bond has begun to form. The substitution of hydrogen for methyl (*cf.* **9** and **10**) has little effect on the reaction profile or the topology of the electron density. The importance of the position of the α-heteroatom was highlighted using **11**, in which TS1 has a relatively high barrier compared to the rest of the amines examined. However, once again, the position of the reactants and the molecular graph was barely changed from that shown in Figure 3.28.

The lowest TS1 of all molecules was found for compound **6**: the molecular graph (Figure 3.29) of this shows the proton of the α-nitrogen forming an interaction (0.021a.u.) with the acrolein oxygen. The formation of this interaction was at the expense of losing a slightly stronger (0.028a.u.) interaction between α-nitrogen and water in the reactant complex. Thus, there appears to be a subtle interplay of formation and loss of hydrogen bonding contacts over the reaction profile, which along with the electronic variation at the reactive amine determines the overall barriers. We will compare barriers to possible reactivity descriptors in a later section (See 3.6)
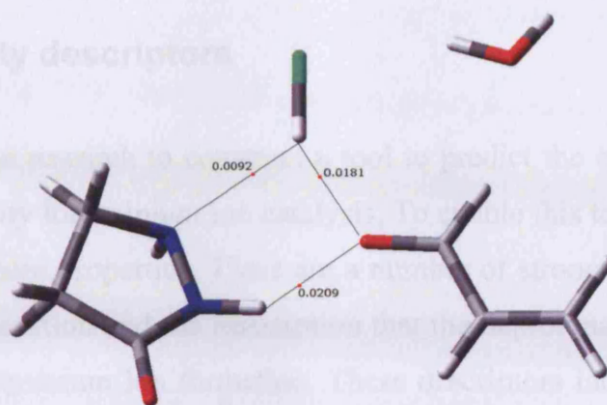
Figure 3.29 Molecular graph of TS1 of **6**, with ρ_{BCP} (a.u.) of significant intermolecular interactions indicated next to each BCP.

Of note was that the scaffold of **6** has shown to give promising results in work carried out by Ogilvie.[7,8] Here the rate determining step was shown to be the cyclisation of the iminium with a diene *i.e.* formation of the reactive iminium ion was very fast. This will be looked at in greater detail in chapter four.

3.3 Reactivity descriptors

It was original goal of the research to construct a tool to predict the effect of functional groups on reactivity and specificity for iminium ion catalysis. To enable this to occur, a candidate has to be described by one or more properties. There are a number of strong candidates for descriptors due to the nature of the reaction and the assumption that the deprotonation of the amine was the rate determining step in iminium ion formation. These descriptors include proton affinity, pKa and electrostatic potential. Less common descriptors such as global hardness and softness along with population analysis are also investigated.

3.3.1 Electrostatic Potentials

The fundamental law of electrostatic is Coulomb's Law (Equation 3.1). The force exerted by a stationary charge on another is given by:

$$F = \frac{q_1 q_2}{r_{12}^{\,2}}$$

Equation 3.1

The electrostatic force, F, exerted is proportional to the product of the charges of the two particles, q_1 and q_2, and inversely proportional to the square of the distance between the particles, r_{12}.

The electrostatic potential (Equation 3.2) of a system is an important value for discussing the interaction between molecules. It is calculated from a cube file by summing the interaction energy of a unit probe charge with the charge at each grid point, *i.e.* :

$$V = \sum \frac{q_i}{r_i}$$

Equation 3.2

Where q_i and r_i are the charge and distance separation of the ith grid point.

The electrostatic potential of a point can be seen as the likelihood of attracting a positive centre toward it. If the value is positive it would indicate a repulsive force toward the cation. If negative, positive centres would be attracted. It is this later effect that we are interested in as a method to quantify the nucleophlicity of an atom.

The electrostatic potential is both a molecular property, in that it depends on the charges in the molecule, and a spatial property, as the position of the charges affects the potential. Because of

the inverse relationship between distance and force a centre closer to the point of interest will have more effect than any other centre present.

The electrostatic potential can be mapped onto an iso-surface of the electron density. Using a program created within the research group the local minima and maxima of the surface electrostatic potential can be isolated. This was achieved by searching an electron density cube file of the molecule in question and isolating all of the desired points (in this case of density $0.001e.au^{-3}$). These points of the grid are transposed onto the electrostatic potential cube file (both of the cube files must be of the same orientation and size).

Using these points, the minimum corresponding to the reactive nitrogen can be found and a value given for that molecule. Difficulty arises when there are a number of minima in close proximity to each other, as the desired minimum may not be found. The program allows for configuration of the scan in the step size, reducing the magnitude of the search vector creates a finer 'net' in which the points can be caught.

To examine the effect of a heteroatom within the framework of a five membered ring we used the above mentioned technique to plot the electrostatic potential of the reactive nitrogen.
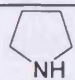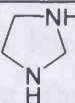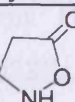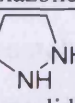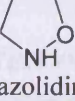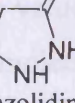
Molecule	Electrostatic potential at Nitrogen (a.u.)
Pyrrolidine	-0.0586
1,3-Pyrazolidine	-0.0568
Isoxazolidine	-0.0548
Pyrazolidine	-0.0543
Isoxazolidinone	-0.0404
Pyrazolidinone	-0.0389

Table 3.2 Electrostatic potential minimum at reactive nitrogen of five membered cyclic secondary amines

58
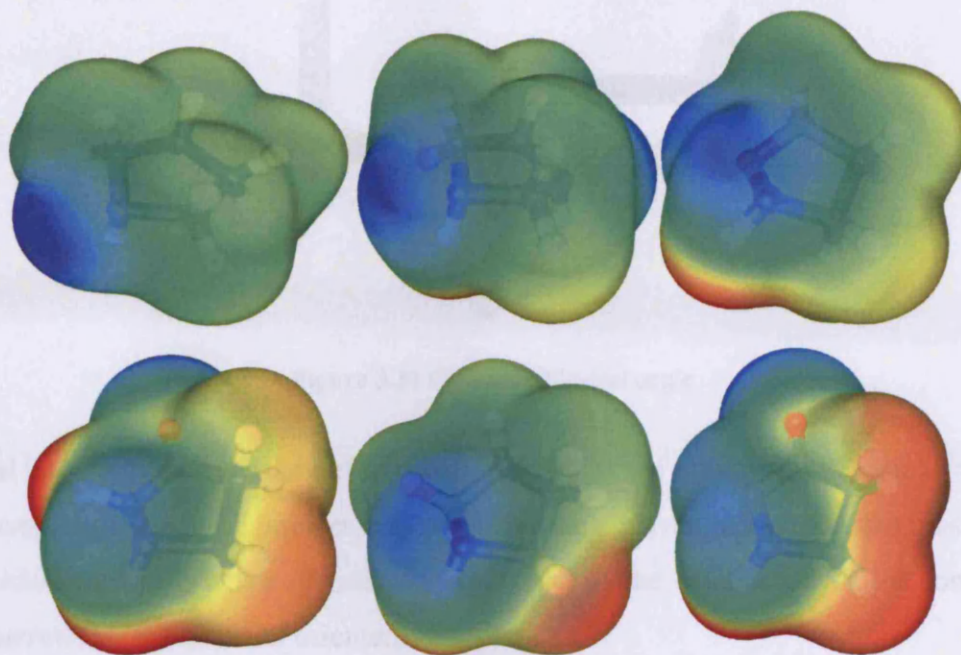
Figure 3.30 Electrostatic potential surfaces at the 0.001a.u. iso-density surface, the most negative points are shown blue and most positive red. Molecules read from top left to bottom right are: Pyrrolidine, 1,3-Pyrazolidine, Isoxazolidine, Pyrazolidine, Isoxazolidinone, Pyrazolidinone

The simplest of the cyclic amines shown in Table 3.2 pyrrolidine, gives the largest value of potential (-0.0586a.u.). The larger the value the less facile the loss of a proton should be at that point. The use of the pyrrolidine can be seen in the work of groups using proline (see chapter 1). The trend in organocatalyst by MacMillan and Jørgenson is to use 1,3-pyrazolidine moieties, which can be seen to give smaller electrostatic potentials (-0.0568a.u.) than pyrrolidine. By moving the second nitrogen to the α-position (pyrazolidine) a less negative value (-0.0543a.u.) was found, oxygen has less of an effect at the α position as shown with isoxazolidine (-0.0548a.u.). The greatest effect on the electrostatic potential was the presence of an endocyclic carbonyl at the β-position. The two smallest values are given for isoxazolidinone (-0.0404a.u.) and pyrazolidinone (-0.0389a.u.). If the electrostatic potential at the nitrogen was of consequence to the formation of the iminium ion then this frame work of an α-heteroatom and a β-endocyclic carbonyl within a five memebered ring could be of use.

Orientation and its effect on electrostatic potential

To successfully compare values of a series, the minimum amount of geometric change has to be made. Within the set of molecules used, particular attention to the dihedral angle of C-X-N-H was needed (Figure 3.31).
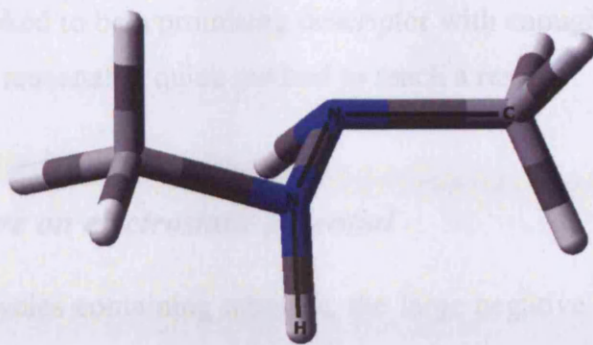
Figure 3.31 C-X-N-H dihedral angle

The dihedral angle of the hydrogen effects the position of the nitrogen lone pair in the molecule. There are two orientations of interest that presented themselves in our calculations. The two C-X-N-H dihedral angles that are of interest are related to the orientation of the lone pair of the nitrogen generating *cis* and *trans* orientations.
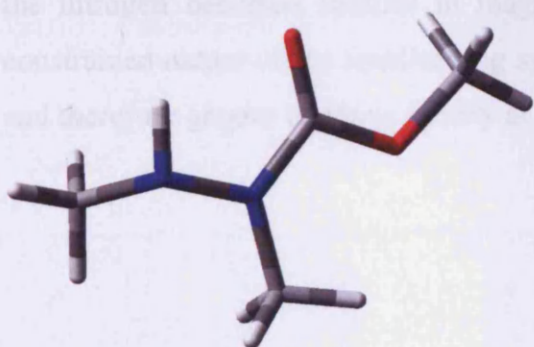
Figure 3.32 *Cis*-orientation
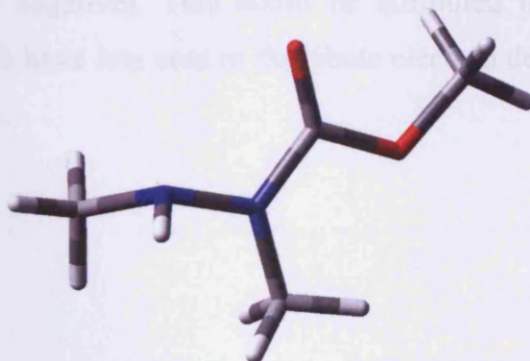
Figure 3.33 *Trans*-orientation

Figure 3.32 shows a *cis*-orientation where the electron density of the lone pair was directed away from the carbonyl. Figure 3.33 illustrates the *trans*-orientation with both electronegative regions in close proximity. This increases the energy of the system by approximately 10kJ mol⁻1. The electrostatic potential for these conformers seen in Figure 3.34 where the large dark blue area indicates a region of negative potential energy.
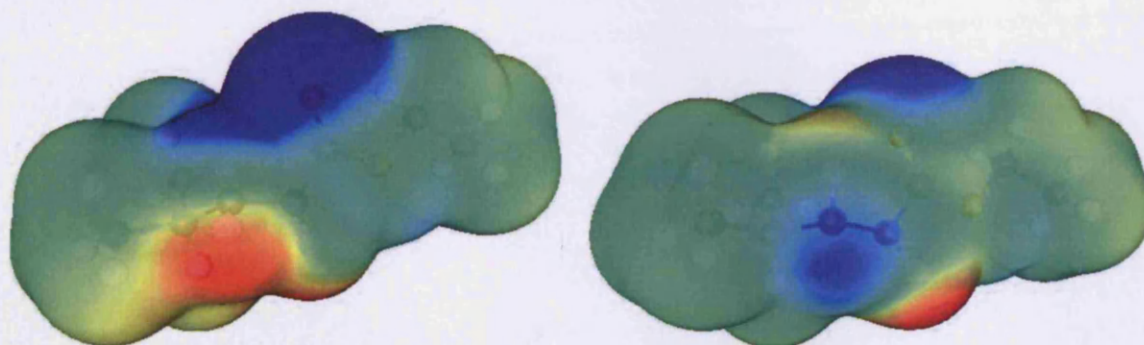
Figure 3.34 Electrostatic potential at the 0.001a.u. iso-density surface of two isomers

Electrostatic potential looked to be a promising descriptor with enough sensitivity to differentiate between molecules and a reasonably quick method to reach a result.

Effect of cyclic structure on electrostatic potential

When looking at heterocycles containing nitrogen, the large negative electrostatic potential over the nitrogen was due to its lone pair. It was this "reactive centre" which was of interest. By looking at four ring sizes and the acyclic dimethylamine, a basic relationship between ring size and nucleophilicity can be built. The heterocycles studied were aziridine, azetidine, pyrrolidine and piperidine with two to five carbons respectively. From surface scans of the $0.001e.au^{-3}$ iso-density surface it was found that the three membered ring of aziridine has the largest negative value of $-0.0645a.u.$ As the number of carbons in the ring increases, the electronic potential at the nitrogen becomes smaller in magnitude (less negative). This could be attributed to the constrained nature of the smaller ring systems which have less area to distribute electron density and therefore greater electron density at the nitrogen.

Considering the goals of the research outlined in Chapter 1.6 a cross section of secondary amines (Figure 3.35) were selected to investigate further molecular properties.

dimethylamine
1

diethylamine
7

1,2-dimethylhydrazine
2

N-methoxymethanamine
3

aziridine
12

azetidine
16

pyrrolidine
4

piperidine
21

pyrazolidine
5

isoxazolidine
22

imidazolidine
11

pyrazolidin-3-one
6

isoxazolidin-5-one
13

2-(trifluoromethyl)pyrrolidine
14

(*S*)-pyrrolidine-2-carbaldehyde
15

(*S*)-methyl pyrrolidine-2-carboxylate
8

1-isopropylpyrazolidine
17

1-(pyrazolidin-1-yl)ethanone
18

pyrazolidine-1-carboxylic acid
19

ethyl pyrazolidine-1-carboxylate
20

9

10

Figure 3.35 Secondary amines evaluated

3.3.2 Proton affinity

Under the acidic conditions of the reaction, the secondary amine will be found mainly as the protonated form with an associated counter ion. It was therefore necessary to deprotonate the reactive nitrogen to allow the reaction with a carbonyl as seen in TS1 (see chapter 3.1). A possible candidate for a descriptor was the proton affinity of the amine, calculated as the difference in enthalpy of the gas phase neutral and protonated forms. This property takes into account the binding of the proton and relaxation of the geometry associated with it. In practice, a proton was added to the reactive nitrogen and the geometry re-optimised to an energy minimum.

Properties were calculated using thermal enthalpies at a temperature of 298K this energy includes the zero point energy correction (ZPE):

$$H = E + RT \hspace{4cm} \textbf{Equation 3.3}$$

where

$$E = E_0 + E_{vib} + E_{rot} + E_{trans} \hspace{2cm} \textbf{Equation 3.4}$$
$$E_0 = E_{elec} + ZPE \hspace{3cm} \textbf{Equation 3.5}$$

Where E_0 is the electronic energy, E_{vib} is the vibrational energy contribution, E_{rot} is the rotational energy contribution and E_{trans} is the translational energy contribution. Using these values should give a better approximation to experimental data.

Figure 3.36 shows the proton affinities of the secondary amines shown in Figure 3.35. The more positive the value the greater the energy needed for abstraction of the proton. Isoxazolidinone (**13**) was given as the most able molecule to donate its proton. The more strongly bound protons are predominantly found in small ring systems and single hetero atom cyclic molecules. The combination of α-heteroatom and cyclic structure gives the largest decrease in proton affinity.
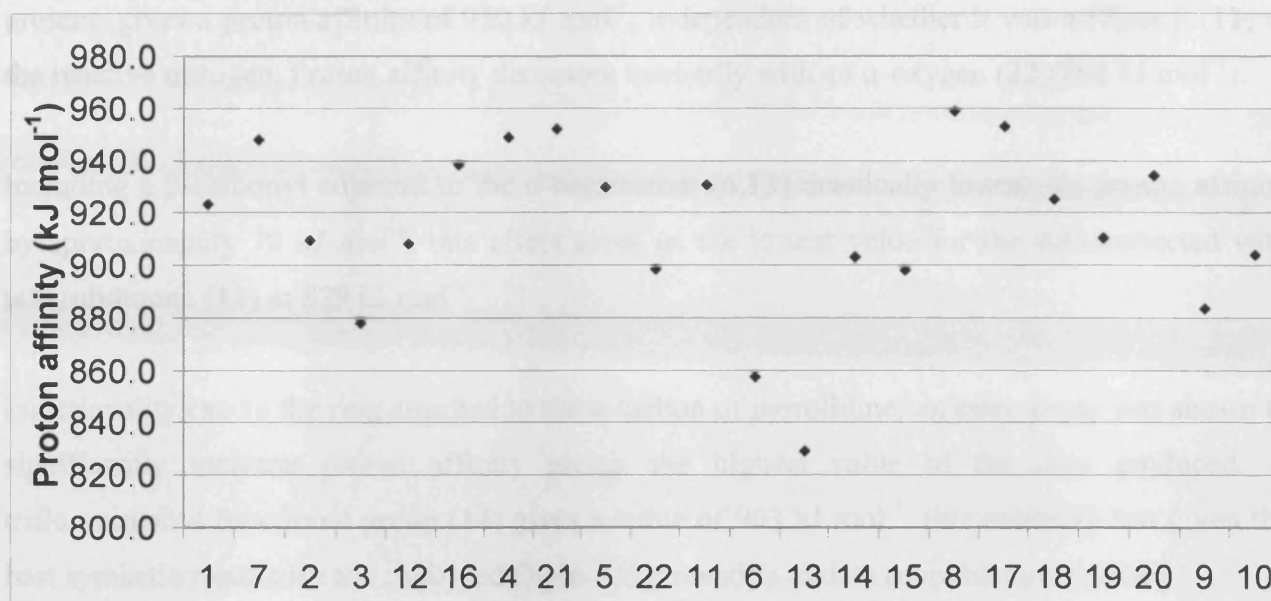
Figure 3.36 Proton affinity of a range of secondary amines, refer to Figure 3.35 for x-axis labels

Seven structural groups can be formed from the data collected for proton affinity, each with a different structural element shared.

The simplest amines are the small acyclic molecules containing only one or two heteroatoms. Dimethylamine (**1**), the simplest secondary amine gives us a reference value of 923kJ mol^{-1}, with the extension of groups to ethyl the proton affinity of diethylamine (**7**) increases to 948kJ mol^{-1}. This can be attributed to the slight electron donating nature of the ethyl group stabilising the cation. Dimethylhydrazine (**2**) and N-methoxymethanamine (**3**) contain α-heteroatoms decreasing proton affinity to 910 kJ mol^{-1} and 878 kJ mol^{-1} respectively. The increase in basicity can be attributed to the increase in electronegativity of the oxygen. From this group we can conclude that an α-heteroatom was of importance when the desired effect was to lower the proton affinity.

The effect of ring size was examined using aziridine (**12**), azetidine (**16**), pyrrolidine (**4**) and piperidine (**21**). It was found that the constrained nature of the smaller aziridine decreased the proton affinity over that of dimethylamine by approximately 15 kJ mol^{-1} the less constrained four, five and six memebered rings all had a larger proton affinities.

Although aziridine gives a smaller proton affinity, it has been found in practice that the best cyclic structure results have come from five memebered rings. Three unsubstituted structures were examined, each with two heteroatoms contained within the ring. Having a second nitrogen

present gives a proton affinity of 930 kJ mol^{-1}, independent of whether it was α (**5**) or β (**11**) to the reactive nitrogen. Proton affinity decreases markedly with an α-oxygen (**22**)(898 kJ mol^{-1}).

Including a β-carbonyl adjacent to the α-heteroatom (**6,13**) drastically lowers the proton affinity by approximately 70 kJ mol^{-1}, this effect gives us the lowest value for the data collected with isoazolidinone (**13**) at 829 kJ mol^{-1}.

Functionality exo to the ring attached to the α-carbon of pyrrolidine: an ester group was shown to significantly increase proton affinity giving the highest value of the data produced. A trifluoromethyl functional group (**14**) gives a value of 903 kJ mol^{-1}, this molecule has given the best synthetic results for the catalysed Diels-Alder reaction to date (unpublished results).

Acyclic structures containing an α-nitrogen and β-carbonyl (**9,10**) were found to have a lower proton affinity than dimethylamine with the ester group contributing a small amount over the α-nitrogen. Comparison of the structures show that a tertiary nitrogen in the α-position with a mildly electron donating methyl group increases the proton affinity.
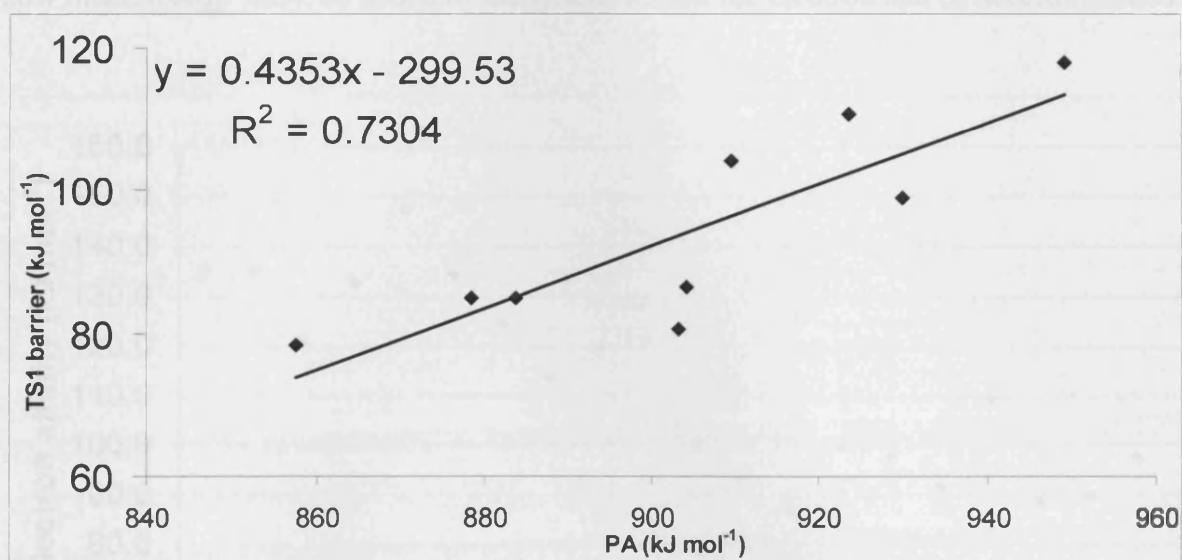
Figure 3.37 Proton affinity vs. TS1 barrier height of a range of secondary amines

The relationship between proton affinity and the TS1 energy barrier was investigated. The values given in Figure 3.37 are all calculated from theoretical data and give a reasonable trend. Molecules **14** and **10** that are the most outlying values in Table 3.3 are both excellent catalysts suggesting that although proton affinity looks to be a good descriptor for TS1. There are other

elements to the reaction that are affecting the overall reaction, however, this may provide a useful guide to the synthesis on new catalytic amines.

Molecule reference	Proton Affinity (kJ mol^{-1})	TS1 Barrier (kJ mol^{-1})
4	948.9	118.0
1	923.4	110.8
5	929.7	99.0
2	909.7	104.2
6	857.5	78.2
9	883.5	84.8
10	904.2	86.4
3	878.2	84.8
14	903.3	80.6

Table 3.3 Proton affinity vs. TS1 barrier height of a range of secondary amines , refer to Figure 3.35 for labels

3.3.3 Electron affinity

The electron affinity was calculated as the difference in thermal enthalpies at 298K between the one electron reduced species and the neutral species. The reduced species energy was calculated by adding an electron to the system without further geometric optimisation. The value describes how much energy must be added to the system so that the electron can be accommodated.
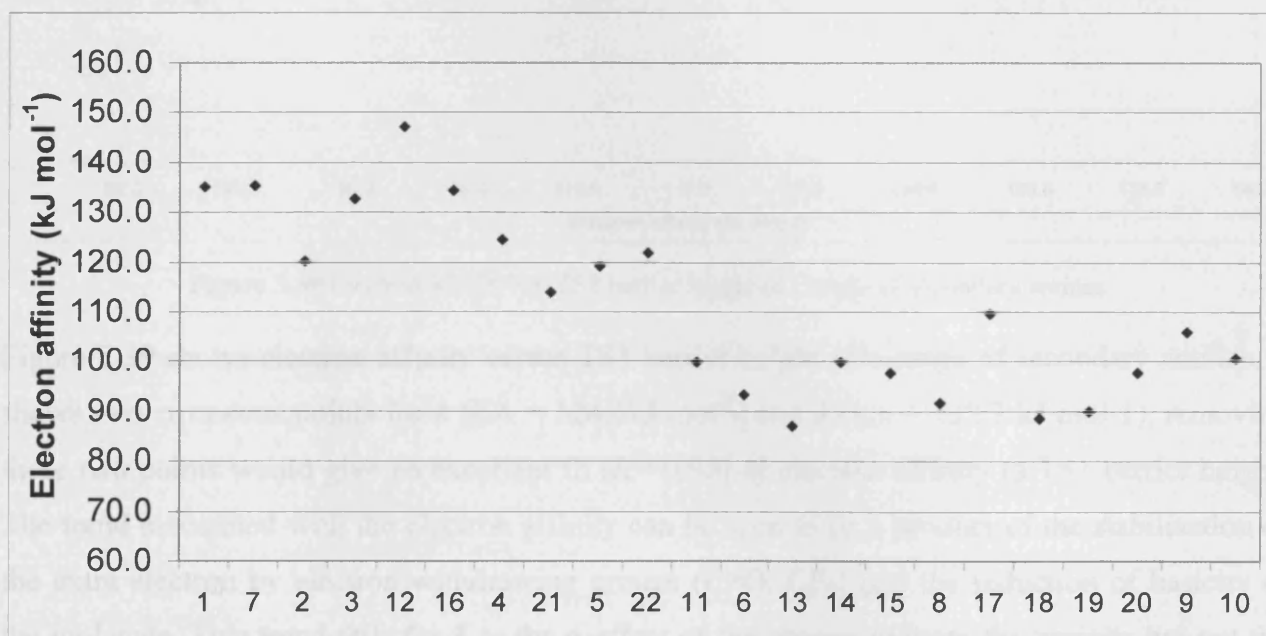
Figure 3.38 Electron affinity of a range of secondary amines , refer to Figure 3.35 for x-axis labels

Electron affinity (Figure 3.38) was shown to decrease steadily with increasing ring size (**12,16,4,21**). The introduction of an α-heteroatom markedly reduces the electron affinity in **2** and

66

3 This reduction was less pronounced in the five-membered cyclic systems of **5** and **22,** with nitrogen lowering the electron affinity more than oxygen. Including an exo-carbonyl group at the beta position lowers the electron affinity markedly with isoxazolidin-5-one (**13**) giving the smallest value of the data. The exo-carbonyl also reverses the order of electron affinity in relation to the α heteroatom where **13** was lower than **6**. Relocating the second heteroatom to a beta position as in imidazolidine (**11**) gives a large drop in electron affinity which has a comparable value to **14** which was shown to give excellent reactivity. Molecules based on a pyrazolidine ring with a carbonyl substituent exo to the α-heteroatom all give low values of electron affinity, isopropyl gives a less pronounced effect. The larger acyclic moieties of **9** and **10** show a lowering of electron affinity over the simpler acyclic molecules but not as much as the five-membered cyclic structures.
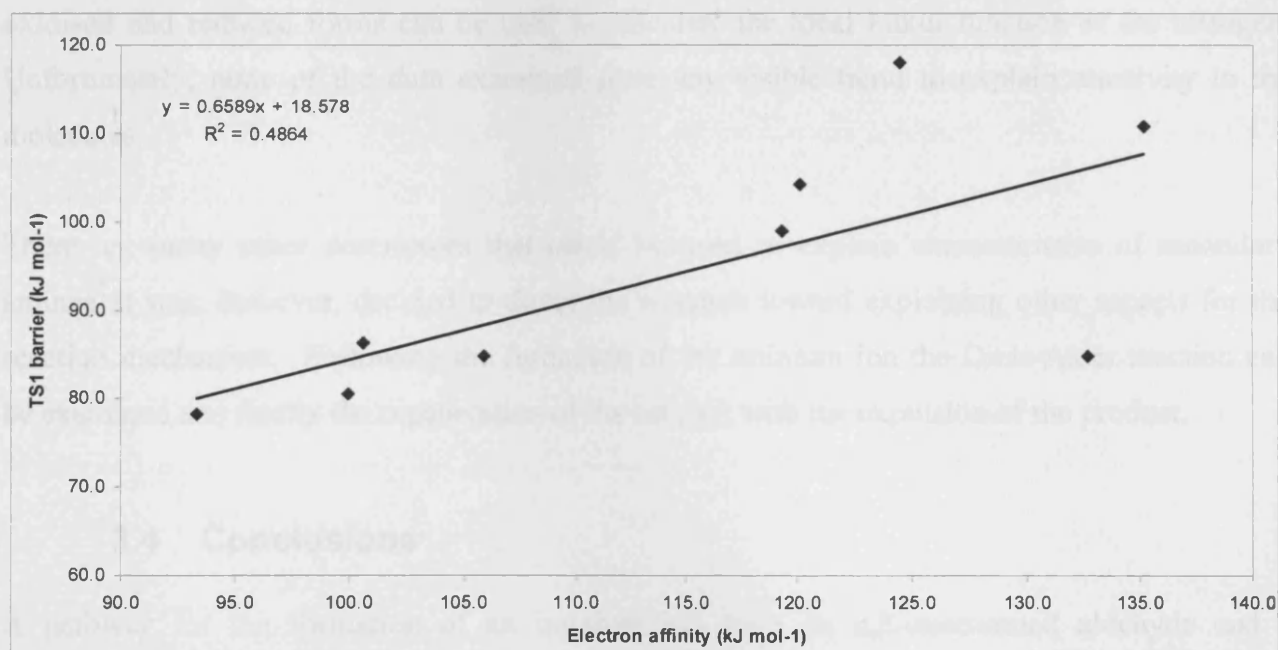
Figure 3.39 Electron affinity vs. TS1 barrier height of a range of secondary amines

Figure 3.39 shows electron affinity versus TS1 barrier height of a range of secondary amines. It shows two erroneous points for **4** (EA = 124.5kJ mol^{-1}) and **3** (EA = 132.7 kJ mol-1), removing these two points would give an excellent fit (R^2=0.95) of electron affinity to TS1 barrier height. The trend associated with the electron affinity can be seen to be a product of the stabilisation of the extra electron by electron withdrawing groups (C=O, CF$_3$) and the reduction of basicity of the molecule. This trend fails for **3** as the α-effect of the oxygen reduces the basicity but not the electron affinity. This property looks to be a chance correlation with the TS1 barrier rather than a good predictor of reactivity.

A number of other molecular and atomic properties were investigated. The chemical potential of each molecule was derived as the sum of the Ionisation energy (I.E.) and the electron affinity (E.A.) divided by two ((IE+EA)/2). This property showed little trend within molecule types and when plotted against TS1 energy, gave a poor R^2 value of 0.03. It was a similar case for the Global Hardness (η) difined as the remainder of the Ionisation energy (I.E.) minus the electron affinity (E.A.) divided by 2. Here there was a slightly better R^2 value of 0.4 but no trend present.

Along with the global properties of the molecules the local Fukui function was also investigated. It was thought that the reactive nitrogen of the amine and its electronic properties would have the greastest effect on reactivity. The natural population of nitrogen gives the electron density present in the nitrogen orbitals. This value along with the natural population of nitrogen of the oxidised and reduced forms can be used to calculate the local Fukui function of the nitrogen. Unfortunately, none of the data examined gave any visible trend to explain reactivity in the molecules.

There are many other descriptors that could be used to explain characteristics of secondary amines, it was, however, decided to direct the research toward explaining other aspects for the reaction mechanism. Following the formation of the iminium ion the Diels-Alder reaction can be examined and finally the regeneration of the catalyst with the expulsion of the product.

3.4 Conclusions

A pathway for the formation of an iminium ion from an α,β-unsaturated aldehyde and a secondary amine was constructed. A model system in the presence of a counter ion and one explicit water molecule allowed for a greater understanding of the formation of this useful intermediate. Each geometry was confirmed via harmonic frequency calculations. Investigating the effect of water on iminium ion formation with the use of explicit molecules and continuum models gave the conclusion that explicit water has the effect of stabilising the reactant complex, allowing for a lower energy reaction profile.

The reaction pathway for the iminium ion formation has been described as a three step deprotonation via water aided proton transfer. The initial deprotonation of the secondary amine was found to be the rate determining step of the iminium ion formation. Differences in DFT geometries were negligible while energies varied mostly in the protonated aminol and TS3

stationary points. Basis set effect showed a lowering of energy of all points bar the sp3 hybridised protonated aminol, with an increase in the number of the basis functions. The type of continuum model for solvent effects was investigated with results showing that PCM models were unable to verify transition state geometries within the software used. The Onsager model allowed for a simple description of the bulk solvent effects. Overall it was found that the B3LYP functional was a sufficient level of theory to use when coupled with the 6-31+G(d,p) basis set. The TS1 activation energy for 2-(trifluoromethyl)pyrrolidine was found to be in good agreement with kinetic data obtained by the Tomkinson group.

The α-effect was found to greatly reduce the activation energies of the rate determining step. An α-Nitrogen allows for extended hydrogen bonding through the reaction profile while a more nucleophilic oxygen decreases the activation barrier by a greater degree than an α-nitrogen. The incorporation of the reactive secondary amine into a five-membered ring increases the activation energy of TS1 with no α-heteroatom present but the combination of both features decreases the activation energy. The addition of an endo-cyclic carbonyl further decreases the activation energy. The presence of carbonyl groups within the catalysts has a large effect on reaction energy and geometry, while reducing the value for TS1, the functional group increases the activation energy for the two remaining transition states. Acyclic carbamates studied gave low energy reaction pathways with some of the lowest TS1 activation energies. All carbamates considered stabilise the intermediate geometry of the iminium ion formation considerably.

The atoms in molecules approach gave further insight into the interactions within stationary point geometries, with inter-molecular interactions being described. Through AIM analysis water was shown to act as a 'proton shuttle' between chloride and the α,β-unsaturated carbonyl. The initial N-C bond formation and the influence of carbamates on transition structure were clearly shown via the presence of a bond critical point. The geometry of a selection of iminium ions were studied with respect to the preferred geometry of the product. There was a slight preference for the Z isomer in asymmetric molecules studied.

A number of molecular descriptors were examined as predictive tools. The electrostatic potential gave insightful information about the reactive nitrogen and the surrounding regions. Proton affinity gave a good relationship with the activation energy of TS1. Experimental data of the Diels-Alder reaction via iminium ions show that although proton affinity looks to be a good

descriptor for TS1, there are other elements to the reaction that are effecting the overall reaction. However this may be a useful guide to the synthesis on new catalytic amines.

3.5 References

(1)   Ahrendt, K. A.; Borths, C. J.; MacMillan, D. W. C. *Journal of the American Chemical Society* **2000**, *122*, 4243-4244.
(2)   Onsager, L. *Journal of the American Chemical Society* **1936**, *158*, 1486.
(3)   Cavill, J. L.; Peters, J. U.; Tomkinson, N. C. O. *Chemical Communications* **2003**, 728-729.
(4)   M. J. Frisch, G. W. T., H. B. Schlegel, G. E. Scuseria, M. A. Robb, J. R. Cheeseman, J. A. Montgomery, Jr., T. Vreven, K. N. Kudin, J. C. Burant, J. M. Millam, S. S. Iyengar, J. Tomasi, V. Barone, B. Mennucci, M. Cossi, G. Scalmani, N. Rega, G. A. Petersson, H. Nakatsuji, M. Hada, M. Ehara, K. Toyota, R. Fukuda, J. Hasegawa, M. Ishida, T. Nakajima, Y. Honda, O. Kitao, H. Nakai, M. Klene, X. Li, J. E. Knox, H. P. Hratchian, J. B. Cross, V. Bakken, C. Adamo, J. Jaramillo, R. Gomperts, R. E. Stratmann, O. Yazyev, A. J. Austin, R. Cammi, C. Pomelli, J. W. Ochterski, P. Y. Ayala, K. Morokuma, G. A. Voth, P. Salvador, J. J. Dannenberg, V. G. Zakrzewski, S. Dapprich, A. D. Daniels, M. C. Strain, O. Farkas, D. K. Malick, A. D. Rabuck, K. Raghavachari, J. B. Foresman, J. V. Ortiz, Q. Cui, A. G. Baboul, S. Clifford, J. Cioslowski, B. B. Stefanov, G. Liu, A. Liashenko, P. Piskorz, I. Komaromi, R. L. Martin, D. J. Fox, T. Keith, M. A. Al-Laham, C. Y. Peng, A. Nanayakkara, M. Challacombe, P. M. W. Gill, B. Johnson, W. Chen, M. W. Wong, C. Gonzalez, and J. A. Pople.
(5)   Edwards, J. O.; Pearson, R. G. *J. Am. Chem. Soc.* **1962**, *84*, 16-24.
(6)   Matta, C. F.; Hernandez-Trujillo, J.; Tang, T. H.; Bader, R. F. W. *Chemistry-a European Journal* **2003**, *9*, 1940-1951.
(7)   Lemay, M.; Ogilvie, W. W. *Organic Letters* **2005**, *7*, 4141-4144.
(8)   Lemay, M.; Ogilvie, W. W. *Journal of Organic Chemistry* **2006**, *71*, 4663-4666.

4. Chapter Four – Structure and Reactions of Iminium Ions

The experimental work carried out by the research group before the commencement of the theoretical investigation was centred around the acceleration of the Diels-Alder reaction.[1] This research showed that the presence of an α-heteroatom lead to significant rate acceleration and a reversal of *endo/exo* selectivity. The presence of an α-heteroatom invariably creates an asymmetric system this difference will permute through the reactions from the point where the catalyst is involved in this reaction scheme that is the formation of the iminium ion. To understand the effect on the formation of the iminium ion a number of questions about the geometry of the molecules must be considered.

4.1. Structure of Iminium ion

The spatial orientation of a molecule can have great bearing on the properties associated with it. This effect is frequently highlighted in the field of enatioselective catalysis. Within the confines of iminium ion formation, there are two spatial arrangements to consider when determining effect on product geometry.

4.1.1. Cis – Trans isomerisation

The reactive centre of an iminium ion is the alkene originating from the carbonyl reactant (Figure 4.1). There is free rotation about the C–C single bond allowing for two diastereoisomers. When both double bonded groups are on the same side the cis-orientation is formed but is sterically disfavoured by the amine structure, therefore the trans-isomer is the more stable form of the iminium species.
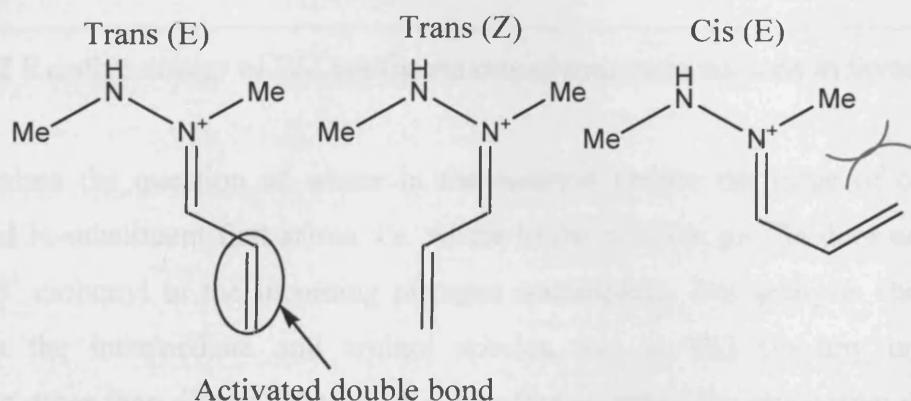
Figure 4.1 Schematic of three orientations of the dimethylhydrazine iminium ion with acrolein.

4.1.2. E and Z conformers

The formation of the N–C double bond essentially locks the geometry of the iminium ion. Conversion between isomers involves disruption of the π-system, and was therefore associated with a large barrier (*e.g.* 231kJmol^{-1} for the iminium ion between acrolein and dimethylhydrazine). The diastereoisomers associated with the N – C bond are assigned names using the Cahn-Ingold-Prelog priority rules. These rules for assigning names to the geometry are identical to that for cis and trans, E is simply the trans orientation and Z the cis (Figure 4.1). One consideration for non-symmetrical amines is the relative energy of *E* and *Z* configurations of the product iminium ion, which may affect subsequent reactions *e.g.* by steric hindrance. The relative energies of *E* and *Z* orientations of four representative iminium ions formed from amines **2**, **3**, **5**, and **9** (Figure 4.2) show, in each case, a small preference for the *Z* configuration.
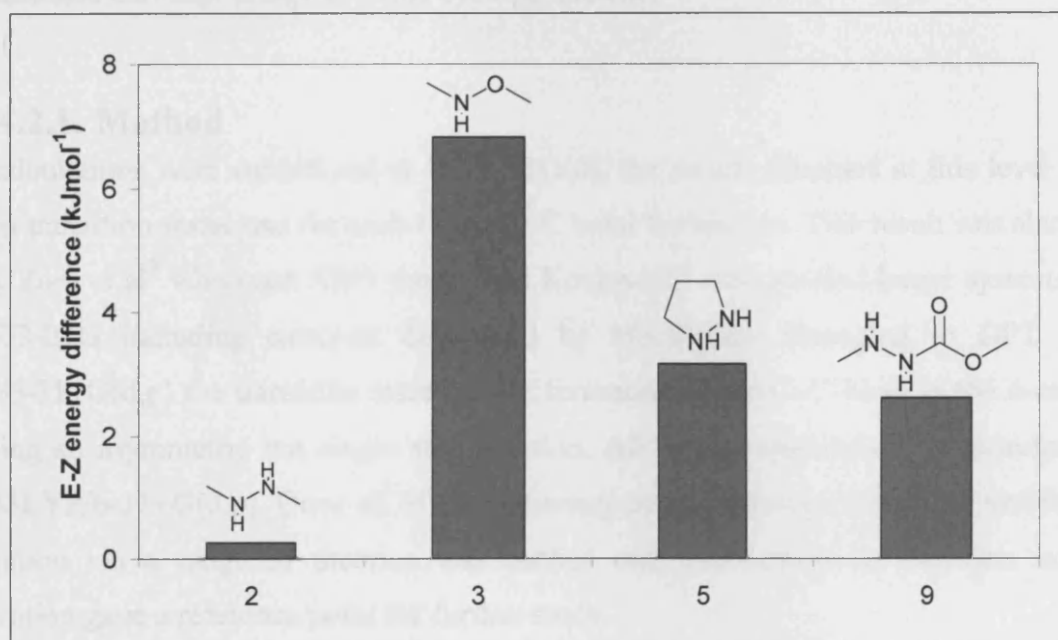
Figure 4.2 Relative energy of E/Z configurations of four iminium ions in favour of Z.

This analysis raises the question of where in the reaction profile the issue of orientation of iminium ion and N-substituent first arises, *i.e.* where in the reaction profile does acrolein rotate to present the δ$^+$ carbonyl to the incoming nitrogen nucleophile. Our analysis shows that this occurs between the intermediate and aminol species, *i.e.* at TS2 for any unsymmetrical secondary amine other than dimethylamine. We therefore searched for alternative geometries of TS2 for amines **2**, **3**, **5**, and **9**, in which the orientation of amine and acrolein was reversed from those shown and discussed in Chapter 3. In three of the four cases, we were unable to find a

transition state corresponding to this altered pathway, so the results in chapter three appear to be the only feasible pathway to iminium formation. In these cases, the direction of rotation of acrolein was such that it leads to the energetically favoured Z-product, *i.e.* both kinetics and thermodynamics favour the formation of one product over another. For amine **5**, two geometries of TS2 were located, but these differ by 7kJmol^{-1}, an essentially negligible difference when compared to the barriers associated with TS1 and TS3.

4.2. Diels-Alder reaction

The Diels-Alder [4+2] cycloaddition is one of the most powerful tools in organic synthesis available. Catalytic variations of the transformation have been given much attention especially in the area of asymmetric variants. This cycloaddition has become one of the central benchmarks for asymmetric catalysts, it was therefore chosen to examine the reaction between the simplest α,β-unsaturated carbonyl compound and cyclopentadiene.

4.2.1. Method

Initial calculations were carried out at HF/6-31G(d), the results obtained at this level of theory gave two transition states one for each of the C–C bond formations. This result was also found in work by Zora et al[2] who used AM1 theory and Kozlowski[3] who studied larger systems at MM3 and HF/3-21G including catalysts developed by MacMillan. Changing to DFT theory at B3LYP/6-31+G(d,p) the transition state for the formation of the C–C bond to the α-carbon was lost giving an asymmetric but single step reaction. All further reactions were therefore carried out at B3LYP/6-31+G(d,p). Once all of the stationary points had been found and verified further investigation via a range of theories was carried out. The results for acrolein uncatalysed cycloaddition gave a reference point for further study.

4.2.2. Systems

Three variations of the system were studied for the dimethylamine iminium reaction with cyclopentadiene; the gas phase cationic reaction (A), solvated two component cationic reaction (B) and solvated neutral reaction containing a chloride counter ion (C). To include the effect of a solvent an Onsager sphere of 8.0Å radius was included. This model proved to be satisfactory for the previous calculations on the formation of the iminium ion. For comparison with the iminium activated reactions, acrolein and cinnamaldehyde were substituted as dieneophiles.
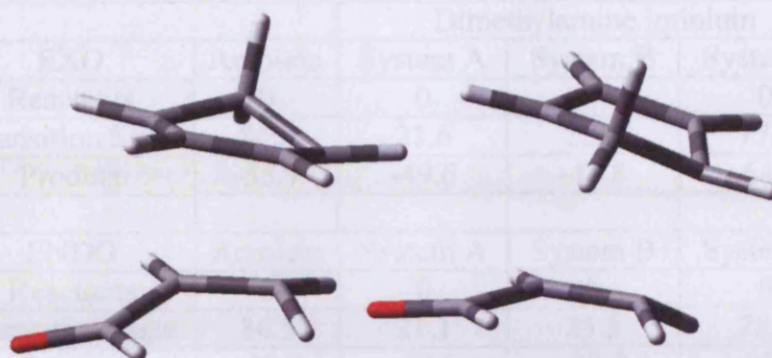
Figure 4.3 Endo (left) and Exo (right) transition states of acrolein addition to cyclopentadiene

The approach of cyclopentadiene to the dienophile has a bearing on the product geometry (Figure 4.3), the nomenclature associated with the product was determined by the relative position of a substituent in the bridged ring system. The prefix endo is given to the isomer with the substituent closest to the longest bridge and the prefix exo is given to the isomer with the substituent closest to the shortest bridge (Figure 4.4).
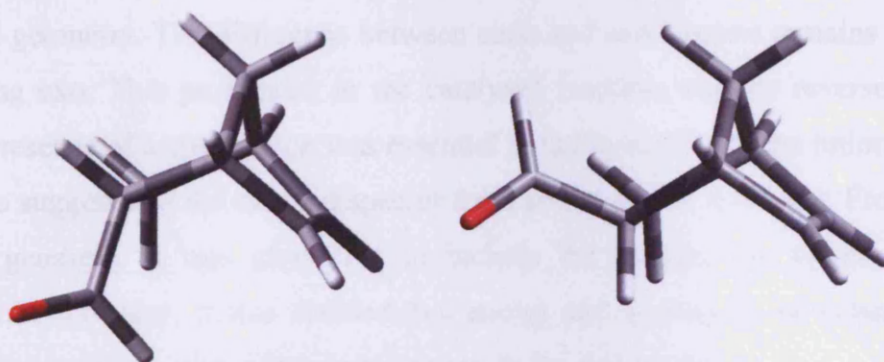
Figure 4.4 Endo(left) and Exo (right) products of acrolein to cyclopentadiene

4.2.3. Results

The Diels-Alder reaction energies of acrolein and the three dimethylamine systems are shown in Table 4.1. Systems A and B that don't include a counter ion have a considerably lower energy pathway that that of acrolein. The use of a solvent model increases the barrier of formation by 4kJmol^{-1} but does little to change the lack of discrimination between formation of endo and exo products.

		Dimethylamine iminium		
EXO	Acrolein	System A	System B	System C
Reactants	0	0	0	0
Transition State	84.8	21.6	25.8	77.8
Product	-55.7	-49.6	-47.8	-64.3

ENDO	Acrolein	System A	System B	System C
Reactants	0	0	0	0
Transition State	84.3	21.1	25.5	78.5
Product	-52.2	-52.8	-50.7	-67.0

Table 4.1 Reaction profile of four Diels-Alder systems (kJmol^{-1}) B3LYP 6-31+g(d,p)

The introduction of a chloride counter-ion causes the barrier to increase to around that of acrolein. The barrier of system C was approximately 5kJ mol^{-1} lower than the respective acrolein system. The underlying reason for the large effect of the chloride ion was most likely due to the charged nature of the species, the close association of the anion with the iminium changes the geometric and electronic nature of the diene substantially. The counter ion drastically alters the geometry of the iminium ion causing the α carbon for the iminium ion to move toward a more sp^3 hybridised geometry. The difference between endo and exo barriers remains small at $\approx$ 1.5kJ mol^{-1} favouring exo. This preference in the catalysed reaction was the reverse of the acrolein system. The presence of a counter ion was essential to the formation of the iminium ion but there was nothing to suggest that the charged species form an ion pair in a solvent. From the change in iminium ion geometry it was clear that to include the counter ion would involve greater representation of solvation. It was decided that energy and geometries of systems A and B are more likely to be representative of the iminium ion in the real system.

The transition state of the reaction was the formation of two carbon-carbon bonds via a non-symmetrical concerted pathway. The terminal carbon bond formation (β relative to the iminium centre) proceeds first, followed by the second bond formation (α relative to the iminium centre). Frequency calculations identified transition geometries and the distances of the forming bonds were recorded (Table 4.2). Atomic distances change marginally with the addition of the counter ion causing the greatest discrepancy in both orientations of the system.

	Orientation	β carbon (Å)	α carbon (Å)	Imaginary frequency (cm^{-1})
System A	exo	2.042	3.127	i284.1
System B	exo	2.039	3.122	i289.3
System C	exo	2.052	2.969	i328.6
System A	endo	2.012	3.068	i303.1
System B	endo	1.949	3.002	i307.0
System C	endo	2.03	2.928	i340.7

Table 4.2 Bond lengths of the transition state geometries in six systems.

The Diels-Alder reaction of a number of other iminium ions were studied at the same theoretical level. Iminium ions based on amines **1 – 4** (Figure 4.5), were chosen to examine the effect of an α heteroatom and the inclusion of the amine in a cyclic structure.
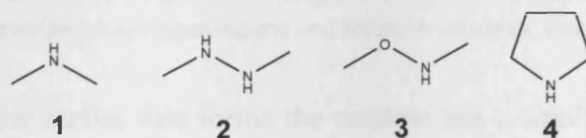
Figure 4.5 Amines used for Diels-Alder models

The energy profiles for the Diels Alder of the systems are presented in Table 4.3.

EXO	Acrolein	Iminium 1	Iminium 2	Iminium 3	Iminium 4
Reactants	0.0	0.0	0.0	0.0	0.0
TS1	84.8	21.6	50.4	14.2	29.9
Product	-52.0	-49.7	-34.9	-50.1	-46.7

ENDO	Acrolein	1	2	3	4
Reactants	0.0	0.0	0.0	0.0	0.0
TS1	84.3	21.1	49.9	13.1	29.4
Product	-52.3	-52.6	-38.6	-53.8	-48.8

Table 4.3 Energy of stationary points of five Diels Alder reactions (kJmol^{-1})

The small barrier height difference between orientations points toward the diastereomeric excess of the product being governed by a factor other than the Diels-Alder reaction, or a failing in DFT to discriminate between transition structure energies. Shown in Figure 4.6 is the profile of the reaction with the endo attack and product. It can be seen that the lowest barrier was of hydroxylamine at 13kJ mol^{-1} and it also has the most energetically stable product in both exo and endo geometries.
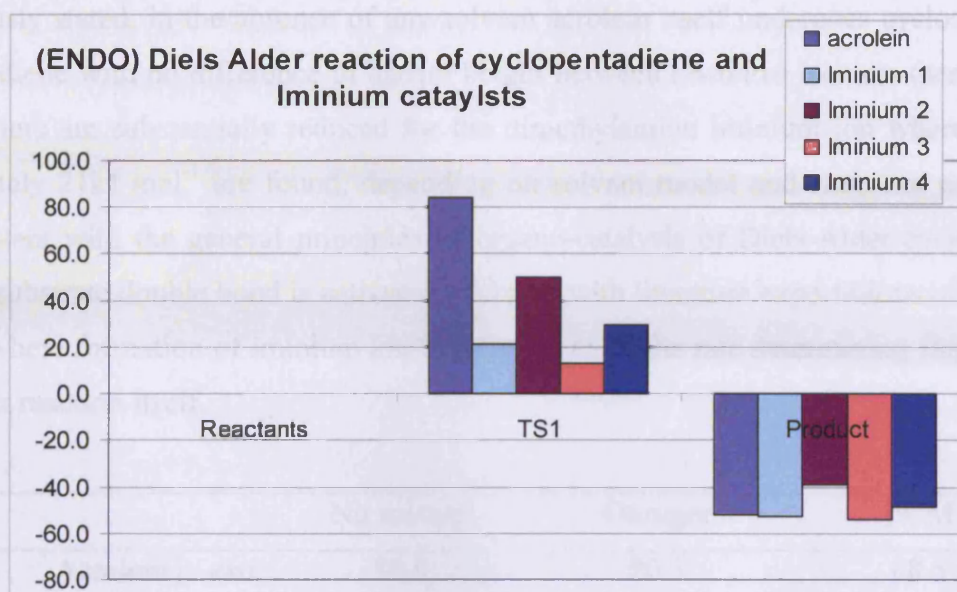
Figure 4.6 Diels Alder reaction of cyclopentadiene and Iminium catalysts, molecules difined in Figure 4.5

Changing the nature of the amine that forms the catalyst has a small effect on the geometry of the transition state (Table 4.4). The distance of the two forming bonds varies by 0.15Å at the β carbon and 0.17Å at the α position. The orientation of cyclopentadiene does affect bond lengths, with dimethylamine and hydrazine having shorter β distances in the endo geometry and the exo orientation having the shorter length for hydroxylamine. The greatest deviation was found in the α carbon bond formation, this increase in distance could be contributing to the lowering of the reaction barrier, the reaction of N-methoxymethanamine (**3**) has the largest difference between α / β bond length but the smallest barrier to formation. Though there was deviation in the transition state geometries no change in β carbon length was larger than 0.15 Å with the larger range of distance originating from the α position. This suggests that if there was enough steric hindrance caused by the amine a stepwise mechanism would be more appropriate.

	Orientation	β carbon (Å)	α carbon (Å)	Imaginary frequency (cm⁻¹)
Acrolein	exo	1.931	2.397	i442.4
	endo	2.049	2.463	i449.4
Iminium 1	exo	2.042	3.127	i284.1
	endo	2.012	3.068	i303.1
Iminium 2	exo	2.006	3.076	i321.1
	endo	1.980	3.029	i326.9
Iminium 3	exo	2.070	3.155	i290.8
	endo	2.100	3.140	i296.5
Iminium 4	exo	2.026	3.093	i298.7
	endo	1.997	3.038	i311.2

Table 4.4 Atomic didstances for the formation of the products with varying catalysts

As previously stated, in the absence of any solvent acrolein itself undergoes cycloaddition with cyclopentadiene with no difference in barrier height between *endo/exo* isomers (see Table 4.5) . These barriers are substantially reduced for the dimethylamine iminium ion where energies of approximately 21kJ mol^{-1} are found, depending on solvent model and *endo/exo* pathway. This was consistent with the general principles of organo-catalysis of Diels-Alder cycloaddition, in which the substrate double bond is activated, and also with literature expectations of iminium ion catalysis, where formation of iminium ion is believed to be the rate determining step and not the Diels-Alder reaction itself.

		No solvent	Onsager	PCM
Acrolein	*exo*	84.8	80.3	68.5
	endo	84.3	83.2	67.7
Cinnamaldehyde	*exo*	111.6	111.6	91.6
	endo	112.4	112.1	102.1
Iminium 1	*exo*	21.6	25.7	31.2
	endo	21.1	25.5	30.7
Iminium 1 with	*exo*	74.3	90.6	77.5
Cinnamaldehyde	*endo*	77.7	94.0	80.1
Iminium 2	*exo*	50.4	52.5	45.2
	endo	49.9	52.2	43.8
Iminium 3	*exo*	14.2	16.3	13.4
	endo	13.1	15.0	12.3
Iminium 4	*exo*	29.9	31.5	33.6
	endo	29.4	31.0	33.1

Table 4.5 Barriers to Diels-Alder cycloaddition reaction (kJ mol^{-1}).

Table 4.5 compares barriers to reaction for amines **1 – 4** in different solvated environments. As Table 4.4 shows, there was little deviation in transition state distances but there are large deviations in energy between complexes which shows that amine structure has some influence on this stage of the catalytic cycle. The iminium ion based on dimethylhydrazine (**2**) has a rather large barrier compared to all other amines, whereas that of **3** has a very low barrier for the reaction. This suggests that it is not only the α-effect that is lowering the energy of the reaction. However, in all cases barriers are substantially lower than for acrolein itself, suggesting that they all activate the dienophile.

Experimental data was obtained using cinnamaldehyde (3-phenylprop-2-enal) rather than acrolein. This was significantly less reactive in the Diels-Alder step than acrolein, with a calculated barrier of 112 kJ mol^{-1}, *i.e.* 30 kJ mol^{-1} more than acrolein under the same conditions. The addition of a phenyl group to the dimethylamine derived iminium resulted in an increase in barrier height of approximately 55 kJ mol^{-1} for the gas phase model, 65 kJ mol^{-1} for Onsager and 50 kJ mol^{-1} for PCM. A further detail to note was that the difference in barrier height between isomers becomes more pronounced with the use of solvent models. For the calculations in Table 4.5 only the two reacting molecules were included, counter ion, explicit and implicit solvent were omitted. We anticipate that phenyl substitution will not have such a large effect on barriers to iminium ion formation. Also throughout, we find no evidence for significant differences in energy barriers between *endo* and *exo* pathways.

4.3. Iminium-ion catalysts based on imidazolidinone systems

One of the leading groups in the study of enantioselective organocatalysis is that of MacMillan. Imidazolidinone catalysts developed by that group are among the most successful molecules in the field of organocatalysis. These molecules give good to excellent yields in reasonable times with range of enantiomeric excesses[4]. The first of these efficient catalysts was reported in 2000[5], from then much work has been done on increasing developing new reactions[6,7]. Other groups have also taken up the challenge working on numerous C–C, N–C bond forming reactions, among these are contributions from Jørgensen[8,9] and List[2,10].

To understand the control these catalysts have on the reaction, it was decided to study the first effective catalyst developed by MacMillan[5] (Figure 4.7), which contain α geminal dimethyl and benzyl groups. The catalyst was reported to give excellent yields (99%) in a short amount of time (8 hours) of the enantioselective Diels-Alder reaction between cyclopentadiene and cinnamaldehyde.
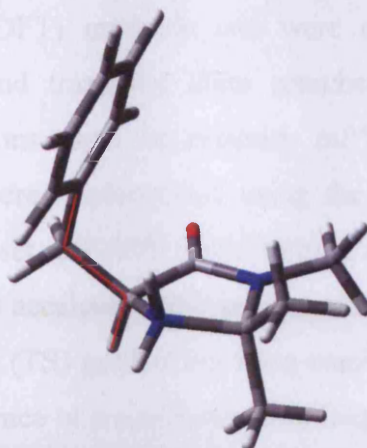
Figure 4.7 Protonated form of imidazolidinone
developed by MacMillan (MM3-9)[11]

In previous theoretical work on this catalyst, Houk et al[12] carried out a conformational search at the B3LYP/6-31G(d) level, exploring both the E/Z configuration of the iminium ion and the orientation of the benzyl arm. They identified two preferred orientations of the benzyl arm, each of which also had E and Z forms, to give a total of four isomers of the iminium ion. MacMillan has also investigated the conformational properties of these catalysts using the MM3 and Monte Carlo simulations[4].

4.3.1. Computational Methods

Due to known deficiencies of B3LYP, and indeed many other common density functionals, in describing the weak interactions that apparently determine the conformation of these molecules, we revisited this work using various theoretical methods, including some recently shown to perform well in describing weak interactions such as $\pi\ldots\pi$ stacking. We also investigate barriers to interconversion of important isomers, and subsequent Diels-Alder reaction of this catalyst.

All density functional theory (DFT) methods and were carried out using the Gaussian03 package. Initial optimisations and transition state searches were carried out at B3LYP/6-31+G(d,p). Subsequent calculations used the methods mPW1PW91[13] and BH&H[14]. Density fitting (DF) MP2 calculations were implemented using the MOLPRO suite of programs and Dunning's aug-cc-pVTZ[15] basis set. DF-MP2 (also termed resolution of identity, RI-MP2, by some authors), has been shown to accelerate MP2 by an order of magnitude with little or no loss of accuracy[16]. All transition state (TS) geometries were confirmed *via* frequency analysis using DFT methods, to ensure the presence of a single negative frequency. To check such structures do indeed link the expected reactants and products, the TS geometry was perturbed both forwards and backwards along the eigenvector corresponding to the negative frequency, and a geometry optimisation performed on the resulting co-ordinates.

4.3.2. Results and Discussion
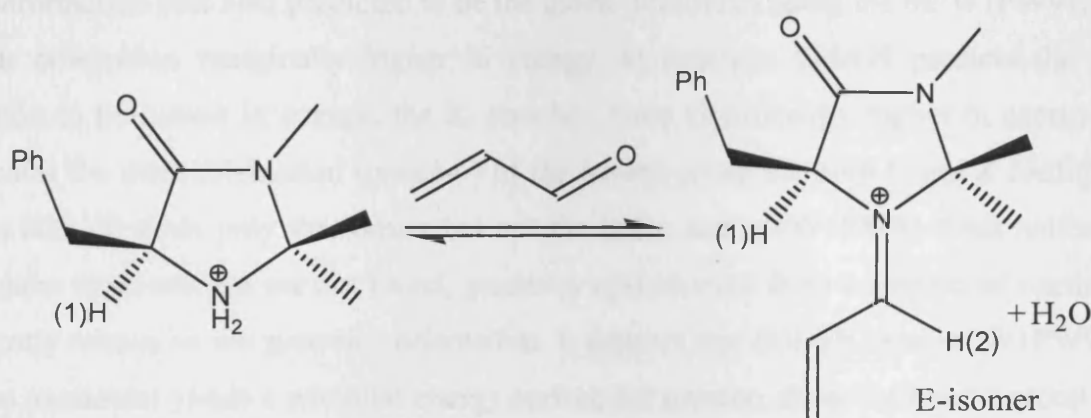
Figure 4.8 Iminium formation of imidiazolidinone, labelling of H(1) and H(2) as reference points.

The relative energies of conformations of the iminium ion calculated with three functionals are reported in Table 4.6. Although not the correct definition, for the purpose of this work E can be described as the configuration in which the C=C bond lies on the same side of the N=C bond as the benzyl group, and Z to that where these groups are opposite one another. The orientation of the benzyl group was reported relative to the proton H1 on the chiral carbon (Figure 4.8). In general, structural parameters determined with the three methods were very similar, but the energetic ordering of conformations varies considerably. There was a clear preference with all methods for the E configuration of the iminium ion, with E-Z differences varying from 4 to 20 kJ mol^{-1}: the origins of this difference are explored in more detail below.

Iminium Configuration	Benzyl Orientation	B3LYP/ 6-31+G(d,p)	mPW1PW91/ 6-31+G(d,p)	BHandH/ 6-31+G(d,p)	DF-MP2/ aug-cc-pVTZ
E	*trans*	1.1	0.3	0.0	0.0
Z	*trans*	10.2	10.0	10.0	10.2
E	*gauche* +	0.0	0.0	6.6	7.9
Z	*gauche* +	4.5	3.9	10.8	15.2
E	*gauche* -	8.4	*	20.5	31.6
Z	*gauche* -	*	*	39.8	53.7

Table 4.6 Optimised iminium ion diastereoisomers relative energies kJ mol^{-1}

(* optimisation reverted to give *gauche* + structure)

Regarding the orientation of the benzyl group, use of a larger basis set (with diffuse basis functions on heavy atoms and polarisation functions on H) changes the energy ordering from that reported by Houk, such that lowest energy conformation found using B3LYP was *E, gauche*+. This conformation was also predicted to be the global minimum using the mPW1PW91, with the *E, trans* orientation marginally higher in energy. In contrast, BH&H predicts the *E, trans* orientation to be lowest in energy, the *E, gauche*+ form significantly higher in energy. BH&H also locates the third orientation (*gauche-*) of the benzyl group for both E and Z configurations, whereas B3LYP finds only the former but not the latter, and mPW1PW91 finds neither. In the cases where these minima are not found, geometry optimisation from a number of starting points consistently returns to the *gauche*+ orientation. It appears that B3LYP (and mPW1PW91 where data was available) yields a potential energy surface for rotation about the benzyl group that was rather flat, *i.e.* that does not discriminate between possible isomers.

While BH&H has been shown to perform well in describing weak intermolecular interactions, its performance for conformations of organic molecules has not yet been tested. Therefore, we carried out single point MP2 calculations on the BH&H optimised structures using DF-MP2. Since all three DFT methods gave essentially identical geometries, DF-MP2 values of B3LYP and mPW1PW91 optimised structures gave similar energies.

Table 4.6 shows generally excellent agreement between MP2 and BH&H, both showing a clear preference for the *trans* orientation of the benzyl group. The relatively high energy of the *gauche+* conformation was in stark contrast to the B3LYP and mPW1PW91 results, which predict this to be slightly lower in energy than *trans*. B3LYP also underestimates the instability of the *gauche-* conformation by a factor of 3 to 4. Thus, it seems the known shortcomings of common DFT methods such as B3LYP leads to poor prediction of the conformations of this iminium ion, but that BH&H can properly describe such structures.

The importance of the orientation of the benzyl arm for catalysis is demonstrated in Figure 4.9, which shows the *trans* and *gauche +* optimised structures. The impressive enantioselectivity of this catalyst has been assigned to the coverage of one face of the C=C double bond by the phenyl ring, preventing approach of a diene at this face. Figure 4.9 indicates that this coverage was best achieved in the *gauche+* structure, *i.e.* that reported as the minimum energy structure by MacMillan. It was notable that the benzyl group was significantly offset from the C=C bond. However, our calculations suggest that the energy minimum structure does not contain this coverage of the C=C bond, and instead that the phenyl ring lies almost perpendicular to both this bond and the mean plane of the imidazolidinone ring.
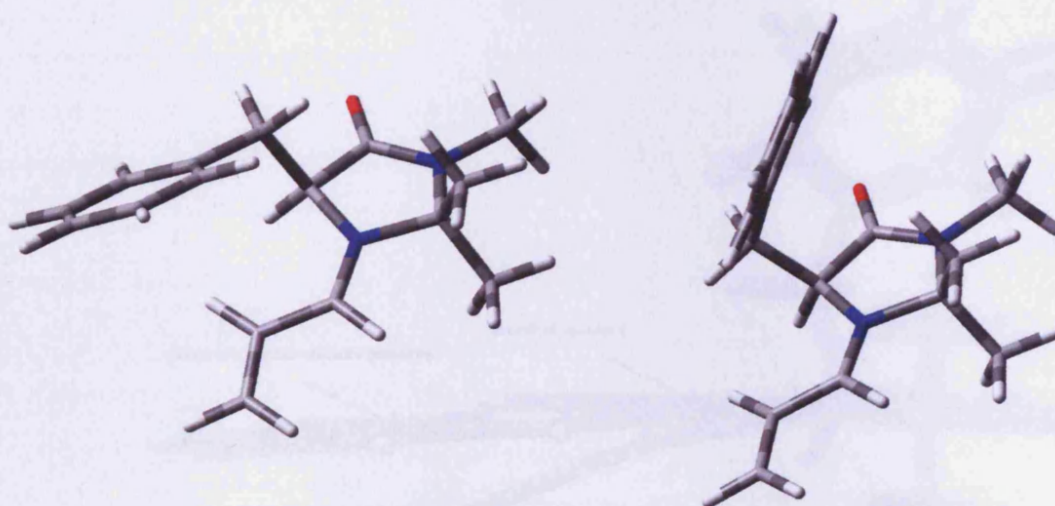

Figure 4.9 Optimised *gauche+* and *trans* structures

It was of note that through research within the group the crystallographic structure of the MacMillan catalyst PF_6 salt has been obtained (Figure 4.10). With this evidence it can be seen that the calculations performed gave the same geometry as the crystal structure.
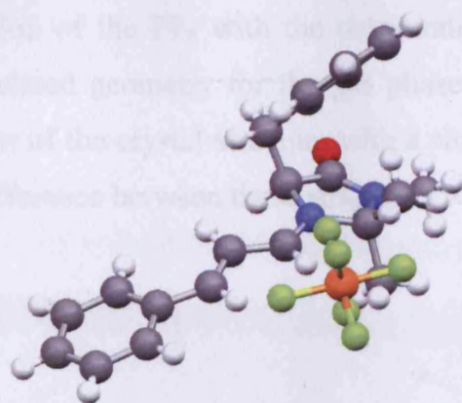
Figure 4.10 Crystal structure of MacMillan PF$_6$ salt with cinnamaldehyde

When comparing calculated and crystal structures it was apparent that the imidazolidinone and benzyl ring are in good agreement. There was a discrepancy in the conjugated vinyl section of the molecule. Calculations for geometry and the Diels-Alder reaction were carried out on the cut-down version of the standard cinnamaldehyde based structure along with the effect of the PF$_6$ salt of the crystal which all contribute to the difference in molecular geometries. In the crystal the C-N=C-C dihedral was 14° from planar and the calculated value was 4.4° for the cut-down molecule. Optimisation of the crystal structure at the same BH&H/6-31+G(d,p) theory results in the dihedral angle being reduced to 6.6° (Figure 4.11).

Figure 4.11 Comparision of crystal and calculated geometries

Within the crystal the interaction of the PF$_6$ with the unsaturated chain induces a bend in the structure. The previously calculated geometry for the gas phase catalyst gives a almost planar conjugated system, optimisation of the crystal structure with a single PF$_6$ counter ion results in a planar structure. The energy difference between these structures was approximately 14kJmol^{-1}.

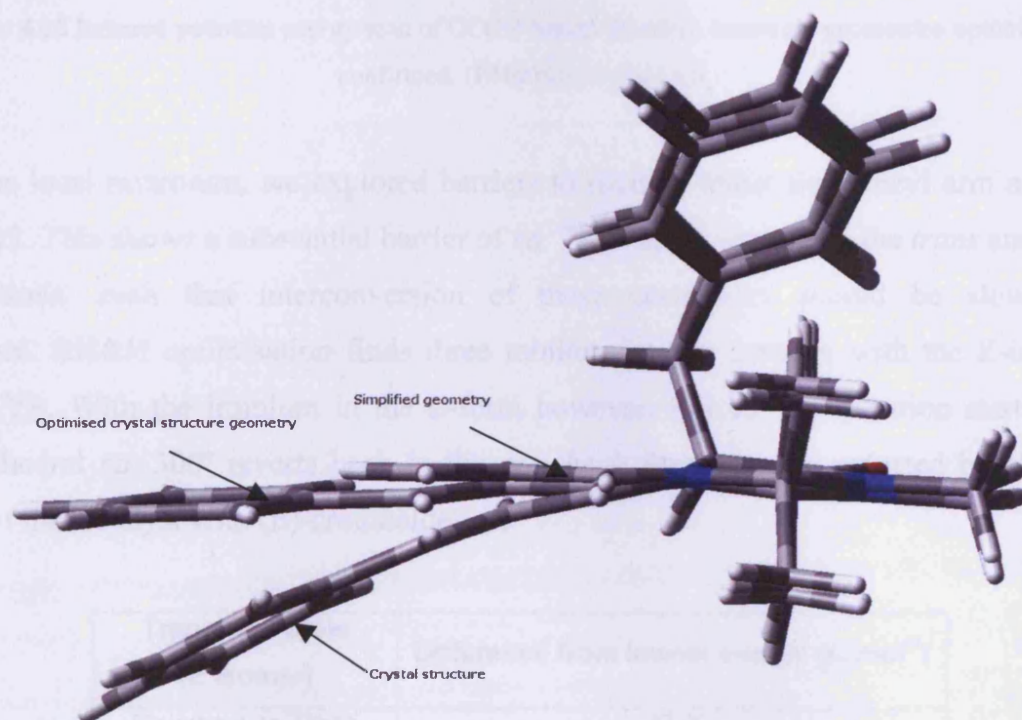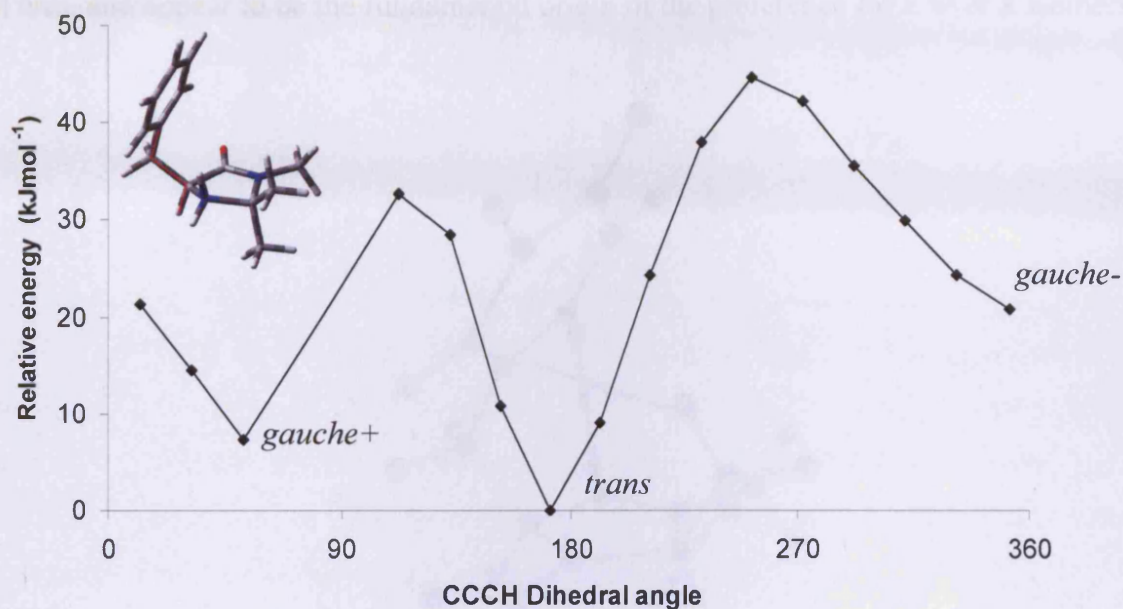**Figure 4.12** Relaxed potential energy scan of CCCH benzyl dihedral, transition geometries optimised and confirmed. (BH&H/6-31+G(d,p))

As well as local minimum, we explored barriers to rotation about the benzyl arm as shown in Figure 4.12. This shows a substantial barrier of *ca.* 35 kJ mol^{-1} separating the *trans* and *gauche +* conformations, such that interconversion of these geometries should be slow at room temperature. BH&H optimisation finds three minima for this rotation with the E-iminium, as does B3LYP. With the iminium in the Z-form however, B3LYP optimisation starting from a CCCH dihedral *ca.* 300° reverts back to the *gauche +* form, as was reported by Houk in the reaction of this catalyst with (E)-crotonaldehyde[12].

Transition State (E isomer)	Difference from lowest energy (kJmol^{-1})
Gauche + to Trans	27.0
Trans to Gauche -	44.4
Gauche - to Gauche +	6.6

Table 4.7 Optimised transition states of benzyl group rotation (BH&H/6-31+G(d,p))

To further explore and rationalise the observed conformational energies of the active catalyst, we turn to Atoms-in-Molecules analysis, which identifies the non-bonding interactions that determine the energetics. The relative instability of the Z isomers (Figure 4.13) was due to H...H interactions between the geminal methyl groups and H2 (see Figure 4.8 for labelling) of the iminium moiety. These interactions are present in all cases, no matter what the orientation of the benzyl arm, and appear to be the fundamental origin of the preference for E over Z isomers.
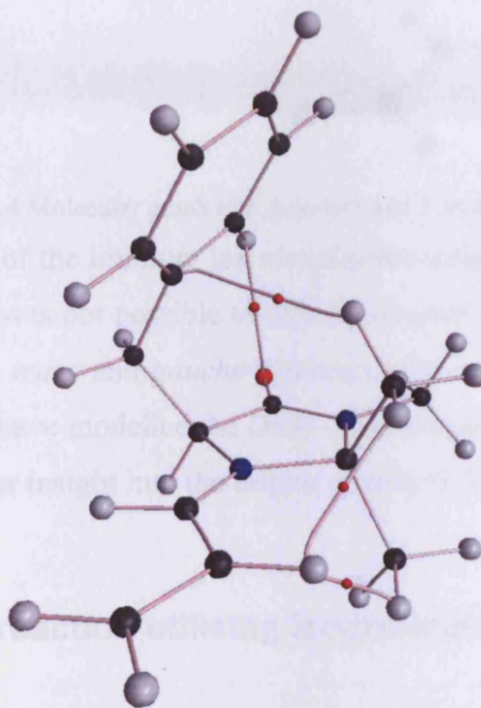
Figure 4.13 Molecular graph of non-bonding interactions of Z isomer of catalyst

E-configurations of the iminium ion, in contrast, show no such interactions between iminium and geminal methyl groups: the lack of these steric clashes seems the likely source of stability. The molecular graph of the *E, gauche+* structure, shown in Figure 4.14, reveals a C—H...π interaction, in which the C—H donor was in the iminium ion group, and the phenyl ring the acceptor. Also present in this structure was an H...H interaction between the benzyl CH$_2$ and one of the geminal methyl groups. In the *trans* conformation we find a C—H...O interaction, from phenyl C—H to carbonyl O, and a C—H...π interaction from methyl C—H to the phenyl ring. These weak (but presumably stabilising) interactions seem to be the origin of the energetic preference for *trans* over *gauche+*. In addition, an H...H interaction between the iminium ion group and the benzyl CH$_2$ group was present.
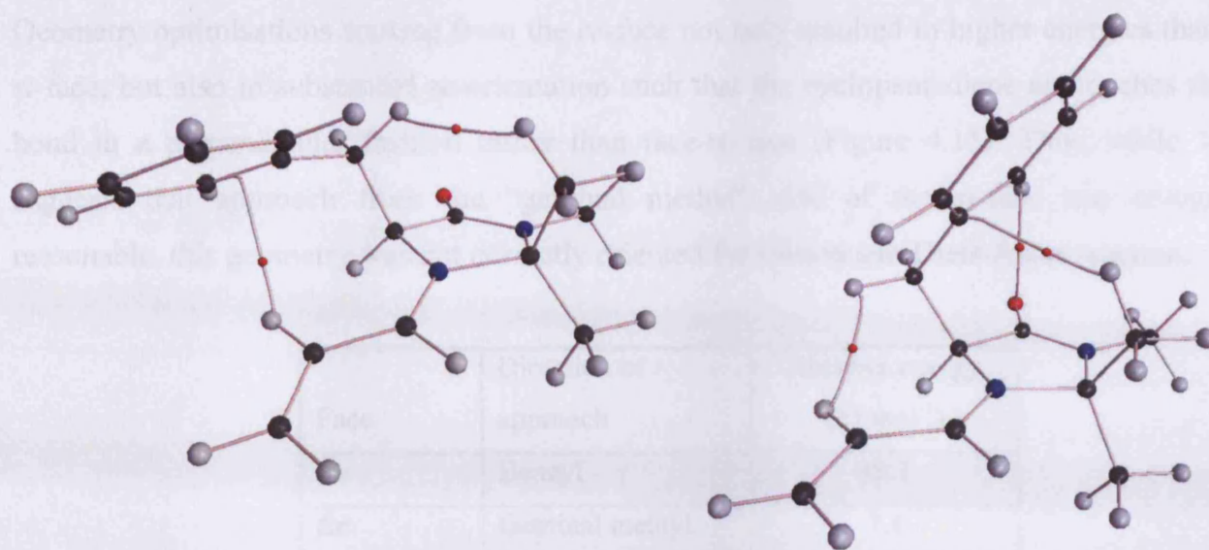
Figure 4.14 Molecular graph of *E,gauche+* and *E,trans* isomers.

While these structural studies of the iminium ion reveal some insight into the relative orientation of benzyl and C=C groups, it was not possible to directly discern the origin of enantioselectivity from these. In particular, both *trans* and *gauche+* interact with and partially 'cover' one face of the C=C bond. Therefore, we have modelled the Diels-Alder reaction of both conformations with cyclopentadiene, to gain further insight into the origins of selectivity.

4.4.   Diels-Alder reaction utilising isoazolidinone derived catalysts

The Diels-Alder reaction of these iminium ions with cyclopentadiene was studied using the same BH&H/6-31+G(d,p) method. In all calculations, the iminium ion was assumed to remain in the *E* configuration. Figure 4.15 suggests that, no matter whether the benzyl arm lies in the *trans* or *gauche+* conformation, approach of the diene from the *si*-face was energetically favoured (Table 4.8).
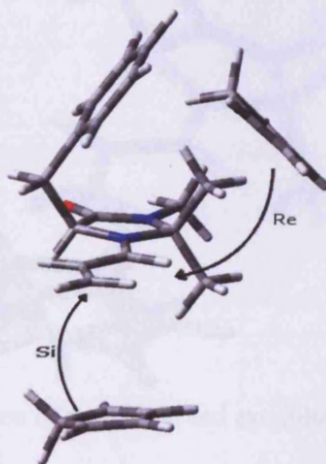
Figure 4.15 *Endo* approach of diene to *re-* and *si-* faces of iminium ion

Geometry optimisations starting from the *re*-face not only resulted in higher energies than at the *si*-face, but also in substantial re-orientation such that the cyclopentadiene approaches the C=C bond in a perpendicular fashion rather than face-to-face (Figure 4.15). Thus, while Table 3 suggests that approach from the "geminal methyl" side of the *si*-face was energetically reasonable, this geometry was not correctly oriented for subsequent Diels-Alder reaction.

Face	Direction of approach	Relative energy (kJ mol^{-1})
Re	Benzyl	49.1
Re	Geminal methyl	7.1
Si	*exo*	6.8
Si	*endo*	0.0

Table 4.8 Minima found from different cyclopentadiene approaches to *E,trans* isomer

Two orientations of approach of cyclopentadiene toward the *si* face, *i.e.* those leading to *endo*- and *exo*- products, were explored for each of the *E,trans*, and *E,gauche*+ conformations. The orientation of approach shown in Figure 4.15 is *endo*, while *exo*- corresponds to 180° rotation of cyclopentadiene relative to the iminium ion, an illustration of this can be seen in Figure 4.16. Binding energies are reported for each orientation in Table 4.9: this data shows that all complexes are rather strongly bound, with values between -40 and -50 kJ mol^{-1}. Interestingly, complexes in the *endo*- arrangement are approximately 6 kJ mol^{-1} more stable than *exo*-.

Figure 4.16 Orientation of endo (red) and exo (blue) reactant complexes

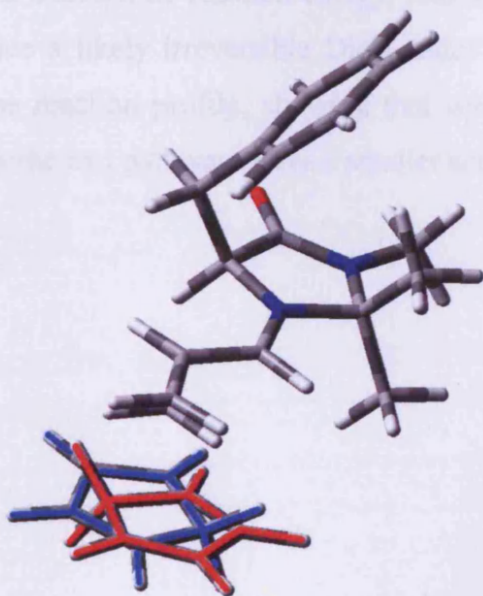Subsequent barriers to Diels-Alder reaction are small, lying in the range 9 to 13 kJ mol^{-1}, compared with a barrier of 52 kJ mol^{-1} for the uncatalysed reaction of cyclopentadiene with acrolein at the same BH&H level. Thus, as seen previously with some model amine catalysts[17], the formation of an iminium ion from reaction of an aldehyde with a secondary amine leads to a substantial lowering of the barrier to Diels-Alder reaction at the α,β- C=C bond, commensurate with the excellent yields for this reaction reported by MacMillan.

	Reactant binding energy	Diels-Alder barrier	Relative rate @ 298K	ΔE reaction
E,trans, exo	-43.4	+8.9	5.4	-192.0
E,trans, endo	-50.0	+11.3	2.1	-196.5
E,gauche+, exo	-40.8	+11.1	2.3	-187.8
E,gauche+, endo	-47.0	+13.2	1.0	-192.8

Table 4.9 Diels-Alder pathway energy changes (kJ mol^{-1})

Several interesting trends are apparent from the data reported in Table 4.9. Firstly, binding energies are more negative (*i.e.* more stable complexes formed) for *endo*- rather than *exo*-complexes. Conversely, for a given orientation of the iminium ion the *exo*- pathway presents a lower barrier to Diels-Alder reaction than does the *endo*- path, albeit with small energy differences of 2.1 - 2.4 kJ mol^{-1}. Secondly, barriers for the *trans*- conformation, *i.e.* the predicted global energy minimum, are lower than for the *gauche+*, again by a relatively small amount. Also of note was the large and exothermic reaction energy, indicating a strong driving force for the forward reaction and hence a likely irreversible Diels-Alder reaction. Figure 4.17 gives a graphical representation of the reaction profile, showing that while the *endo* pathways have a lower reactant complex energy the exo pathways have a smaller activation barrier.
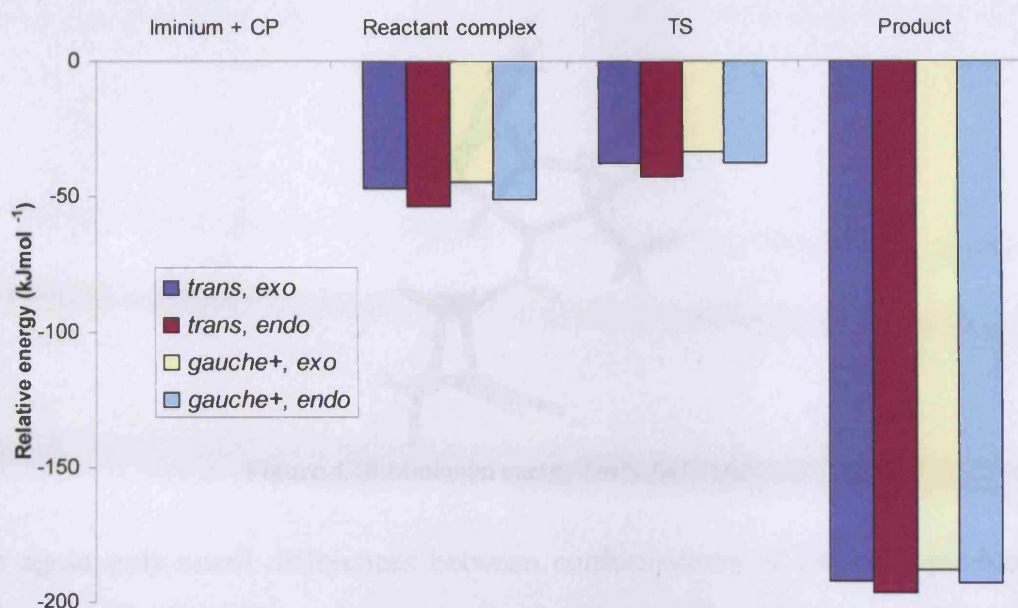
Figure 4.17 Diels-Alder profile of four orientations, all with *E* iminium ion conformation

Thus, our results indicate that barriers to rotation between conformations of the iminium ion catalyst are substantially bigger than that of Diels-Alder reaction. One would therefore expect reaction to take place rather more quickly than interconversion of isomers, and hence both the *trans* and *gauche+* isomers to contribute to the overall reaction rate, according to their relative Boltzmann populations (Table 4.10). It was particularly significant, therefore, that in both conformations the *exo-* reaction presents a lower barrier than the *endo-*.

	Trans (E) EXO	Trans (E) ENDO	Gauche + (E) EXO	Gauche + (E) ENDO
Relative energy (kJ mol^{-1})	0	2.4	2.1	4.2
Boltzmann Population @ 298K (%)	50.0	19.1	21.6	9.3

Table 4.10 Boltzmann populations (@298K) of four isomers.
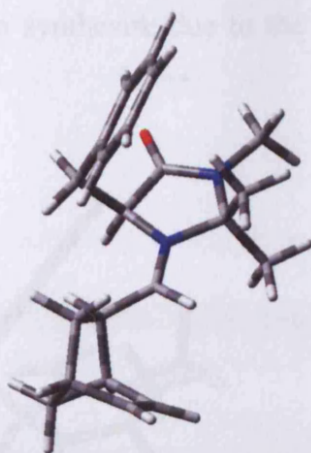
Figure 4.18 Minimum energy Diels-Alder product

There are again only small differences between conformations of the final product, the most stable being that formed from *endo*- approach of cyclopentadiene to the *trans*- iminium ion, as shown in Figure 4.18. Unlike orientations of the iminium ion, the energy ordering of these four reaction products are relatively insensitive to the theory level used (Table 4.11). AIM analysis shows this product retains the C—H...π and C—H...O contacts seen in the catalyst, along with two new C—H...π interactions involving the newly formed bicyclic moiety.

|	180 (E) EXO	180 (E) ENDO	60 (E) EXO	60 (E) ENDO
B3LYP/6-31+G(d,p)	2.3	0.0	6.0	3.7
BHandH/ 6-31+G(d,p)	4.5	0.0	15.2	10.2
mPW1PW91/6-31+G(d,p)	3.2	0.0	8.9	4.5

Table 4.11 Energy differences of four isomers of product and varying theory level (kJ mol^{-1})

The role of the C—H...O interaction involving the carbonyl group in determining the conformation of the benzyl group has been previously documented by Houk.[12] To investigate this effect further, three hypothetical modifications to the ring structure used by MacMillan were investigated (Figure 4.19). In these, the carbonyl was replaced with (a) a thiocarbonyl (C=S) group, (b) an alkenyl group (C=CH$_2$), and (c) a methylene (CH$_2$) group, and the conformation of the resulting iminium ions optimised. As might be expected, the thiocarbonyl group does not significantly affect the geometry of the iminium ion, which remains in the *trans* conformation discussed above. The alkenyl-substituted structure was similar, with a slight loss of planarity of the ring. Removal of the carbonyl altogether leads to larger changes, with a non-planar ring and a twist in the CCCH benzyl dihedral from 110° to 87°, *i.e.* with the phenyl ring further from the geminal methyl groups and closer to the iminium moiety. The reduction of the carbonyl looks

partially interesting as a molecule to synthesise due to the large structural effect on the central ring structure.
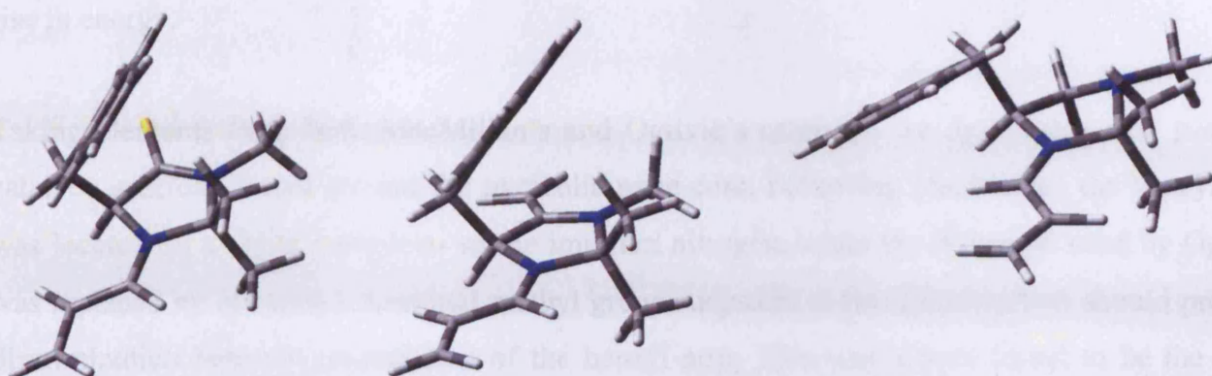
Figure 4.19 Minimum energy geometries of a) thiocarbonyl, b) alkenyl, and c) CH$_2$ modifications of MacMillan catalyst. (BH&H/6-31+G(d,p))

Recently, Lemay and Ogilvie[18,19] reported a novel catalyst architecture with similarities to MacMillan's but based instead on pyrazolidinone five-membered ring system (Figure 4.20). This catalyst includes the benzyl arm used by MacMillan, but locates this on an α nitrogen, and also a bicyclic structure that effectively locks in chirality on two ring carbons, giving impressive stereo-selectivity. We found this report particularly interesting since in section 3, we predicted that an unsubstituted pyrazolidinone ring should have the lowest barrier to iminium ion formation of all amines considered.
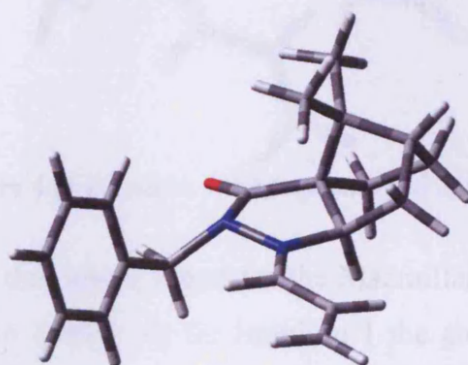
Figure 4.20 Iminium ion formed from Ogilvie's catalyst and acrolein, optimised at BH&H/6-31+G(d,p) (E isomer)

We have therefore used the methods described above to study the geometry of the iminium ion formed from Ogilvie's structure with acrolein. With the benzyl group attached to the α-nitrogen, a loss of planarity was observed at this centre and the positioning of the benzyl group was more flexible than in the systems discussed above. Optimisation of both E and Z-configurations (note that due to the change in ring system from isoazolidinone to pyrazolidinone , this notation has

reversed from section 4.3) yields minimum energy conformations where the significant change in geometry was that of the conjugated C=C bond. Energetically the E isomer was 18 kJmol^{-1} more stable with steric interaction between the benzyl and C=C bond the most likely cause of the rise in energy.

Taking elements from both MacMillan's and Ogilvie's catalysts, we designed a new possible catalytic scaffold, based around the pyrazolidinone core. Following MacMillan, the benzyl arm was located on a chiral carbon α- to the iminium nitrogen, while the N-benzyl used by Ogilvie was replaced by N-methyl. Geminal methyl groups adjacent to the chiral carbon should provide discrimination between orientations of the benzyl arm. This was indeed found to be the case, with the E, *gauche*+ structure found to be the lowest energy conformation by ≈6 kJmol^{-1}. In this conformation, shown in Figure 4.21, the phenyl ring was located directly over the C=C bond, providing an ideal orientation to direct subsequent Diels-Alder reaction. These hypothesis are to be tested by synthetic colleagues to evaluate their potential.
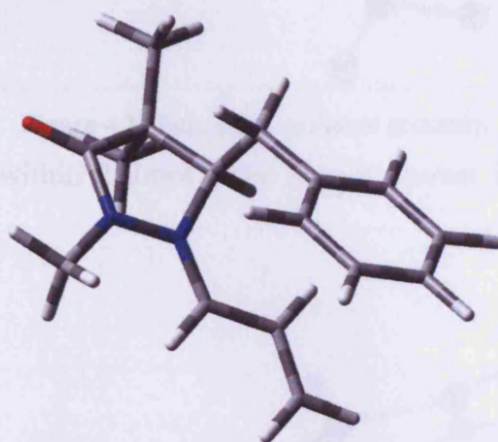
Figure 4.21 E Gauche + stable geometry of Iminium 1

The four iminium geometries that where found for the Macmillan catalyst where also minimised for this structure. As shown in Table 4.12 for Iminium 1 the gauche E geometry gives a lower energy minimum (6.3kJmol^{-1} lower than next minimum). When the hydrogen of the α carbon of the ring was substituted for a methyl (Iminium 2) the preferred geometry was gauche Z isomer albeit less stabilising *cf.* the gauche E of design 1 (1.8kJmol^{-1} lower than next minimum). The orientation of the benzyl could have further affect on the selectivity of the catalyst. Although both orientations are *Si* face directing the *gauche* direction seems to give a superior coverage of the C = C face.

	trans E	trans Z	gauche E	gauche Z
Iminium 1 (h)	6.3	18.1	0.0	9.7
Iminium 2 (me)	10.2	7.6	1.8	0.0

Table 4.12 Energies of iminium ions of two similar molecules (kJmol⁻¹)

Analysis continued with AIM showing interaction of the benzyl group with iminium for design 1 minimum (Figure 4.22), the lack of other interaction shows a well spaced geometry.

Figure 4.22 Iminium 1 minimum geometry

Design 2 has two minium within 2kJmol⁻¹, the lowest shown in Figure 4.23 has three non bonding interactions present.

Figure 4.23 Iminium 2 minimum

94

The pathway of the Diels-Alder reaction between acrolein and cyclopentadiene via an iminium ion intermediate was examined and possible routes to products identified. Although differences in *endo/exo* stationary point energies are small, the effect on rate was noti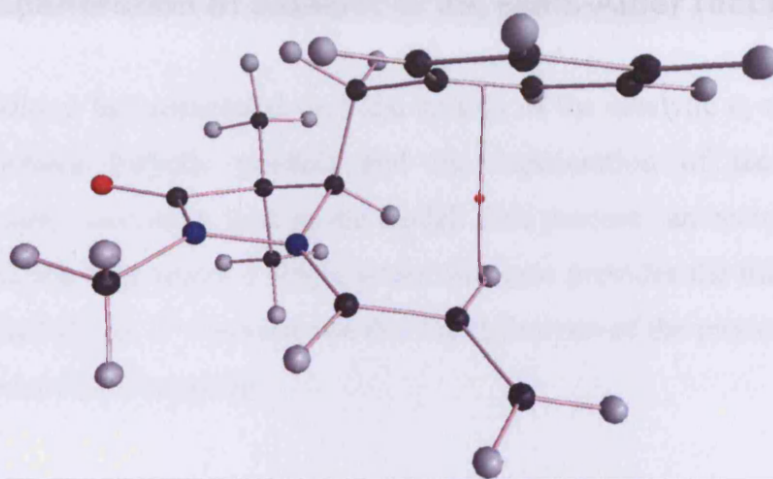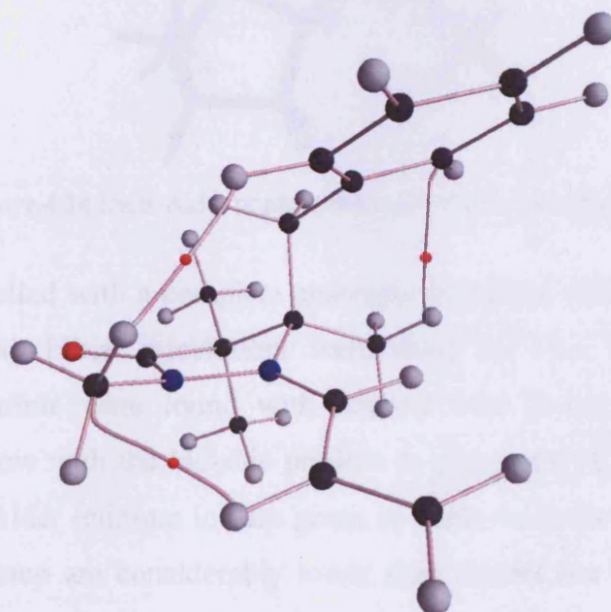ceable with this work giving good structural analysis of a successful catalysis. Our results suggest a theoretically accessible catalyst which has good differentiation between conformational isomers. This differentiation should carry through to the product of subsequent reactions which rely on the orientation of the catalyst.

4.5. Regeneration of catalyst of the Diels-Alder reaction

Once the cycloaddition has completed the final section of the catalytic cycle was the hydrolysis of the newly formed bicyclic product and the regeneration of the catalyst. Here the dimethylamine system was again used as the model. This process can occur as the reverse of the iminium ion formation step where a single water molecule provides the means for separation of the final product and amine. It was assumed that the hydrolysis of the product follows the reverse profile of the iminium ion formation.
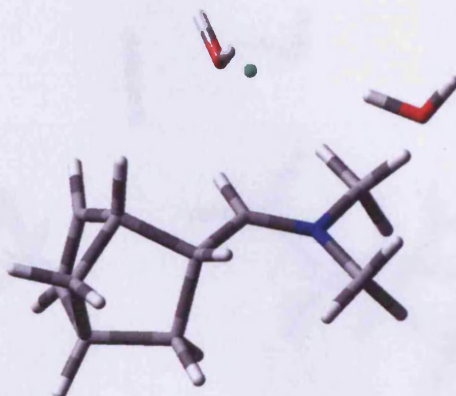
Figure 4.24 Diels-Alder product ensemble of dimethylamine catalyst

The reaction was modelled with a complete ensemble including chloride and two explicit water molecules (Figure 4.24). Initial calculations went along the lines of the reverse iminium ion formation. Energy minima were found with relative ease giving similar geometries to the forward reaction but now with the bicyclic product in place of C=C. Energies of the stationary points from the Diels-Alder iminium ion are given in Table 4.13, the reaction barriers associated with the regeneration step are considerably lower than that of the formation process with the largest barrier for aminol to TS6 of 76kJ mol^{-1}.

	Difference from DA iminium (kJmol^{-1})
Diels-Alder product iminium + 2H$_2$O + Cl$^-$	0
TS5	60.9
Diels-Alder product Aminol	-19.7
TS6	56.4
Diels-Alder product intermediate	48.8
TS7	82.4
Diels-Alder product and catalyst	-28.6

Table 4.13 Energy of stationary points of the regeneration of amine cataylst.

From the assumption that the regeneration of the catalyst follows the same path as the formation of the iminium we have been able to isolate each stationary point in the transformation. For this section the largest energy barrier was associated with the final protonation of the amine, this was conducive with the initial steps of the cycle (Figure 4.25). The size of this barrier was 18kJ mol^{-1} lower in energy than the first deprotonation of the amine in the catalytic cycle.
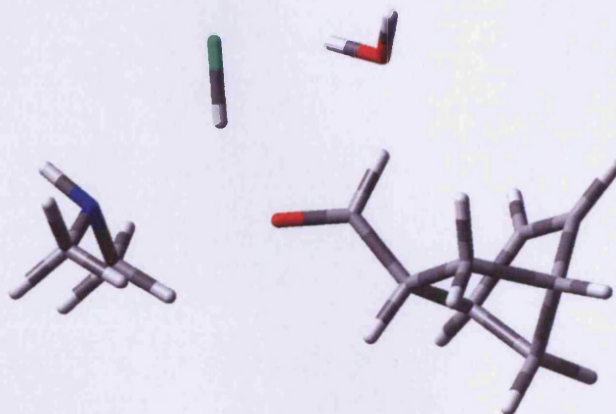
Figure 4.25 TS7 geometry of Diels-Alder adduct hydrolysis using dimethylamine as catalyst.

With results found for the formation, reaction and regeneration of the catalyst a complete pathway can be constructed for the entire catalytic cycle (Figure 4.26). Stationary points that were found without the presence of the atoms contained in cyclopentadiene had the energy of an optimised cyclopentadiene in an 8Å methanol solvent model included. What can be seen from Figure 4.26 is that TS1 gives the largest energy barrier to the forward reaction, also the stabilisation in energy of forming two C – C bonds at TS4 essentially stops any reverse process taking place. Our investigation has focused upon the design of the amine catalyst to lower the energy of TS1, if this energy was sufficiently reduced it is possible that another reaction barrier will become the rate determining step. This could be the case for the catalyst developed by Ogilvie[18,19] where it has been shown that the Diels-Alder reaction itself was the limiting factor to the reaction.
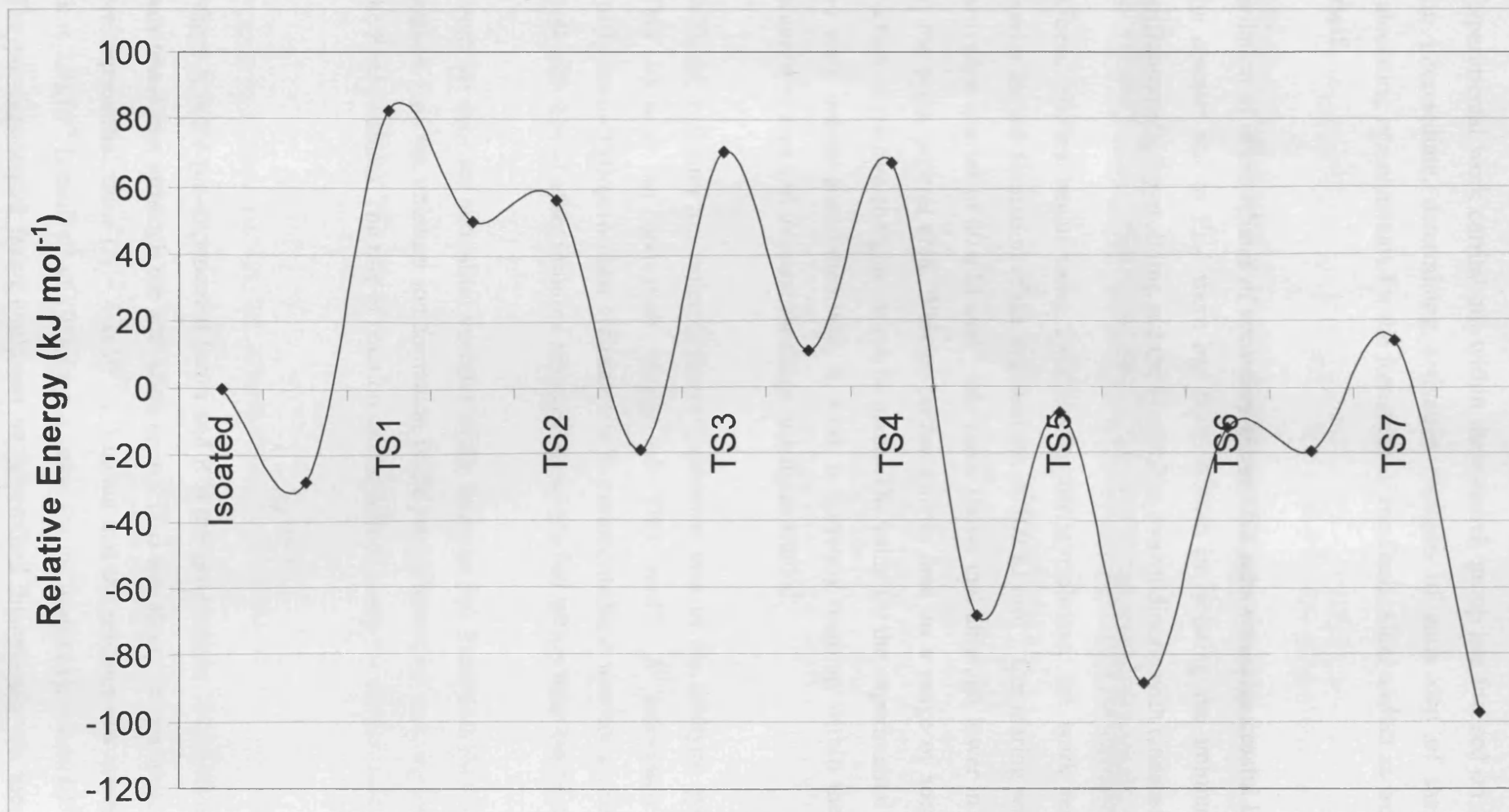
Figure 4.26 Complete reaction profile for the cycloaddition of acrolein with cyclopentadiene via a dimethylamine catalyst

Experimental work carried out within the research group has focused on isolating the iminium ion intermediate, determining activation energies of each step of the catalytic cycle and calculating rate constants for the formation of the Diels-Alder adduct as well as the iminium ion itself.

Isolation of intermediates of secondary amine HCl salts was unsuccessful however, by changing the counter ion to PF_6^- there has been success in isolating the iminium ion adducts of 2-(trifluoromethyl)pyrrolidine and the MacMillan oxazolidinone with cinnamaldehyde.

Kinetic studies began using 2-(trifluoromethyl)pyrrolidine, the work recorded an activation barrier for the formation of the iminium ion of 102 kJ mol^{-1}. Comparing with the calculated TS1 activation barrier of 80.6 kJ mol^{-1}, this value shows that although lower in energy the values are in the same general area. Without further kinetic data on a range of secondary amines a true picture of relative energies cannot be made. The value for the experimental activation energy has no error values accosiatied with it, work is currently ongoing within the group to gain more accurate values and increase the range of amines studied.

With the iminium ion isolated, the cycloaddition step of the catalytic cycle was then studied. This showed an activation energy of 57kJ mol^{-1}. A calculated value for the 2-(trifluoromethyl)pyrrolidine cyclisation with cyclopentadiene was not available, but the value fits well with that of other iminium ion cyclisations studied which were between 14-74kJ mol^{-1}.

From the data for activation energies of the iminium ion formation and cycloaddition, it would suggest that the iminium ion formation is the rate determining step (ignoring the hydrolysis of the final product). The rate of reaction can be defined using the Arrhenius equation:

$$k = Ae^{-Ea/RT}$$

<div align="right">**Equation 4.1**</div>

where A is the pre-exponential factor and R is the gas constant. From the experimental results it was found that although the activation energy (E_a) was larger for the iminium ion formation the pre-exponential value ($A = 4.2 \times 10^{15}$ s^{-1}) meant that the reaction was much more likely to occur ($k = 2.7 \times 10^{-3}$ L mol^{-1}s^{-1} at 293K) c.f. a value for cyclisation ($k = 4.6 \times 10^{-4}$ L mol^{-1}s^{-1} at 293K). The pre-exponential factor could not be determined theoretically via the methods used within this body of work, but the results for the activation energies were encouraging.

The main focus of the research was centred on the formation of the iminium ion and the Diels-Alder reaction with cyclopentadiene. This reaction was looked at for a number of iminium ions, from the simple dimethylamine case to the efficient reaction using MacMillan's imidazolidinone. These studies allowed the postulation of a new catalyst that should show good rates and high levels of asymmetric induction.

To further examine the use of secondary amines in organocataylsis the process of α-acyloxylation via an enamine intermediate was investigated.

4.6.   Mechanistic study of α-acyloxylation of carbonyl compounds

A simple and effective method of the α-functionalisation of carbonyl compounds has been reported by Tomkinson[20] who proposed that the mechanism proceeded via a concerted pericyclic rearrangement. The reaction was shown to be viable for a wide range of functional groups and was operational in the presence of air and water with little or no heating (Figure 4.27).
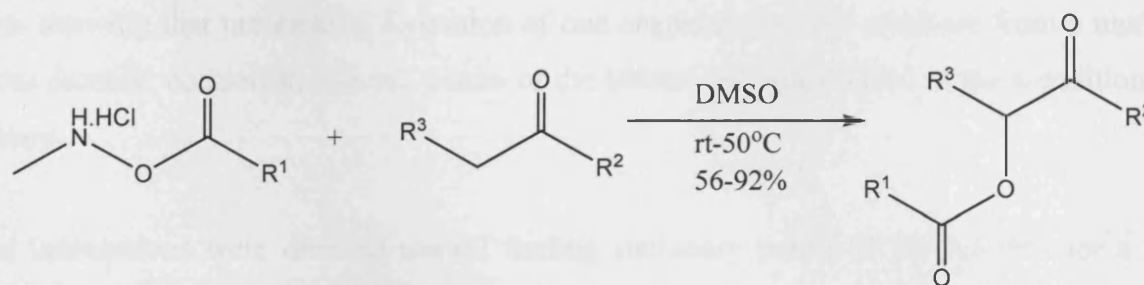
Figure 4.27 Generalised reaction of α-acyloxylation of carbonyl compounds

Secondary amines are commonly used in organocatalysis via enamine pathways. This class of reaction allows for the easy formation of a carbanion equivalent where the lone-pair of the nitrogen is the driving force for the attack onto electron deficient species such as a carbonyl carbon. In reactions such as aldol condensations proton transfer is also important, this is facilitated by the enamine as conversion to the imine form is more favourable than a similar keto – enol tautomerisation.

Preparation of the reagent is achieved via a three step process (Figure 4.28) that results in a secondary amine from which iminium ion formation can occur. A mechanism for this step has been extensively studied in chapter three. After the formation of an iminium ion, the neutral

enamine is formed via the loss of a proton. Through a [3-3]-sigmatropic rearrangement the carbonyl attacks the double bond of the enamine causing dissociation of the N – O bond to form an imine. The product is formed in the final hydrolysis and the reagent is regenerated via a secondary process.
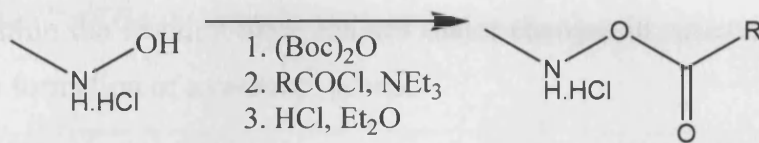
Figure 4.28 Formation of reactive species

The aim of the study was to present a theoretical mechanism of the reaction from enamine to product. Previous studies have given a detailed account for the formation of iminium ion between secondary amines and carbonyl compounds, therefore the focus will be on the rearrangement itself. Through the use of radio-labelling the reaction has been shown to proceed via a pericyclic rearrangment with reactants in a chair-like configuration (Tomkinson – Unpublished results). Stereoselectivity of the reaction has been studied experimentally with results showing that preferential formation of one enantiomer could originate from a number of sources namely; cocatalyst, solvent, nature of the ketone and substituents at the α-position of the auxiliary.

Initial calculations were directed toward finding stationary points of the reaction for a simple model system with no preference for product (Figure 4.29) from which we can increase the complexity of the system.

Figure 4.29 Model system 1

Each stationary point was optimised at HF/6-31G(d), B3LYP/6-31+G(d,p) and mPW1PW91/6-31+G(d,p) with transition states confirmed via frequency calculations. HF produced a large reaction barrier in comparison to the Hybrid DFT functionals. Within this family the barrier height still varies by approximately 20 kJmol^{-1} with B3LYP the lower at 96 kJmol^{-1}. The reaction process was particularly exothermic with a change of approximately 150.0 kJmol^{-1} for DFT methods, within the reaction there are two major changes in structure; a dissociation of an N – C bond and a formation of a carbonyl group.
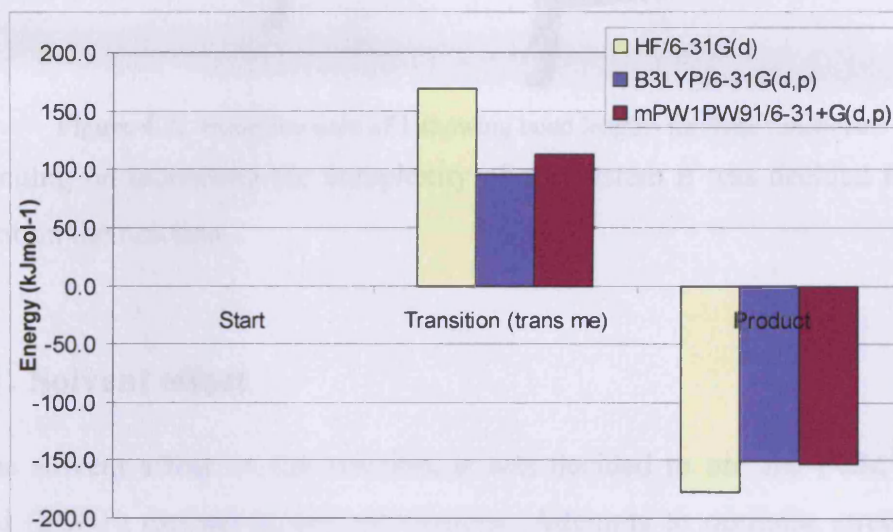
Figure 4.30 Effect of theory on α-acyloxylation of carbonyl compound 1

The transition state was quite asymmetric with bond lengths showing little variation between theories. N – O and C – O distances reported between 1.92-1.98Å and 2.42-2.51Å respectively (Figure 4.31) give a more reactant like geometry. To verify that the correct transition state had been found the geometry was perturbed along the negative eigenvector in both directions. These calculations led to the calculated reactant and product stationary points confirming previous calculations of these minimum.

HF/6-31G(d)   = 1.98Å
B3LYP/6-31+G(d,p) = 1.96Å
mPW1PW91/6-31+G(d,p) = 1.92Å

HF/6-31G(d) = 2.42Å
B3LYP/6-31+G(d,p) = 2.51Å
mPW1PW91/6-31+G(d,p) = 2.42Å
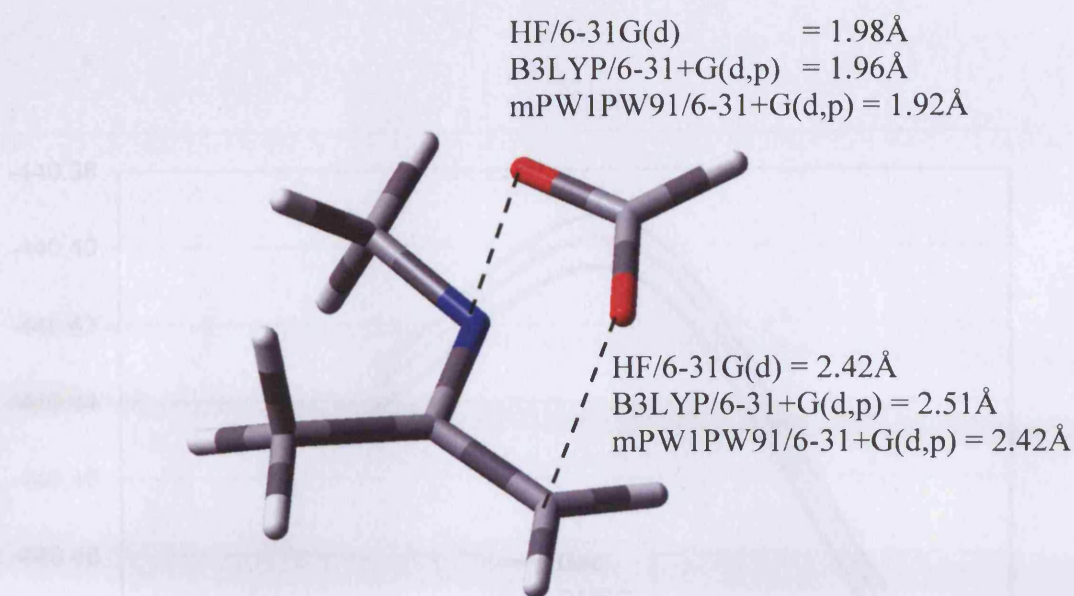
Figure 4.31 Transition state of 1 showing bond lengths for three functionals

Before continuing on increasing the complexity of the system it was decided to investigate the role of solvent on the reaction.

4.6.1. Solvent effect

To model the solvent effect on the reaction, it was decided to use the PCM[21] self-consistent reaction field (SCRF) method in our calculations. Attempts to optimise structures within the solvent cavity were unsuccessful, the B3LYP/6-31+G(d,p) optimised geometry was used for single point calculations using the self–consistent reaction field as implemented in Gaussian 03. Within a dimethylsulfoxide (DMSO) dielectric cavity the absolute energy of the system lowered by an average of 30.0 kJmol^{-1} when compared with the gas phase system. The overall forward activation barrier was lowered by approximately 6.0 kJmol^{-1}. The less polar solvent toluene was also tested for its effect on the mechanism. As predicted, toluene had a lesser effect on the lowering of the reaction energy with an average of 13.0 kJmol^{-1} stabilisation over gas phase calculations and 3.0 kJmol^{-1} lowering for the activation energy.
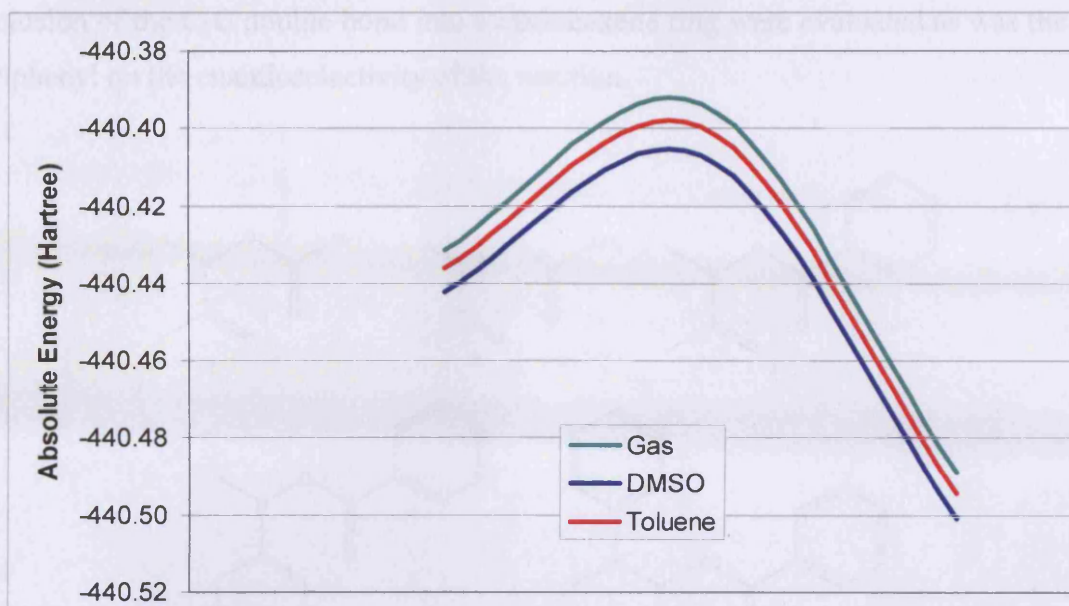
Figure 4.32 Reaction profile of 2 using PCM solvent models

The magnitude of the solvent correction was sufficiently small to allow us to continue calculations in the gas phase without significant loss of accuracy.

From the stationary points found for the simple model system larger ensembles were created. Initially the proton of the carbonyl carbon was substituted by methyl (Figure 4.33) and phenyl groups (Figure 4.34). There was no appreciable change in N – O bond length between structures, C – O distances varied the most at HF/6-31G(d) between **2** and **3** by 0.03Å. This indicates that the transition state geometry looks to be only slightly affected by substitutions at the carbonyl carbon.

HF/6-31G(d)	= 1.97Å
B3LYP/6-31+G(d,p)	= 1.95Å
mPW1PW91/6-31+G(d,p)	= 1.91Å

HF/6-31G(d)	= 2.38Å
B3LYP/6-31+G(d,p)	= 2.46Å
mPW1PW91/6-31+G(d,p)	= 2.37Å
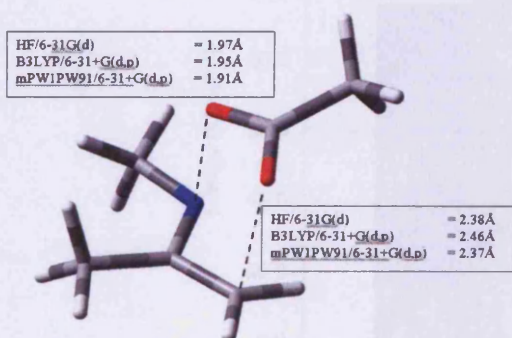
Figure 4.33 Transition state of 2

HF/6-31G(d)	= 1.97Å
B3LYP/6-31+G(d,p)	= 1.94Å
mPW1PW91/6-31+G(d,p)	= 1.90Å

HF/6-31G(d)	= 2.41Å
B3LYP/6-31+G(d,p)	= 2.47Å
mPW1PW91/6-31+G(d,p)	= 2.38Å
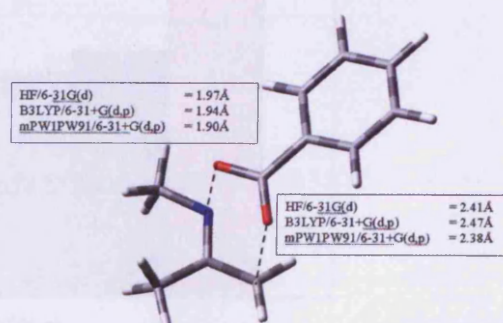
Figure 4.34 Transition state of 3

From the calculations performed it can be said that the substitution of the carbonyl position has no appreciable effect on the geometry of the transition state. Reaction profiles were calculated for a further four systems with increasing complexity (Figure 4.35). The presence of a phenyl

and inclusion of the C-C double bond into a cyclohexene ring were evaluated as was the effect of N-ethylphenyl on the enantioselectivity of the reaction.
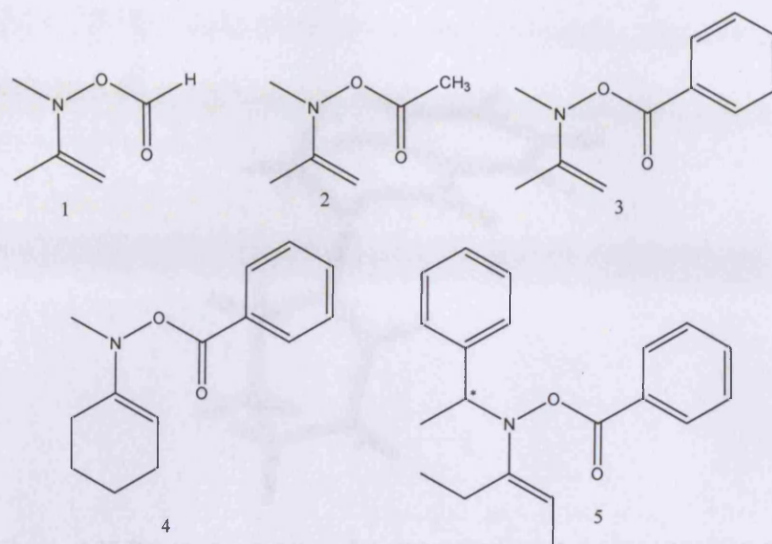
Figure 4.35 Molecules investigated

Changing the functional group of the ester has only a small effect on the barrier to reaction. Methyl substitution (**2**) increases the barrier by approximately 3.0 kJ mol^{-1} over **1** while a bulky phenyl (**3**) has a stabilising effect of the same magnitude. This can be seen as stabilisation of the electron density of the transition state via the aromatic nature of the substituent.
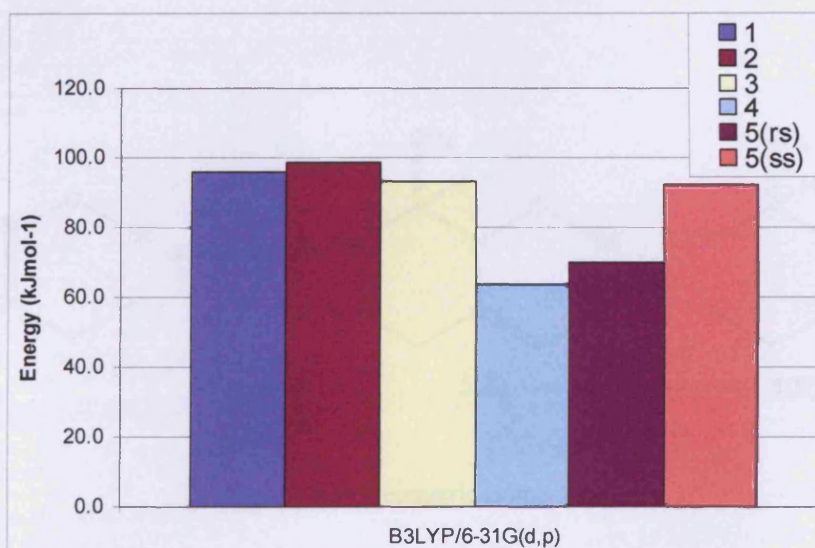
Figure 4.36 Energy of activation of six systems

Figure 4.36 shows that the lowest transition state energy was that of the molecule with the enamine contained within a hexene ring (**4**). This structure promotes a substantial drop in activation energy but still lacks enantioselectivity. The orientation of the N-methyl group can

allow for further geometrical variation, the preferred geometry of the N-methyl was on the opposite face to the reaction centre. This arrangement allowed for a sterically unhindered approach to the transition state geometry (Figure 4.37).
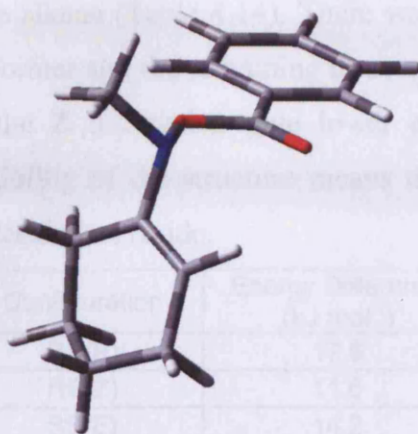
Figure 4.37 Reactant geometry of system with lowest energy transition state

Molecule **5**, can show preference to form a specific diastereoisomer. The reagent itself contains one stereogenic centre, adjacent to the nucleophilic nitrogen. The absolute geometry was defined by two labels; the first label describes the α-Carbon stereochemistry while the second gives the stereochemistry of the chiral centre to be formed. Experimentally, the former was fixed as **R**, leading to preferential formation of **RR** over the **RS** product.
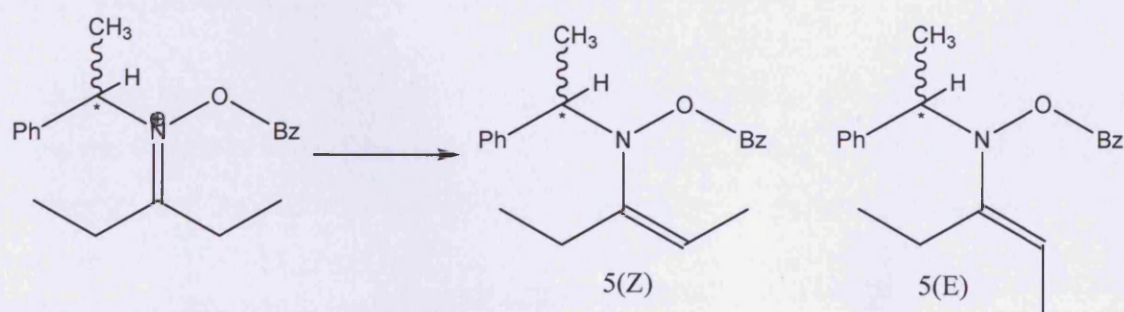
Figure 4.38 Geometric isomers of 5

The preferred geometry of the reactant depends on the stereocentre. Fixing the geometry of the α-carbon as **R**, four possible reactant geometries were identified, i.e. with the benzyl group oriented over the pro-**R** or pro-**S** face on the C=C bond, which can in turn have **E** or **Z** orientation. The relative energies of these geometries can be seen in Table 4.14. Note that

although the second stereocentre has not yet been formed here, we term these **RS** and **RR** for simplicity.

Results show that the preferred geometry for the reactant was the **RR** configuration at the chiral centre with **Z** orientation of the alkene (Table 4.14). There was a substantial energy difference between the lowest energy conformer and the remaining three conformers studied. Also it can be seen that both isomers with the **Z** orientation give lower energies than the comparable **E** orientation. The rotational flexibility of the structure means that there was a large number of conformations in which the molecule can reside.

Configuration	Energy Difference (kJ mol^{-1})
RS(E)	17.9
RS(Z)	11.6
SS(E)	14.2
SS(Z)	0.0

Table 4.14 Energy difference of reactant geometries of 5 at B3LYP/6-31+G(d,p)

The transition states for formation of four diastereoisomers from **5** were isolated. The geometry of the **RS** transition states has a 'chair like' configuration as visible in the achiral examples of **1-4**. The change in enantiomer for R to S invokes a change in transition state geometry, there was a loss of the chair like structure that was found with the R enantiomers. The steric effect of the chiral centre of the **S** enantiomer gives a more perpendicular approach to the rearrangement observed (Figure 4.39). This tilted structure has a slightly increased activation energy.
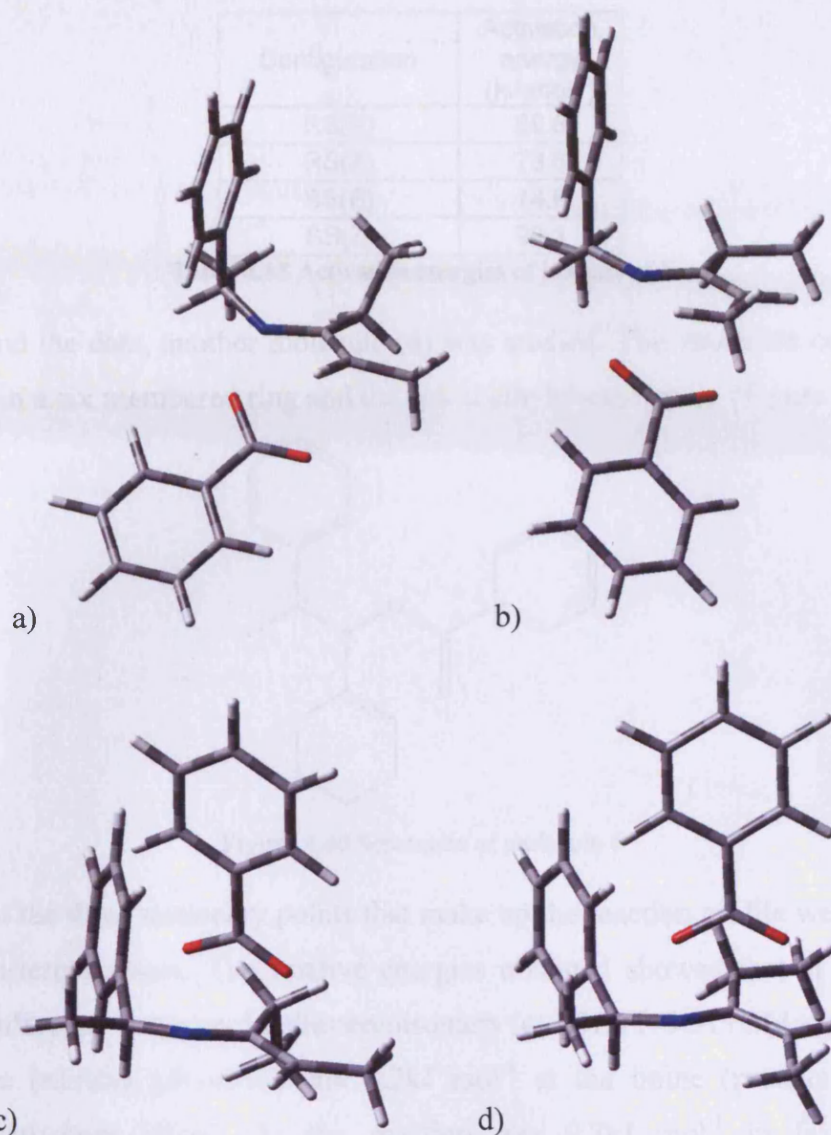
Figure 4.39 Transition state of 5 from top left to bottom right; a) **RS**(E), b) **RS**(Z), c) **RR**(E) and d) **RR**(Z)

From the transition state calculations, it was found that formation of both **RS** enantiomers has a lower activation barrier than either of the **RR** enantiomers (Table 4.15). The largest activation barrier (92.1kJ mol⁻¹) was found for **RR**(Z) geometry which was shown to be the lowest energy reactant geometry. This suggests that that although **RR**(Z) was the most stable configuration for the reactant, it was the RS geometry that was the most likely to react. The reorientation from pro-R to pro-S face was likely to be relatively low in energy compared to the barriers shown in Table 4.15, since this only involves rotation about single bonds.

Configuration	Activation energy (kJ mol^{-1})
RS(E)	69.8
RS(Z)	73.6
SS(E)	74.6
SS(Z)	92.1

Table 4.15 Activation energies of isomers of 5

To further expand the data, another molecule (**6**) was studied. This molecule contained both the alkene 'locked' in a six membered ring and the chiral ethylphenyl group (Figure 4.40).
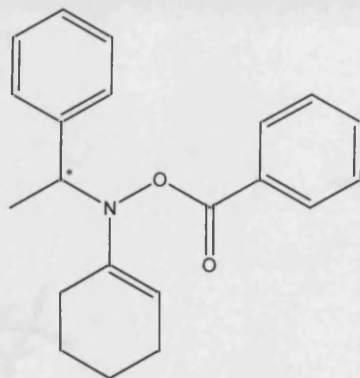
Figure 4.40 Schematic of molecule 6

Optimisations of the three stationary points that make up the reaction profile were carried out for **RS** and **RR** diastereoisomers. The relative energies obtained showed that at the local energy minimum the difference between the diastereoisomers (at B3LYP/6-31+G(d,p)) was 1.2kJ mol^{-1} for the enamine (starting geometry) and 0.2kJ mol^{-1} at the imine (product geometry). The difference in activation energy for the reaction was 0.7kJ mol^{-1} in favour of the **RR** diastereoisomers (Table 4.16).

Enamine	Transition state	Imine
1.2	1.9	0.2

Table 4.16 Increase in energy of RS over RR (kJ mol^{-1})

The lack of discrimination between these rotamers in this case was surprising, but could be attributed to subtle inclination of the benzyl group or a longer range of solvent on the reaction that previously anticipated. Through figures 4.42 to 4.45 it can be shown that there was substantial rotation of the 3-carbon group in the reaction. The ease in the speed of this rotamer factor in the fact although appearing in the charge of the chargroups of rotamer. As the difference in energy of these rotamers was minimal, the overall activation energy for the reaction was smaller compared to the other reactions studied. Therefore this reaction was expected to proceed quickly but with little chiral discrimination, unlike in the acyclic case. The activation energy for the acetyl transfer in this acyclic case was found to be 42 kJ/mol.

Figure 4.41 RS Start geometry
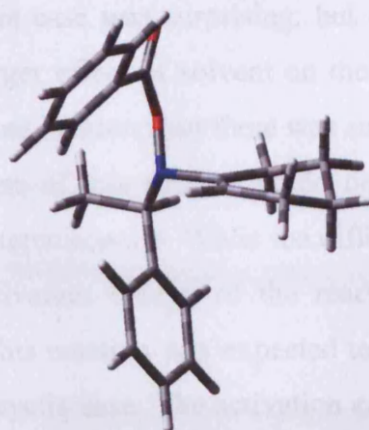
Figure 4.42 RR Start geometry

The calculations performed for molecule 6 may concern the change in the chiral nature of the reactant, with some rotamer producing a second chiral centre of R configuration. In this it is appreciable that in each case the inhibition of the groups the attitude of attack in such the R product would then be the preferred.
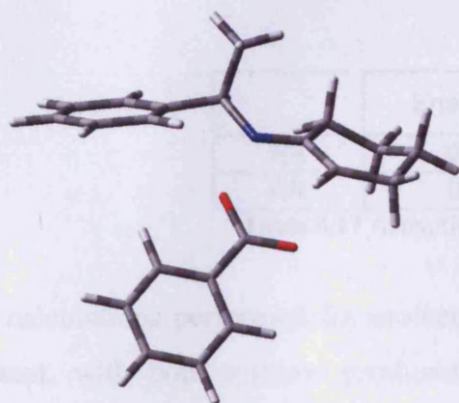
Figure 4.43 RS TS geometry

Figure 4.44 RR TS geometry

4.6. Conclusions

The associations with the kind reasonably active has been determined in the experimental images. The geometries have been discussed and although the structures were quite approximated it possible that image produced by the calculations with the DFT calculations gave a reasonable transition transition states but this was not accurate in energy because functionals were often inadequate and that a HF optimisation followed by a DFT single point energy calculation is useful, and even for further work it may however it was found in this investigation that it was necessary for the structure to contain subsidiary structure such as to be stabilised enough were acceptable, but it seller adequate interactions between the alkyl chains and aromatic groups. Though the combination this choice it was clear that HF gave incorrect geometries for this kind of system.

Figure 4.45 RS product geometry

Figure 4.46 RR product geometry

110

The lack of discrimination between diastereoisomers in this case was surprising, but could be attributed to subtle interaction of the benzyl group or a larger effect of solvent on the reaction than previously envisage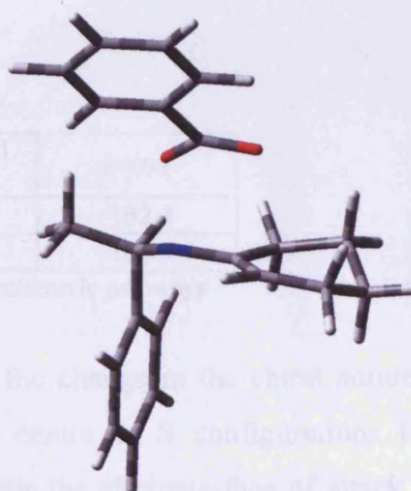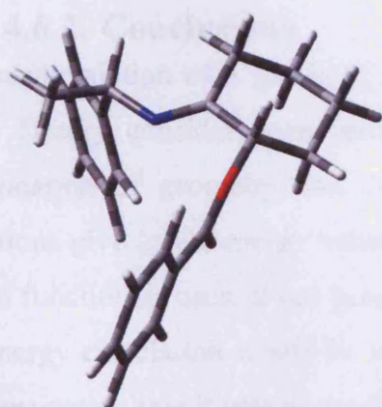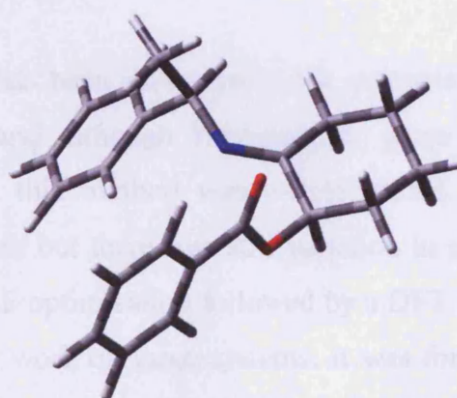d. Through figures 4.43 to 4.48 it can be seen than there was substantial rotation of the benzyl group through the reaction. The ease of this rotation could be another factor in the lack of discrimination in the energy of the diastereoisomers. While the difference in energy of diastereoisomers was minimal, the overall activation energy of the reaction was smaller than any of the other reactions studied. Therefore this reaction was expected to proceed quickly but with little chiral discrimination, unlike in the acyclic case. The activation energy for the reaction was approximately 38kJ mol^{-1} (Table 4.17).

	Enamine	Transition state	Imine
RS	0.0	38.5	-182.1
RR	0.0	37.8	-181.1

Table 4.17 Activation energies of two enantiomeric pathways

The calculations performed for molecule **6** only concern the change in the chiral nature of the reactant, with both systems producing a second chiral centre of **S** configuration. To fully appreciate the extent of asymmetric induction of the groups the alternate face of attack to give the **R** product would need to be calculated.

4.6.2. Conclusions

The α-acyloxylation of a group of secondary amines has been investigated via computational means. Theory considerations have been discussed and although Hartree-Fock gives good approximation of geometry, the energy produced by this method was overestimated. DFT calculations give lower energy values for transition states but there was still variation in energy between functionals used. It has been suggested that a HF optimisation followed by a DFT single point energy calculation would be sufficient for further work on large systems. It was found in this investigation that it was dependent on the structure in question. For rigid structures such as **6** or smaller systems such as **1-4** this was acceptable, but **5** relies on subtle interactions between the alkyl chains and aromatic groups. Through the optimisation procedure it was clear that HF gave incorrect geometries for this flexible system.

As the process studied here was not the rate determining step with the reagent being destroyed it was unclear on how to proceed with modifying the bond forming step of the reaction, what was of interest was that it is possible to observe control of stereochemistry through changes to one area of the molecule. A decrease in activation barriers has been found mainly due to the initial formation of the system with the attack of a carbonyl by a secondary amine, (cyclohexanone in **4**, pentan-3-one in **5**).

4.7. References

(1)   Cavill, J. L.; Peters, J. U.; Tomkinson, N. C. O. *Chemical Communications* **2003**, 728-729.
(2)   Zora, M. *Journal of Molecular Structure-Theochem* **2002**, *619*, 121-133.
(3)   Kozlowski, M. C.; Panda, M. *J. Org. Chem.* **2003**, *68*, 2061-2076.
(4)   Northrup, A. B.; MacMillan, D. W. C. *Journal of the American Chemical Society* **2002**, *124*, 2458-2460.
(5)   Ahrendt, K. A.; Borths, C. J.; MacMillan, D. W. C. *Journal of the American Chemical Society* **2000**, *122*, 4243-4244.
(6)   Paras, N. A.; MacMillan, D. W. C. *Journal of the American Chemical Society* **2001**, *123*, 4370-4371.
(7)   Austin, J. F.; MacMillan, D. W. C. *Journal of the American Chemical Society* **2002**, *124*, 1172-1173.
(8)   Halland, N.; Hansen, T.; Jorgensen, K. A. *Angewandte Chemie-International Edition* **2003**, *42*, 4955-4957.
(9)   Halland, N.; Aburel, P. S.; Jorgensen, K. A. *Angewandte Chemie-International Edition* **2004**, *43*, 1272-1277.
(10)   Yang, J. W. p.; Fonseca, M. T. H. p.; List, B. p.
(11)   Jen, W. S.; Wiener, J. J. M.; MacMillan, D. W. C. *Journal of the American Chemical Society* **2000**, *122*, 9874-9875.
(12)   Gordillo, R.; Carter, J.; Houk, K. N. *Advanced Synthesis & Catalysis* **2004**, *346*, 1175-1185.
(13)   Adamo, C.; Barone, V. *Journal of Chemical Physics* **1998**, *108*, 664-675.
(14)   Becke, A. D. *Journal of Chemical Physics* **1993**, *98*, 1372-1377.
(15)   Kendall, R. A.; Dunning, T. H.; Harrison, R. J. *Journal of Chemical Physics* **1992**, *96*, 6796-6806.
(16)   Hill, J. G.; Platts, J. A.; Werner, H. J. *Physical Chemistry Chemical Physics* **2006**, *8*, 4072-4078.
(17)   Evans, G. J. S.; White, K.; Platts, J. A.; Tomkinson, N. C. O. *Organic & Biomolecular Chemistry* **2006**, *4*, 2616-2627.
(18)   Lemay, M.; Ogilvie, W. W. *Organic Letters* **2005**, *7*, 4141-4144.
(19)   Lemay, M.; Ogilvie, W. W. *Journal of Organic Chemistry* **2006**, *71*, 4663-4666.
(20)   Beshara, C. S.; Hall, A.; Jenkins, R. L.; Jones, K. L.; Jones, T. C.; Killeen, N. M.; Taylor, P. H.; Thomas, S. P.; Tomkinson, N. C. O. *Organic Letters* **2005**, *7*, 5729-5732.
(21)   Tomasi, J.; Mennucci, B.; Cances, E. *Journal of Molecular Structure: THEOCHEM* **1999**, *464*, 211-226.

5 General conclusions

The research undertaken throughout this project has aimed to answer a number of questions that were found in the literature and experimental data from the Tomkinson group at Cardiff university. Through computational means some notable questions have been answered, and inevitably more questions posed.

A pathway for the formation of an iminium ion from an α,β-unsaturated aldehyde and a secondary amine was constructed. A model system in the presence of a counter ion and one explicit water molecule allowed for a greater understanding of the formation of this useful intermediate. Each geometry was confirmed via harmonic frequency calculations. Investigating the effect of water on iminium ion formation with the use of explicit molecules and continuum models gave the conclusion that explicit water has the effect of stabilising the reactant complex, allowing for a lower energy reaction profile.

The reaction pathway for the iminium ion formation has been described as a three step deprotonation via water aided proton transfer. The initial deprotonation of the secondary amine is found to be the rate determining step of the iminium ion formation. Differences in DFT geometries were negligible while energies varied mostly in the aminol and TS3 stationary points. Basis set effect showed a lowering of energy of all points bar the sp^3 hybridised aminol, with an increase in the number of the basis functions. The type of continuum model for solvent effects was investigated with results showing that PCM models were unable to verify transition state geometries within the software used. The Onsager model allowed for a simple description of the bulk solvent effects. Overall it was found that the B3LYP functional was a sufficient level of theory to use when coupled with the 6-31+G(d,p) basis set. The TS1 activation energy for 2-(trifluoromethyl)pyrrolidine was found to be in good agreement with kinetic data obtained by the Tomkinson group.

The α-effect was found to greatly reduce the activation energies of the rate determining step. An α-Nitrogen allows for extended hydrogen bonding through the reaction profile while a more nucleophilic oxygen decreases the activation barrier by a greater degree than an α-nitrogen. The incorporation of the reactive secondary amine into a five-membered ring increases the activation energy of TS1 with no α-heteroatom present, but the combination of

both features decreases the activation energy. The addition of an endo-cyclic carbonyl further decreases the activation energy.

The presence of carbonyl groups within the catalysts has a large effect on reaction energy and geometry, while reducing the value for TS1, the functional group increases the activation energy for the two remaining transition states. Acyclic carbamates studied gave low energy reaction pathways with some of the lowest TS1 activation energies. All carbamates considered stabilise the intermediate geometry of the iminium ion formation considerably.

The atoms in molecules approach gave further insight into the interactions within stationary point geometries, with inter-molecular interactions being described. Through AIM analysis water is shown to act as a 'proton shuttle' between chloride and the α,β-unsaturated carbonyl. The initial N-C bond formation and the influence of carbamates on transition structure were clearly shown via the presence of bond critical points.

The geometry of a selection of iminium ions were studied with respect to the preferred geometry of the product. There was a slight preference for the Z isomer in asymmetric molecules studied.

A number of molecular descriptors were examined as predictive tools. The electrostatic potential gave insightful information about the reactive nitrogen and the surrounding regions. Proton affinity gave a good relationship with the activation energy of TS1. Experimental data of the Diels-Alder reaction via iminium ions show that although proton affinity looks to be a good descriptor for TS1, there are other elements to the reaction that are effecting the overall reaction. However this may be a useful guide to the synthesis on new catalytic amines.

For the Diels-Alder reaction of cyclopentadiene and an α,β-unsaturated carbonyl, the inclusion of counter ion species is shown to be problematic due the charges present in the system. Iminium ion mediated Diels-Alder reactions have a significantly lower activation energy *cf* uncatalysted reaction with acrolein and proceed in an asymmetric concerted pathway.

The presence of an α-heteroatom drastically reduces the activation energy for the Diels-Alder reaction. The more electronegative hydroxylamine incurs the lowest barrier of the systems

studied that used acrolein as the carbonyl reagent. The use of cinnamaldehyde as the carbonyl reagent gives a rise in activation energy of 30kJ mol^{-1} over acrolein and 65kJ mol^{-1} over the dimethylamine based catalyst. Actual values of the transition state energies and reaction as a whole are dependent on the solvent model used but all trends studied are the same regardless of solvent model. The difference in barrier height between isomers becomes more pronounced with the use of solvent models.

The choice of theory level is important for the study of imidazolidinones developed by McMillan et al. Good results were found using the BH&H DFT functional (6-31+G(d,p)) with the more common B3LYP functional using the same basis disagreeing with results. The calculated geometry for the imidazolidinone iminium ion was confirmed via crystallographic methods. Atoms in molecules analysis provided useful interpretation of the interactions present. Intramolecular interactions of the catalyst have been given as a possible cause for preferred geometries and allowed for the development of a number of catalyst candidates.

The Diels-Alder reaction employing the imidazolidinone catalyst of McMillan was studied, with results showing a slight preference for the exo product. It is shown that the binding energy of reactants in the endo configuration is greater than that of the exo. The exo transition states are seen to be lower in energy than both endo geometries, also the large exothermic nature of the reaction is evident.

Hydrolysis to the final product of the Diels-Alder reaction was examined using a model system of dimethylamine. It was found that the process occurred via the reverse of iminium ion formation. The reaction barriers associated with the regeneration step are considerably lower than those of the formation process. The regeneration of the catalyst completes the catalytic cycle for the iminium ion catalysed Diels-Alder reaction.

Finally the process of α-acyloxylation of carbonyl compounds was investigated. Theory considerations have been discussed, and although Hartree-Fock gives good approximation of cyclic geometries it has difficulty with flexible systems. DFT calculations give better energy values for transition states over HF methods, but there is still variation in energy between functionals used.

Reasons for the observed stereoselectivies in experiment work were not clearly uncovered for the systems studied. Although differences in activation energies are found to be small, the description of the system could be improved through solvent models which could have an influential effect on stereoselectivity. As the process studied here is not the rate determining step with the reagent being destroyed it is unclear on how to proceed with modifying catalytic step of the reaction, what is of interest is that it is possible to observe control of stereoselectivity through changes to one area of the molecule.

There is much scope in the continuation of this subject area. Many aspects of the research could be expanded upon such as an increase in accuracy in solvent models of the iminium ion formation and charged systems. Reliable reactivity descriptors still remain a goal of the project which could demand more attention. The Diels-Alder reaction is an extensively studied system but there is scope for a greater understanding in the stereoselectivites of asymmetric organocatalysis. Prediction of viable catalysts for synthesis remains the ultimate goal of the research, the work conducted within this report gives a platform to do just that, with a number of catalysts already suggested for synthesis.